PROTON TRANSFER IN BIOENERGETIC PROTEINS

by

ÁGNES MARÓTI MD

DISSERTATION

Submitted in partial fulfilment of the requirements
for the degree of Doctor of Philosophy in Clinical Medicine Sciences
in the Graduate School of the
University of Szeged, Hungary

Supervisor: Csaba Bereczki MD, PhD
Head of the Department of Paediatrics
University of Szeged, Hungary

Department of Paediatrics University of Szeged, Hungary

Szeged

2015.

The dissertation is based on the following **PUBLICATIONS**:

I. Ágnes Maróti, Colin A. Wraight and Péter Maróti: The rate of second electron transfer to Q_B^- in bacterial reaction center of impaired proton delivery shows hydrogen-isotope effect. *Biochim. Biophys Acta, Bioenergetics,* 1847 (2015) 223–230.

II. Ágnes Maróti, Colin A. Wraight and Péter Maróti: Protonated rhodosemiquinone at the Q_B binding site of M265IT mutant reaction center of photosynthetic bacterium *Rhodobacter sphaeroides. Biochemistry,* American Chemical Society (2015) DOI: 10.1021/bi501553t

III. Ágnes Maróti, Colin A. Wraight and Péter Maróti: Equilibrium- and kinetic isotope effects of electron transfer in bacterial reaction center of photosynthetic bacteria. COST conference, Visegrád, (2014), talk.

IV. Ágnes Maróti, Colin A. Wraight and Péter Maróti: Spectroscopic evidence for protonated semiquinone in reaction center protein of photosynthetic bacteria. Molecular Machines Conference, Ringberg, Germany (2014) poster.

ACKNOWLEDGEMENTS

I would like to thank Dr. Csaba Bereczki MD, PhD, head of the Department of Pediatrics at the University of Szeged who allowed me the freedom to prepare this work which would not have been possible without his generous support.

I am also indebted to Dr. Colin Wraight, professor of biochemistry and biophysics at the University of Illinois, Urbana-Champaign IL. USA, whose impact on me as a scientist and a person is undeniable.

I would also like to thank Dr. Eiji Takahashi (University of Illinois, Urbana-Champaign, IL, USA) providing me the site directed mutations to the reaction centers used in this work. In particular, Eiji's knowledge of the art of molecular biology was crucial.

Additionally, I owe a lot to Gábor Sipka, PhD student at the Department of Medical Physics and Informatics who helped me to prepare the fascinating atomic structures of the molecules and the 3D representation of Fig. 4.8.

Finally, I am indebted to my family particularly my mother and father for their constant support. They always loved me and had faith in me.

TABLE OF CONTENTS

1. INTRODUCTION

The external energy sources (food) and stimulations (sound, light, etc) are converting to metabolic energy forms and neural responses, respectively, almost exclusively by chemiosmotic mechanisms in which oxidation-reduction (redox) free energy is changed into transmembrane proton (H^+ ion) and electrical gradients (Mitchell's chemiosmotic theory, Nobel Prize 1978).[1,2] The vast majority of these reactions occur not in solution but in proteins bound to membranes. About one third of all proteins are redox active and an overlapping one third are membrane proteins. The chemistry is performed by various redox and photobiological cofactors (hemes, metal clusters, quinones, flavins, pterins, etc) that are invested with extraordinary properties by the proteins that bind them. The protein-cofactor interactions are the same as those that operate on a substrate in an enzyme active site. The membrane proteins of respiration, photosynthesis, methanogenesis, etc provide ideal systems for studying the catalysis with astonishing specificity and revealing concepts, realities and design that can be related to similar systems of higher complexity. The present dissertation is inspired by that concept and will demonstrate the abundance of this approach.

The transfer of protons in living organisms can be classified into two (not fundamentally different) categories: reactions of 1) acid-base catalysis and 2) proton transport. In the former, the proton transfer events are highly localized and occur generally pair wise between adjacent groups (e.g. an amino acid and a substrate) in the active site. The importance of acid-base catalysis in enzyme activity is well known and documented in several fields of medical sciences including the control of pH balance of blood or gastric juice. In the latter, the transport of protons is usually coupled to electron transfer or conformational changes induced by light (e.g. vision) or hydrolysis of ATP (e.g. gastric proton pump). It is effective over long distance and typical in bioenergetics. The primary purpose of the proton transfer is to translocate protons into and across the membrane, e.g., of the mitochondrion or cells. The transport necessarily involves many elementary proton transfer steps constituting proton delivery pathway in permanent or transiently formed structure of the protein where proton donors and acceptors line up and form bucket-brigade mechanism to transport H^+ ions.[3] There are not only energetic constraints (e.g. pathway should be formed) but also kinetic limitations, because usually high rate of proton delivery is needed to reduce the dissipation (losses) of the available free energy by competing additional processes. Below, the

transfer of protons in some selected channels and bioenergetic proteins will be introduced to demonstrate the design of functionality of long distance proton transport of medical (biological) interest.

1.1 Proton transport in some bioenergetic proteins.

Human carbonic anhydrase catalyzes the rapid interconversion of carbon dioxide and water to bicarbonate and protons to maintain acid-base balance in blood and other tissues, and to help the transport of carbon dioxide out of the tissues:

$$CO_2 + H_2O \leftrightarrow HCO_3^- + H^+, \qquad (1.1)$$

where the proton is taken up (or released) as part of the stoichiometric turnover.[4] The proton transfer occurs over a distance of 8-10 Å and is associated with the regeneration of the active site Zn^{2+}-OH^- complex:

$$Zn^{2+} - OH_2 + His^{64} \leftrightarrow Zn^{2+} - OH^- + His^{64}H^+ \qquad (1.2)$$

The communication between the zinc-bound water and the aqueous phase is mediated by a short chain of 2-3 water molecules and the histidine (His64) side chain, which is in contact with the bulk phase (Fig. 1.1).

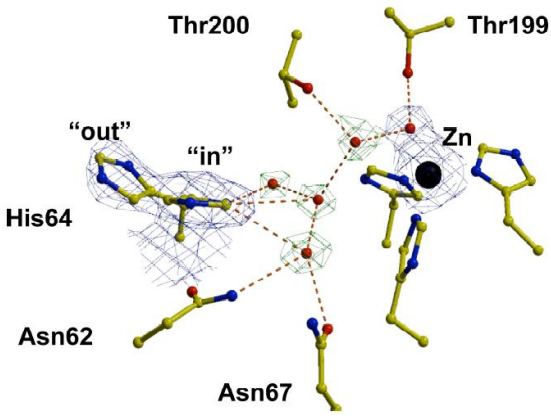

Figure 1.1 The active site of carbonic anhydrase II. The reactive water/hydroxyl is bound to a zinc(II) ion (black), which is liganded by three histidines. The fourth histidine, His64, is at the entrance of the active site cleft and is observed in two distinct configurations – the "out" position is essentially in the bulk phase and the „in" position is connected to the Zn^{2+} ion by four bridging water molecules (red). Image from www.med.ufl.edu/pharm/facdata/silvermn/silvermn.html.

The reaction rate of carbonic anhydrase is one of the fastest of all enzymes, and somewhat surprisingly, the transport of H^+ in and out of the active site is the rate limiting step. Typical catalytic rates of the different forms of this enzyme are ranging between 10^4 and 10^6 s^{-1}. The reverse reaction is relatively slow (kinetics in the 15 second range) in the absence of a catalyst.

This is why a carbonated drink does not instantly degas when opening the container; however it will rapidly degas in the mouth when it comes in contact with carbonic anhydrase that is contained in saliva.

The H^+/K^+ ATPase proton pump causes the exchange of a proton against a potassium ion through the membrane:

$$H^+(\text{in}) + K^+(\text{out}) + \text{ATP} + H_2O \leftrightarrow H^+(\text{out}) + K^+(\text{in}) + \text{ADP} + P_i . \qquad (1.3)$$

This pump is present in the colon, the kidney, but especially the stomach where it is particularly active: controls the secretion of protons into the gastric fluid which becomes acid. It generates a gradient of pH of more than 6 pH units: whereas the blood pH is 7.3 that of the gastric fluid is about 1.

The H^+/K^+-ATPase is located at the apical pole, i.e. luminal, of the parietal cells of the gastric mucosa. The pumps are normally inactive inside the vesicles which are activated through a signaling pathway (acetylcholine, histamine, and gastrin) to move toward the lumen. The inorganic phosphate (P_i) produced from the hydrolysis of ATP drives a conformational ($E_1 \leftrightarrow E_2$) change in the enzyme resulting release of H^+ into the highly acidic environment in exchange for extracellular K^+ ions.[5]

The H^+/K^+-ATPase is a heterodimeric protein. The α subunit of the enzyme is an ~1000-amino acid protein containing the catalytic sites and the pore that allows the transport of ions through the cell membrane. It is responsible for the hydrolysis of ATP. The β subunit is an ~300-amino acid protein with a 36-amino acid N-terminal cytoplasmic domain, a single transmembrane domain, and a highly glycosylated extracellular domain. Its function is poorly understood. The β subunit stabilizes the α subunit and is required for function of the enzyme. It also appears to contain signals that direct the heterodimer to membrane destinations within the cell, although some of these signals are subordinate to signals found in H^+/K^+ ATPase α subunit. HCl is formed when chloride ions (Cl^-) passively flow out through the Cl^- channels into the lumen to maintain electroneutrality. The source of Cl^- ions comes from a Cl^-/HCO_3^- exchanger. Blood CO_2 and H_2O produce HCO_3^- and H^+ through the enzyme carbonic

anhydrase (see above). The HCO_3^- is secreted into the interstitial fluid (which enters the blood) in exchange for Cl^- ions into the parietal cell.

The proton transport in gastric H^+/K^+-ATPase is illustrated in Figure 1.2. In the E_1 conformation, water molecules in the cytosolic medium are transported to cation binding sites 1 and 2. H^+ ions in the cytosolic medium are transported (in the form of H_3O^+) to the H_2O molecule in site 2 via the charge transfer pathway (H_3O^+-Lys-164 -Gln-161-Glu-345-H_2O). Charges of H_3O^+ in site 2 are transported to the water molecule in site 1 via the water wire and the charge transfer pathway (H_3O^+-Asn-941-Glu-797-H_2O). Finally, H_3O^+ in sites 2 and 1 are transported to the lumen during the conformational transition from E_1 to E_2.

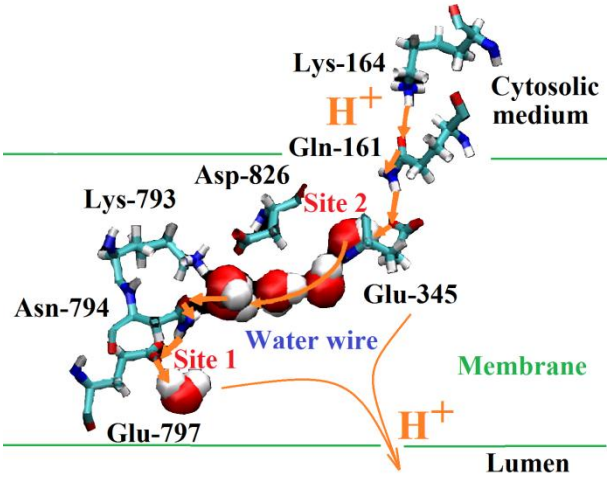

Figure 1.2 Charge transfer from Glu-345 in site 2 to Glu-797 in site 1. Charge is transferred from Glu-345 to H_2O in site 2 and then to a water wire, which transfers the charge to H_2O that is trapped by hydrogen bonds with Asp-826 or Lys-793. Then it is transferred to H_2O near Asn-794. Finally, it is transferred to Glu-797 via the charge transfer pathway (H^3O^+-Asn-794 -Glu-797). Adapted from Morii et al. 2008.

Bacteriorhodopsin relates to vertebrate rhodopsins that sense light in the retina. Although rhodopsins also contain retinal, the functions of rhodopsin and bacteriorhodopsin are different. Bacteriorhodopsin captures light energy and uses it to move protons across the membrane out of the cell.[6] The action is partitioned between two domains—the extracellular and cytoplasmic domains, separated by the photoactive retinal-lysine Schiff base. The network of protonatable amino acids and water molecules is a fundamental constituent of proton delivery pathway and its transient modifications are essential to the H^+ pumping mechanism of the bacteriorhodopsin photocycle. Following light absorption, the all-trans retinal isomerizes to a 13-cis, 15-anti configuration, which is held in a highly twisted form by constraints of the protein. Subsequent relaxation of the 13-cis form drives protein conformational changes and coupled pK_a shifts that lead to *i*) proton release from the extracellular space and *ii*) proton uptake from the cytoplasmic side (Fig. 1.3).

i) Proton release. In the extracellular domain, a proton is transferred from the protonated Schiff base of retinal-Lys216 to Asp85 within about 500 μs. Coupled to this, Arg82 moves down and away from Asp85, and a proton is transferred to the protein surface from the proton release group, formed by Glu194, Glu204 and about 4 water molecules. This proton escapes to the bulk phase on a much slower time scale, which roughly corresponds to reprotonation of the Schiff base from the cytoplasmic side. The reprotonation of the Schiff base occurs via proton transfer from Asp96 over a distance of about 11 Å, and involves the structuring of water molecules to act as a bridge between donor and acceptor. As the reprotonated Schiff base returns to its all-trans configuration, Asp85 transfers its proton to the proton release group, Arg82 recovers its original position, and the resting state is restored.

ii) Proton uptake. The proton conducting structure linking the cytoplasm to the Schiff base is assembled from scratch by structural changes that draw in water from the aqueous phase. This allows transfer of a proton from Asp96, which is protonated in the ground state; it is subsequently reprotonated from the cytoplasmic medium. These events are initiated by relaxation of the 13-cis retinylidene, which forces movement of helices F and G that opens a channel and draws water in from the bulk phase. A proton transfer pathway is established between Asp96 and the deprotonated Schiff base and, at the same time, structural changes around Asp96, including water movements, lower the pK_a of Asp96 thereby driving the proton transfer to the Schiff base. The water chain from Asp96 to the protein surface, which allows reprotonation of the acid, is completed as the inner water chain to the Schiff base is collapsing.

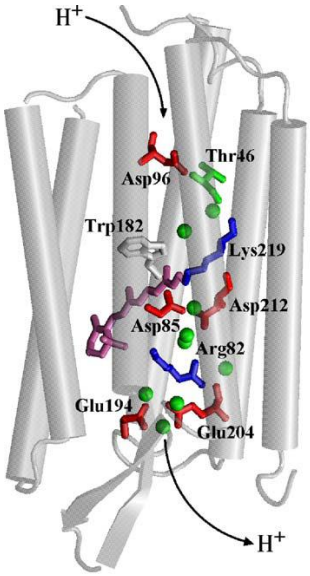

Figure 1.3 The light-adapted all-trans retinal (mauve) is covalently linked to Lys219, forming a protonated Schiff base (–HC=NH^+–). The retinal chromophore isomerizes in less than 1 ps, and the resulting strains on the protein give rise to several early intermediates. Relaxation of these strains cause deprotonation of the Schiff base to yield conformation state M_1. The proton is released to the extracellular phase. Further relaxation completes the bond rotations in M_2, which switches accessibility of the Schiff base from the extracellular to the cytoplasmic side. After this major conformational switch, the Schiff base is reprotonated by proton uptake from the cytoplasmic side. This facilitates the reisomerization back to the all-trans state. Structure file: 1c3w.pdb, at 1.55 Å.

The respiratory cytochrome oxidase catalyses oxygen reduction in cell respiration and pumps hydrogen ions simultaneously out of the mitochondrion:

$$4e^- + 8H^+(\text{in}) + O_2 \rightarrow 2H_2O + 4H^+(\text{out}). \qquad (4)$$

The overall process leads to generation of an electrical membrane potential and a pH gradient across the membrane, which may be used to form ATP by another enzyme in the same membrane.

Electron input from the respiratory chain occurs via cytochrome *c* (cyt. *c*) into the Cu_A center on the outside of the membrane (Fig. 1.4).[7] From there electrons are transferred, one at the time, via heme *a* to the binuclear heme a_3/Cu_B centre where dioxygen is reduced to water. The latter redox centers lie at a dielectric depth within the membrane. The chemistry of oxygen reduction is completed by uptake of protons from the inside of the membrane (orange arrow) into the binuclear site. A water-filled channel, the D-pathway, delivers at least 6 (and possibly 7) of the 8 protons consumed or transferred in the full turnover of cytochrome oxidase. The K-channel delivers the minority of protons to the binuclear center.

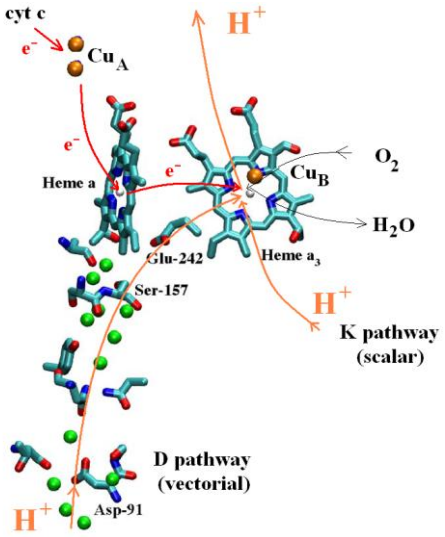

Figure 1.4 The atomic details of the D-pathway of protons in cytochrome oxidase. The path begins with an aspartic acid (Asp-91) at the mitochondrial matrix (or bacterial cell cytoplasm) side and ends at a glutamic acid (Glu-242), close to heme *a* and the binuclear center (heme a_3 and Cu_B). Waters (green) shown are crystallographic; none are present in the last 6–7 Å before Glu-242. The binuclear center is also empty of waters in the fully oxidized and reduced resting states of the enzyme. Structure file: 1v54.pdb, for fully oxidized bovine cytochrome c oxidase at 1.80 Å resolution.

The main part of the D channel is lined by several polar amino acid residues which are stabilizing the water column. The D pathway has a substantially complete hydrogen bonded chain of (crystallographic) water molecules, extending about 16 Å from a ring of three asparagines, near the entrance, up to Glu-242. However, the chain is incomplete in the last 7 Å between Ser-157 and Glu-242. Computational methods have been used to place additional waters to effectively fill the channel, up to the entrance to the central cavity between heme *a* and the binuclear center (heme a_3-Cu_B). In the central cavity, the PT path must branch in

order to deliver protons alternately to the oxygen reduction chemistry at the binuclear center, on the one hand, and the proton pumping mechanism, on the other. Neither of these paths is defined at the current level of resolution (<2 Å) and it seems likely that highly mobile water molecules are involved.

The proton transfer in the respiratory cytochrome oxidase is coupled primarily to electron transfer and not to conformational changes. Similar coupling is observed in reaction center proteins of photosynthetic organisms. Here, we will discuss the proton transfer in reaction center from photosynthetic bacteria as its relative simplicity can be utilized *i*) to understand the transfer mechanism down to atomic level and *ii*) to apply this knowledge to more sophisticated systems.

1.2 Bacterial reaction center.

The membrane bound photosynthetic reaction center proteins (RC) from purple bacteria take up protons upon light excitation and reduce quinone to quinol:

$$Q + 2\,e^- + 2\,H^+ \leftrightarrow QH_2\,. \qquad (1.5)$$

The most striking feature of the RC structure is a marked two-fold symmetry of cofactors and protein (Nobel Prize 1988, Fig. 1.5).[8,9] The RC from *Rhodobacter sphaeroides* comprises three subunits, a heterodimer of similar, but non-identical L and M subunits, and subunit H, which caps LM on the cytosolic side of the membrane. The LM dimer binds all the cofactors, while subunit H stabilizes the structure and is involved in H^+-ion uptake and transfer associated with electron transfer to the quinones.

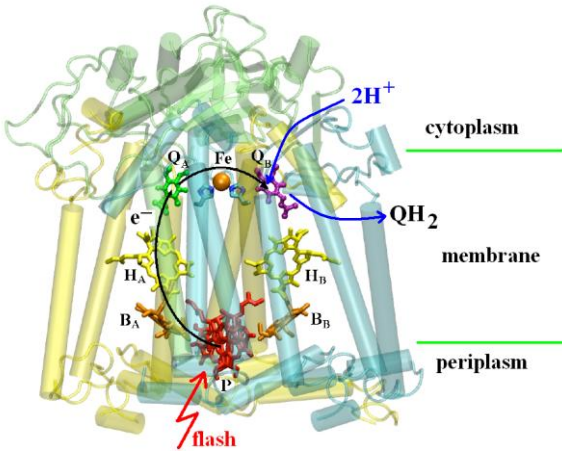

Figure 1.5 The cofactors in reaction center complex from *Rhodobacter sphaeroides* are arranged around a quasi-2-fold rotational symmetry axis, normal to the plane of the membrane and passing through the primary donor (P), the special pair dimer of bacteriochlorophylls, and a non heme iron (Fe^{2+}) midway between the two quinones Q_A and Q_B. Upon flash excitation of P, electron (e^-) transfer proceeds from P*, via the A-branch of cofactors to the secondary quinone, Q_B. By taken up $2H^+$ ions, QH_2 will be exported into the membrane. (Figure prepared in VMD.)

In spite of the evident structural symmetry, only the A cofactor branch is active in electron transfer from the primary donor, P (BChl dimer), *via* B_A ($BChl_A$) and H_A ($BPhe_A$), to the primary quinone, Q_A. The electron is then transferred across the symmetry axis to the secondary quinone, Q_B, forming a long-lived semiquinone (Q_B^-) state. A second turnover of the light-driven electron transfer, accompanied by proton uptake, fully reduces Q_B to quinol (or hydroquinone, QH_2), which unbinds and is replaced by an oxidized quinone to complete the acceptor quinone cycle (Fig. 1.6). The released quinol serves as a reductant to fuel electron transfers in other membrane-bound enzymes, resulting in an electrochemical gradient of protons across the membrane that drives the chemiosmotic processes of ATP synthesis, ion and substrate transport, reversed electron transport, and flagellar rotation.

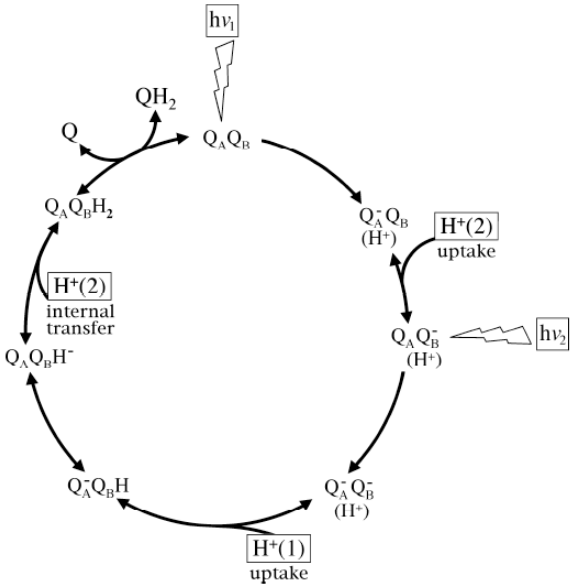

Figure 1.6 The acceptor quinone reduction cycle in RC. Following each flash, an electron is transferred to the acceptor quinones. After the first flash, the anionic semiquinone charge on Q_A and subsequently on Q_B induces pK_a changes in some ionizable amino acid residues in the Q_B binding pocket and substoichiometric amount of H^+ ions („Bohr protons") are taken up to the protein. After a second flash, the transfer of the second electron from Q_A^- only takes place after Q_B^- has been protonated (it binds $H^+(1)$ „chemical" proton). After the first proton binding, the Bohr protons provide the 2nd („chemical") proton, $H^+(2)$, which are transferred from amino acids to Q_B after the second flash.

The involvement of protons is crucial for both electron transfers to Q_B. Electron transfers between Q_A and Q_B redistribute charge within the protein dielectric, causing electrostatic responses (changes in pK_a values) in the ionizable side chains of the protein. After a single flash, proton uptake and internal transfers accompany the formation of the anionic semiquinone states ($Q_A^-Q_B \longleftrightarrow Q_A Q_B^-$). Proton affinities (p$K_a$s) are somewhat higher in the Q_B^- state, and proton uptake by the protein contributes significantly to the relative stabilization of the electron on Q_B rather than Q_A. After a second flash, the double reduction of Q_B to Q_BH_2 requires delivery of two protons to the quinone headgroup, itself. These are long range proton transfers from solution, over a distance of about 15 Å, and a cluster of ionizable residues near the secondary quinone binding site, Q_B, is known to be involved in

this delivery pathway (Fig. 1.7). However, although site directed mutations have implicated several acidic residues, the distinction between a true proton carrying activity and a role in influencing the electrostatics of other residues – or even buried water molecules - has always been difficult to make. As for acid-base catalysis in physical organic chemistry, a Brönsted relationship between kinetics and pK_a (driving force) can be established[10] similarly as the Marcus theory describes the kinetics of electron transfer (Nobel Prize 1992).[11] These works successfully identified the entry point of H^+ ions into the RC, and the midpoint of the pathway and provided significant insight into the design of proton translocating pathways which constitutes the major theme of the present study.

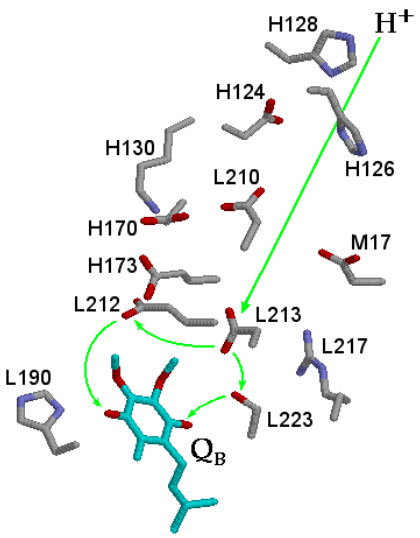

Figure 1.7 Proton delivery pathway from the aqueous cytoplasmic phase to the secondary quinone Q_B. The approximate pathway includes the proton entry site (surface histidines H126 and H128), the Q_B site acid cluster, labeled by residue number and the destination of the proton transfer, Q_B. The bucket-brigade mechanism of transfer occurs via several carboxylates, and structured water molecules where necessary to bridge the gap between remote protonatable groups. The acidic amino acids of the cluster are in strong interaction that modifies the intrinsic pK_a values of the groups significantly. The path bifurcates at AspL213 toward GluL212 and SerL223 to deliver $H^+(1)$ and $H^+(2)$ to the two carbonyls of the quinone, respectively.

1.3 Aims of the thesis

Although bacterial RCs do not carry out transmembrane proton pumping, which is characteristic of gastric H^+/K^+ ATPase, cytochrome oxidase and bacteriorhodopsin, the uptake associated with quinone reduction constitutes the first half of a proton translocating redox loop that is completed with the oxidation of quinol by the cytochrome bc_1 complex. Furthermore, H^+ transfer to the buried Q_B quinone site is over similar long distances to those that are encountered in pumping mechanisms, and the lack of gating in the RC provides a useful simplification in the study of the essential features of proton conduction pathway(s) in proteins. Indirect coupling of electron transfers to proton uptake is also seen in the reponse to the light induced perturbation of the charge distribution of the protein.

In spite of the two-fold symmetry of the RC protein, it is broken so that each separate cofactor has a non-functional, or differently functional, partner. Therefore, the RC is ideally suited for studying how protein-cofactor interactions induce unique properties in bound cofactors and substrates. We should like to capitalize on these features, using the RC from the purple photosynthetic bacterium, *Rhodobacter (Rba.) sphaeroides,* to investigate how the protein environment controls proton (and electron) transfer and tunes the functional properties of the cofactors with special interest on Q_B.

The rich sructural and functional information about the RC provides a unique (model) system for studying the intraprotein proton transport and dielectric responses of proteins. The kinetics of proton transport if it is the rate limiting step, should be sensitive to deuterization i.e. to change of H^+ ions to D^+ ions in the aqueous cytoplasmic phase and to modification of the p*K* value of the quinone at the Q_B binding site. These experiments will be carried out and we hope the results will shed some more light to the principles of electron transport coupled proton uptake in bacterial RC.

2. MATERIALS AND METHODS

2.1 Chemicals and reagents.

UQ_{10} ($ubiquinone_{10}$, UQ-50, 2,3-dimethoxy-5-methyl-6-decaisoprenyl-1,4-benzoquinone) was purchased from Sigma. RQ (rhodoquinone; 2-amino-3-methoxy-6-methyl-5-decaisoprenyl-1,4-benzoquinone) was obtained from *Rhodospirillum rubrum* grown photosynthetically under anaerobic conditions. Separation of RQ from the quinone extractions was performed using preparative TLC plates. The concentration of RQ in ethanol was determined from optical absorption coefficient of 1 $mM^{-1} \cdot cm^{-1}$ at 500 nm. Ferrocene (Eastman Kodak), ethyl ferrocene, cytochrome-*c* (horse heart grade VI) and DAD (diaminodurene) were used to reduce the oxidized dimer (P). Ethanolic solutions of the electron donors ferrocene and DAD were prepared fresh prior use. The water soluble cytochrome-*c* was reduced (>95%) by hydrogen gas on platinum black and filtered (0.2 μm pore size acetate filter). The interquinone electron transfer inhibitors terbutryne and stigmatellin (Chem. Service) were solubilized in ethanol.

The experiments were carried out in mixture (2-2 mM) of buffers whose pK_a values were close to the pH value of the solution. The buffer mix contained the following buffers: 2-(N-morpholino)-ethanesulfonic acid (MES; Sigma), succinate or citric acid (Calbiochem) between pH 4.5 and pH 6.5; 1,3-bis[tris(hydroxymethyl) methylamino]propane (Bis-Tris propane; Sigma) between pH 6.3 and pH 9.5; Tris–HCl (Sigma) between pH 7.5 and pH 9.0; 3-(cyclohexylamino) propanesulfonic acid (CAPS; Calbiochem) above pH 9.5. All pH(D) measurements were carried out by a glass electrode (Radiometer, Copenhagen, Denmark) that had been standardized with conventional buffer mixtures (in H_2O) at pH 7.0 and 11.0 (alkaline range) or 4.0 (acidic range) at room temperature. In heavy water (D_2O) experiments, the pD value was derived as pD = apparent pH + 0.40, which included the correction D^+-ion concentration for the glass electrode solvent isotope artifact. The "apparent pH" means the actual pH meter reading. Acid HCl (deuterated acid, DCl) and base NaOH (deuterated base, NaOD) were used for pH (pD) adjustment.

2.2 Cell growth and isolation and preparation of photosynthetic reaction centers

The details of the molecular biological techniques in generating *Rhodobacter (Rba.) sphaeroides* mutants, methods of cell growth and RC isolation have been well documen-

ted.[12-15] The RC isolation was greatly simplified by using His-tagged proteins.[16] All mutant RCs used here were expressed in *Rba sphaeroides*. Depending on the particular mutation, the mode of bacteria growth varied between anaerobic, semiaerobic and aerobic conditions. In all cases, the basis of the growth medium was Sistrom's minimal medium but with malate used as the carbon source, in place of succinate. RCs referred to as "wild type" in these studies are from the 2.4.1 strain with a polyhistidine tag inserted at the C-terminus of the M-subunit. The gene encoding the M subunit, *pufM*, was cloned into the phage plasmid M13 and histidine codons were inserted via the oligonucleotide insertion method. The *puf* operon was reassembled in a pRK plasmid and inserted into a strain of 2.4.1, in which the *pufL* and *pufM* genes on the chromosome were deleted, called ΔLM1.1. The plasmid carrying the RC also contained the gene for tetracycline resistance. These cells were grown in malate Sistrom's medium containing 2 μg/ml of tetracycline in 1 liter bottles covered with red filters (to protect tetracycline from photodegradation). The cells were grown photosynthetically and anaerobically under an array of 40 watt incandescent light bulbs. For large-scale growth, the 1 liter stock is transferred to 12 liter carboys containing no antibiotic. When inoculated with this concentration of cells, there were few contamination issues in the final cell harvest.

The pRK plasmid containing specific mutations to the L and M subunits was transferred into a *Rba. sphaeroides* background containing no light harvesting complex (courtesy of Dr. E. Takahashi). These cells grow very inefficiently under photosynthetic conditions, as used for the His-tagged 2.4.1 strain. However, *Rba. sphaeroides* is also capable of growing aerobically in the absence of light and these mutants were grown in Sistrom's medium supplemented with yeast extract, shaking, in the dark. Pigmentation in *Rba. sphaeroides*, including RC biosynthesis, is under oxygen control and can be induced under semi-aerobic conditions. Initially, therefore, 450 ml of Sistrom's medium supplemented with 0.1% yeast extract was inoculated with cell stock. At the mid logarithmic growth stage, (typically ~3 days after initial inoculation) an additional 1 liter of Sistrom's medium supplemented with 0.6% yeast extract was added to the flasks and, the rate of shaking was reduced from 300 rpm by increments of ~50 rpm daily to a final rate of ~100 rpm, to maximize RC expression. Strains of *Rba. sphaeroides* containing RC mutations carried a resistance to both tetracycline and kanamycin. The Sistrom's medium typically contained

both antibiotics (tetracycline at 2 μg/ml and kanamycin at 25 μg/ml) at the initial stage of growth, but only tetracycline was present in the additional 1 liter of medium.

When it appeared that the cultures had reached a maximum density (estimated from the color) the cells were harvested from the carboys, bottles or flasks by a combination of filtration and centrifugation. The His-tagged 2.4.1 strain, grown phototrophically in bottles or carboys, typically contained very few large particulates and most of the liquid medium could be easily removed by filtration. The cells could then be collected by centrifugation at 8000 rpm in 250 ml bottles. However, semi-aerobic growth would sometimes generate a large amount of precipitate that could clog the filter. Additionally, there was always some risk of cell loss when concentrating by filtration. Therefore, despite the cost in time, it was prudent to collect these cells exclusively by centrifugation.

Regardless of whether cells were frozen post collection or used immediately, the cell pellets were combined with buffer containing 100 mM NaCl, 10 mM Tris at pH 7.9, and 50 μM EDTA, and stirred at 4 °C overnight. The buffer maintains ionic strength and chelates divalent ions, thereby inhibiting some protease activity. Cells were washed and recollected via centrifugation two times (or more if the supernatant is still very cloudy). Following the final wash, cells were suspended in a volume of buffer at ~0.5 g/ml, and were broken by passage through a French press at 18,000 psi (pounds per squere inch). To maximize the yield of breakage, the suspension was routinely run through the French press twice. Unbroken cells were separated by centrifugation at 15,000 rpm for 20 minutes. If the quantity of unbroken cells was substantial, the pellet was resuspended in buffer and French pressed again.

The result of crushing cells in the French press is the formation of chromatophores. These are small vesicles reformed after disruption of the cell membrane folds that contain the RCs and other membrane proteins. In the isolation of RCs that do not contain the poly-his tag, the chromatophores would be purified by centrifugation to remove some soluble proteins. However, this step is not required for His-tagged RCs and the membrane proteins were immediately solubilized by addition of the detergent lauryldimethylamine-N-oxide (LDAO). In order to maximize the efficiency of detergent solubilization, the broken cells were diluted in buffer prior to the addition of 1% LDAO. The degree of dilution is somewhat arbitrary but, for a typical preparation with less than 100 g of starting material, the total volume was increased to 290 ml buffer, which conveniently fits into twelve 25 ml ultracentrifuge tubes

after the addition of 10 ml of LDAO (1% total LDAO from 30% stock). Because of the selectivity of the His-tag, there was no need to take care to not over solubilize the membranes with detergent, as in previously published procedures. To ensure maximum solubilization, the suspension was stirred at room temperature for one hour in buffer with 1% LDAO. Solubilized proteins were separated from insoluble proteins and aggregates by centrifugation at 40,000 rpm for 90 minutes – solubilized RCs were in the supernatant.

After solubilization, the His-tag was used to purify the RCs. The supernatant following 40,000 rpm centrifugation (approximately 250 ml for a prep smaller than 100 g) was diluted to a total volume of 500 ml in buffer containing 100 mM NaCl, 10 mM Tris at pH 7.9, 10 μM EDTA, 0.045% LDAO, and 4 mM imidazole (TL045 + 4 mM imidazole). This solution was loaded onto a column of Ni-NTA (Qiagen) resin at a rate as slow as could be generated with the valve on the gravity-fed column, typically taking up to 12 hours (overnight), in order to get the majority of His-tagged protein to adhere to the nickel column.

Washing the Ni-NTA column with approximately 500 ml of TL045 buffer provided the best compromise between removing as much unwanted cell residue and protein from the column as possible, yet preventing RCs from leaking off the column or any denaturation. The RCs were removed from the Ni-NTA column with an elution buffer comprised of TL045 and 150 mM imidazole. In order to ensure that the RCs are eluted from the column at the highest possible concentration, the flow rate was set as slow as was manageable in the gravity fed column.

5 ml fractions were collected from the column and assayed for RC concentration. RC concentration is based on the extinction coefficient at 802 nm of 0.288 μM^{-1} cm^{-1}. A typical 2.4.1 RC isolation, starting with 100 g of cells, yields at least two 5 ml fractions with a concentration of ~50 μM. The yield of high concentration fractions from mutant RCs grown semi-aerobically was highly variable, but seemed to correlate to the quantity of RCs expressed during cell growth. It was very unlikely to produce a single high concentration 5 ml fraction in preparations starting with less than 50 g of cells. Purity of the RCs was assayed via the ratio of the 802 nm absorption versus the typical tryptophan 280 nm protein absorption. A 280:802 ratio of approximately 1.2 is considered to be very pure. However, samples of 280:802 ratios closer to 1.4-1.6 have been frequently used and produced satisfactory results.

The reason for this is unclear, but it is possible that extensive purification of RCs removes lipids from the sample that stabilize the RC throughout the cleaning procedure and storage.

While the data presented in this thesis are nearly exclusively from His-tagged RCs, all methods were also tested with the wild type "Ga" or carotenoidless strain "R26". All RCs showed similar spectroscopic properties and His-tagged RCs were routinely used due to the simplicity of isolation.

2.3 RC sample analysis: steady state and kinetic absorption measurements

The pigments present in RCs make UV and visible light spectroscopy useful in analyzing isolated RCs (Fig. 2.1).

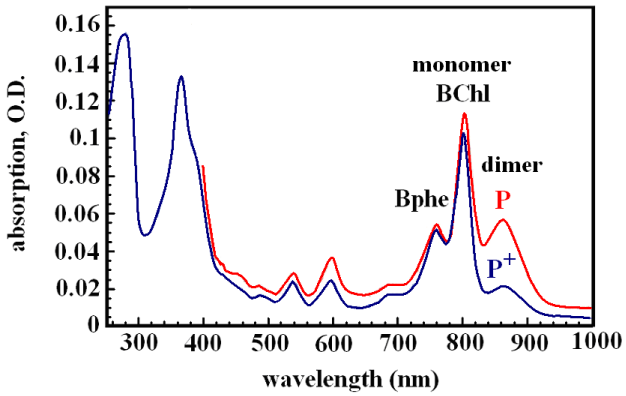

Figure 2.1 The steady state optical spectrum of a typical RC fraction after purification (red). The 755 nm peak is ~50% of the 802 nm peak. The 860 nm peak in the blue trace shows the bleaching that is often observed due to light activation from the measuring beam. The red trace shows the spectrum with dithionite added to fully reduce the sample.

RCs from *Rba. sphaeroides* have three characteristic peaks between 700 and 900 nm due to light absorption by the bacteriopheophytin and bacteriochlorophyll. The peak at 860 nm is readily bleached and largely disappears when the primary donor is oxidized. A reducing agent such as Na-dithionite, ascorbate or ferrocene can be added to the cuvette to reduce P and maximize intensity at 860 nm. The 802 nm peak is routinely used to measure the concentration of RC samples and the ratio of this peak to the peak at 280 nm (tryptophan absorption) is used to determine RC purity. However, the three peaks must be viewed as a whole. Free bacteriochlorophyll dissociated from light harvesting complex or degraded RCs can contaminate the 755 and 802 nm peaks causing them to be artificially high, and intact light harvesting complexes can distort the 802 and 860 nm peaks If the ratio of peak intensities isn't correct, it is likely the concentration and purity calculated from the intensity of the 802 nm peak will be inaccurate.

Measuring the rate of the $P^+Q^- \rightarrow$ PQ back reaction can provide insight into the kinetics and relative energetics of the acceptor quinones in the RC. The rate of this reaction

reflects the equilibrium between Q_A^- and Q_B^- and changes in the measured rate can be related to changes in the free energy difference between the two quinones. The back reaction is measured by flash spectroscopy at 430 nm and the rate is expected to be on the order of 1 s^{-1} for RCs with active Q_B vs. 0.1 s for RCs with Q_A only. Analysis of the kinetics is done by fitting the trace to a biexponential decay. The fast component is attributable to relaxation of $P^+Q_A^-$ in RCs lacking Q_B activity. Introducing an inhibitor (e.g., 100 μM terbutryn) to block electron transfer to Q_B reveals this component. Figure 2.2 shows a typical measurement. These samples show a charge recombination rate on the order of 1.3 s^{-1}, which is typical for wild type RC.

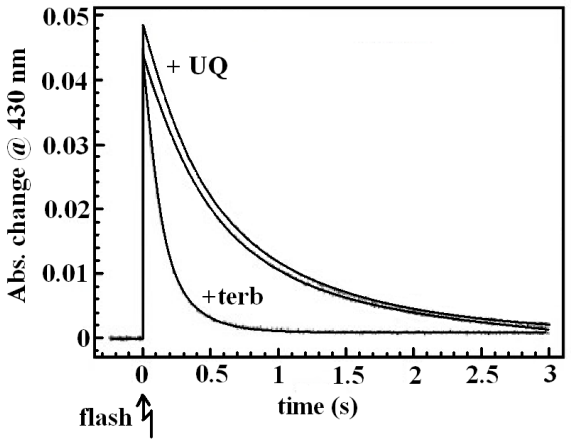

Figure 2.2 The back reaction in wild type RC in a buffer containing 10 mM Tris at pH 8, 2.5 mM KCl and 0.002% LDAO. The two slower traces represent samples with no additional quinone added after the preparation (lower) and with an additional 50 μM ubiquinone-10 (upper). The fast trace is from RCs in the presence of the inhibitor turbutryn to block electron transfer to Q_B. The recombination rate constants of the fast and slow traces are 10 s^{-1} and 1.3 s^{-1}, respectively.

The rate constants of the second electron transfer to Q_B^-, $k^{(2)}_{AB}$ were determined by monitoring the decay of semiquinone absorbances (Q_A^- and Q_B^-) at wavelength 450 nm following a second saturating flash in RC solution containing exogenous reductants to re-reduce the oxidized dimer P^+ before the second flash (Fig. 2.3).

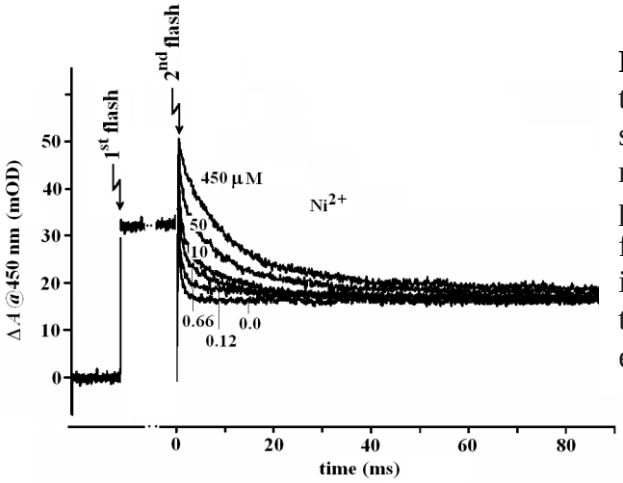

Figure 2.3 Kinetics of the second electron transfer followed by the disappearence of the semiquinones Q_A^- and Q_B^- monitored at 450 nm after the second saturating flash in the presence of external electron donor, ferrocence, to P^+. The divalent cation, Ni^{2+}, inhibits the 2nd electron transfer by blocking the proton uptake of the RC at the proton entry point.

Depending on the magnitude of $k^{(2)}_{AB}$, different donors were applied to reduce P^+: mammalian cytochrome *c* or cytochrome c_2 (fast donation) and various forms of ferrocene (slow donation at low (2-10 μM) concentrations and fast donation at high (400 μM) concentration). With the use of different donors, their disadvantages were tried to minimize. A small fraction of cytochrome c^{2+} under our conditions did follow a relatively slow photo-oxidation (in the range of several hundreds of microseconds) after the second flash, and it could have kinetic contribution to the observed absorption change at 450 nm. To avoid the overlap in the (sub)millisecond range, ferrocene, a much slower donor than the cytochrome c^{2+} was also applied. Although the redox changes of ferrocene did not have contribution in this optical range, the observed kinetics included the large absorption change from P/P^+ and its separation from that of Q/Q^- needed careful multiexponential peeling of the traces carried out by Marquardt's least square method.

3. THE RATE OF SECOND ELECTRON TRANSFER TO Q_B^- IN BACTERIAL REACTION CENTER OF IMPAIRED PROTON DELIVERY SHOWS HYDROGEN-ISOTOPE EFFECT

3.1 Background and inspiration

Proton transfer reactions of crucial significance in biology need well defined atomic structure, substantial energetic constraints and, in many cases, are coupled to conformation changes or electron transfer. In photosynthetic reaction center (RC) from purple bacteria, the proton coupled electron transfer is evoked by two subsequent saturating flashes and results in full reduction of quinone (Q) at the secondary quinone binding site Q_B: $Q + 2e^- + 2H^+ \rightarrow QH_2$. The same proton path, formed by acidic cluster around Q_B is used to deliver protons both on the first and on the second electron transfers (Fig. 3.1).

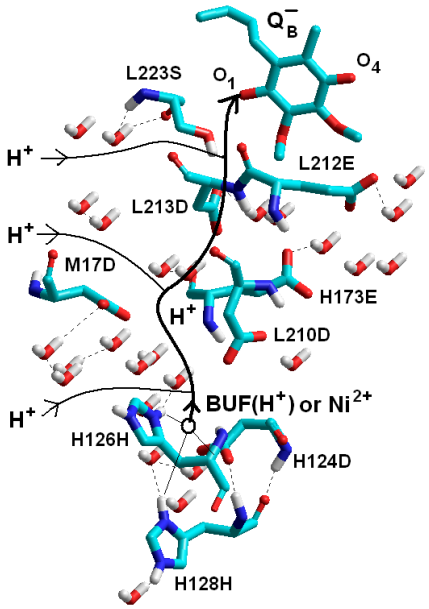

Figure 3.1 Key protonatable amino acids and water molecules of the proton delivery pathway from the proton entry point BUF(H^+) to Q_B^- semiquinone after the second flash in native RC of *Rba. sphaeroides*. The proton transport is severely hindered by ligation of bivalent transition metal ions (e.g. Ni^{2+}) to the H126H/H128H/H124D cluster or by replacement of the protonatable amino acids to nonprotonatable residues by single (or double) mutations. The alternative (by-pass) proton pathways are connected to the main pathway above the deletion sites. The structure was taken from Brookhaven Protein Databank 3I4D (www.rcsb.org).

The nature of the proton accepting group(s), however, is quite different. On the first flash, the protons are accepted by an array of ionizable residues in the cluster as their pK_a values increase in response to the Q_B^- formation. On the second flash, the proton is trapped at any pH by Q_B^- itself. The rate of the $Q_A^-Q_B^- + H^+ \rightarrow Q_AQ_BH^-$ second electron transfer depends on the free energy gap $\Delta G_{AB}^{(2)}$, as has been shown by driving force assay using RC preparations with Q_A replaced by low-potential quinines. This finding has been interpreted as an evidence of a fast, non-rate-limiting protonation of a semiquinone anion ($Q_B^- + H^+ \rightarrow Q_BH$) followed by a rate-limiting nonadiabatic ET reaction ($Q_BH \rightarrow Q_BH^-$) with rate constant $k_{et}^{(2)}$ (Fig. 3.2).

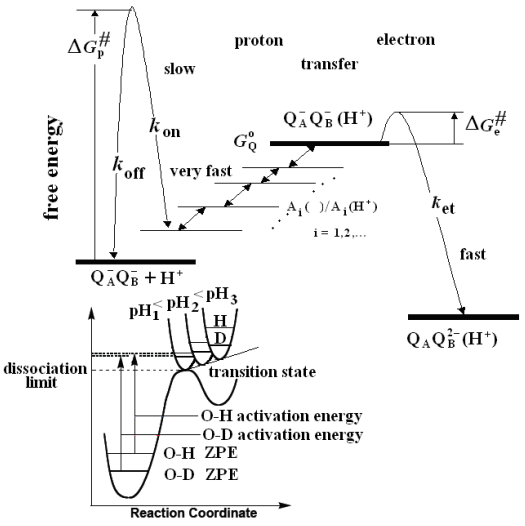

Figure 3.2 Proton coupled second ET in bacterial RC. The fast interquinone ET (k_{et}) is proceded by faster (WT) or slower (PT variants) proton equilibration with Q_B^-. The rate limiting step of proton delivery to Q_B^- is attributed to enhanced proton activation energy ($\Delta G_p^{\#}$) with k_{on} and k_{off} forward and back PT rate constants, respectively. Depending on mutations and ways of impedence in the proton pathway, the bottle neck can occur in different locations (amino acids, A_i) of the proton delivery network. Kinetic isotope effect is attributed to difference of the zero point energies that can show pH-dependence. Notations: G^o_Q – standard free energy level of semiquinone at Q_B, A_i – intermediate protonatable residue (amino acid or water) in the chain and ZPE – zero point energy of O-H(D) vibration.

Thus, the 2nd electron transfer proceeds with an observed rate of

$$k_{AB}^{(2)} = k_{et}^{(2)} \cdot f(Q_BH), \qquad (3.1)$$

where $f(Q_BH)$ is the fraction of the semiquinone in the protonated state.[17,18]

In contrast to the first electron transfer, there is no conformational control on the second electron transfer. It is not surprising, because both Q_B- and the ubiquinol-anion Q_BH^- are likely to be fixed in similar positions. However, the contribution of the protonic relaxation to the kinetics of the 2nd electron transfer is an open question. Due to the low pK_a value of the Q_B^-/Q_BH couple, the absence of a notable protonic relaxation can be expected in wild type and in mutants where the electron transfer is the rate limiting step. On the other hand, in mutants of PT limitation, the rate becomes independent of $\Delta G_{AB}^{(2)}$ and thereby the proton relaxation control over the second electron transfer might be imposed.

The recognition of protonic relaxation modes could be facilitated by the notion that the protonic component should depend on the H/D isotope substitution as shown below by two examples: 1) The slow (1–30 μs) phase of the reduction of the photo-oxidized primary donor of the photosystem II ($P680^+$) by a redox-active tyrosine Y_Z is sensitive to the H/D substitution and has been attributed to the protonic relaxation. 2) The two hydrogen-bonded protons associated with Q_A of reaction centers from *Rba. sphaeroides* can be exchanged with deuterons from solvent D_2O. The rate of $P^+Q_A^- \rightarrow PQ_A$ electron-transfer, k_{PA} was found to increase slightly with deuterium exchange up to a maximum $k_{PA}(D^+)/k_{PA}(H^+) = 1.06$. The

solvent isotope effect indicates that these protons play a role in the vibronic coupling associated with electron transfer of charge recombination.

There seems to be great potential in H/D exchange experiments while light-induced proton binding/unbinding is taking place in bacterial RC. Incubation in D_2O caused pH (pD)-dependent slowing of the H^+/D^+ binding rate after the first flash.[19] A maximum isotope effect of the apparent proton binding rate constant $k_{on}(H)/k_{on}(D) = 3.0$ was found. It is worth to carry out similar isotope measurements with the 2nd ET of various proton transfer RC variants. These RCs impede the normal fast function of the bucket brigade mechanism of PT at well defined locations: native RC treated with divalent metal ions at the proton entry point, L210DN/M17DN double mutation between L210D and M17D and L213DN single mutation at L213 close (< 5Å) to Q_B. The proton delivery with significantly increased free energy of activation will be the bottle neck of the observed 2nd ET (Fig. 3.2). The proton equilibrium partitioning (see Eq. (3.1)), and therefore the fraction of protonated sites of Q_B^- may be affected by H/D exchange (equilibrium isotope effect). Additionally, if proton pathways are limited by bond-breaking steps, the observed rate will be sensitive to deuteration of the RC (kinetic isotope effect). These effects can be used to elucidate the PT mechanisms including rate limiting steps, transition states and alternate pathways.

3.2 Results

Rate of second electron transfer, $k^{(2)}_{AB}$ and operational pK_a of Q_B^-/Q_BH

The proton-coupled ET rate $k^{(2)}_{AB}$ ($Q_A^-Q_B^- + H^+ \rightarrow Q_AQ_BH^-$) was measured by monitoring the absorption changes at 450 nm due to the disappearance of two (Q_A^- and Q_B^-) semiquinones after the second saturating flash in the presence of an exogenous donor. The donor was selected to make the electron donation to the RC either faster (cytochrome *c*) or slower (various ferrocene compounds at low concentrations) than the second ET because of kinetic separation of the second ET from P^+ donation (cyt c^{2+} $P^+ \rightarrow$ cyt c^{3+} P) and/or elimination of the charge recombination ($P^+Q_A^-Q_B^- \rightarrow PQ_AQ_B^-$). The rate $k^{(2)}_{AB}$ measured in native RC was not greatly affected in L210DN, M17DN and H173EQ electron transfer mutants (Fig. 3.3a). The decrease from the native value was small (about 3-fold) in L210DN and M17DN mutants but significantly larger (about 200-fold) in H173EQ mutant. In contrast, the PT mutants (L213DN single mutant and L210DN/M17DN double mutant together with

native RC poisoned by transient bimetal ions) show much larger (up to 4 orders of magnitude) decrease relative to that of the native value (Fig. 3.3b) in nice agreement with earlier measurements.[20]

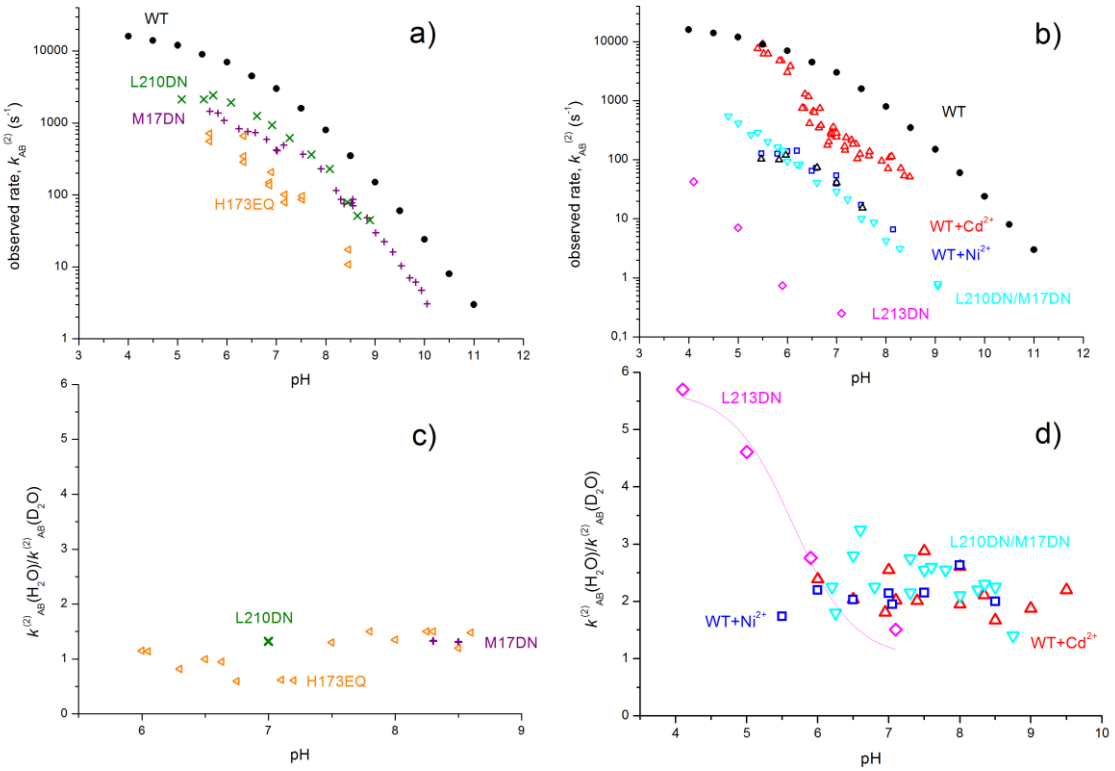

Figure 3.3 pH dependence of the observed rate constants ($k^{(2)}_{AB}$, panels *a* and *b*) and solvent isotope effect ($k^{(2)}_{AB}$(H)/ $k^{(2)}_{AB}$(D), panels *c* and *d*) of second ET for various RC strains of ET (panels *a* and *c*) and PT (panels *b* and *d*) limitation. The pH-dependence of the isotope effect in the L213DN mutant is approximated by a Henderson-Hasselbalch function with amplitude of 5.7 and pK = 5.65 (panel *d*). Symbols: ● (WT), □ (WT+Ni^{2+}), Δ (WT+Cd^{2+}), ◊ (L213DN), × (L210DN), + (M17DN), ◁ (H173EQ) and ▽ (L210DN/M17DN).
Conditions: 1.0 – 4.0 μM RC, 0.02% Triton X-100, 40 μM UQ_{10}, 5 mM KCl, T = 293 K, 2-2 mM buffer mix, 20 μM cyt c^{2+} or 2-8 μM/300-500 μM (ethyl-, methyl)ferrocene (depending on $k^{(2)}_{AB}$, see Material and Methods) and 100 μM $CdCl_2$ or 1 mM $NiCl_2$ in metal treated WT RC.

The pH profiles of $k^{(2)}_{AB}$ of electron and proton transfer limited RCs show marked differences. The logarithms of $k^{(2)}_{AB}$ of PT variants display (with good approximation) linear pH dependence throughout the entire pH range from 4 to 9. The electron transfer RC mutants, however, describe monotonously decreasing function with gradually increasing slope: it is small in the acidic pH range, becomes more pronounced in the neutral and slightly alkaline

pH regions and approaches the limiting value of –1 in the highly alkaline pH range. The measured rates are pH-dependent because the population of Q_BH is pH dependent. In native (and other ET mutant) RCs, the rate limiting ET is preceded by very fast proton equilibrium $Q_A^-Q_B^- + H^+ \leftrightarrow Q_A^- Q_BH$. In the simplest case, the protonated fraction, $f(Q_BH)$ follows the Henderson-Hasselbalch equation, but the complex electrostatics of the protein interior results in an extended pH-dependence that can be formally approximated by a Henderson-Hasselbalch function with pH-dependent (operational) pK_a values:

$$f(\mathrm{Q_BH}) = \frac{10^{pK_a(pH)-pH}}{1+10^{pK_a(pH)-pH}} \tag{3.2}$$

By insertion of Eq. (3.2) into Eq. (3.1) and taking $k^{(2)}_{et} = 1\cdot10^6$ s^{-1}, the pH-dependence of the operational pK_a of Q_BH can be derived from the measured $k^{(2)}_{AB}$ values in wild type and some other ET mutant RCs (Fig. 3.4).

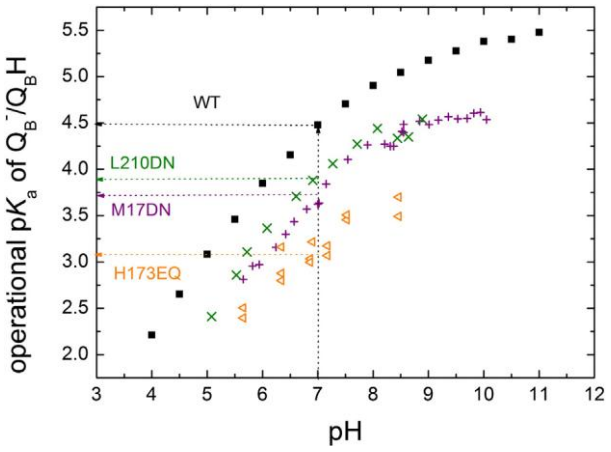

Figure 3.4 pH-dependence of the operational pK_a values of Q_B^-/Q_BH calculated from the rate constants of the second electron transfer limited by ET (Fig. 3.3a) according to Eqs. (3.1) and (3.2). The rate of intrinsic electron transfer was taken $k_{et}^{(2)} = 1\cdot10^6$ s^{-1}. The operational pK_a values for some electron transfer mutants at pH 7 are indicated by arrows.

At pH 7, the operational pK_a values of the native semiubiquinone-10 are 4.5 (WT), 3.9 (L210DN), 3.7 (M17DN) and 3.1 (H173EQ) which are in good accordance with values obtained from temperature dependence of the second ET.[21] In absence of any electrostatic interactions between RC and Q_B^-, one would expect a constant pK_a value throughout the pH scale. This is clearly not the case. In the acidic pH range, the increase of the operational pK_a is steep (close to 1) and levels off in the alkaline pH region.

Solvent isotope effect of $k^{(2)}_{AB}$

The solvent isotope effect was studied by comparison of $k^{(2)}_{AB}$ measured in water (H_2O) and in heavy water (D_2O) under otherwise identical conditions. The proton → deuterium exchange in the protein was initiated at t = 0 by injecting the concentrated stock of RC into D_2O (Fig. 3.5).

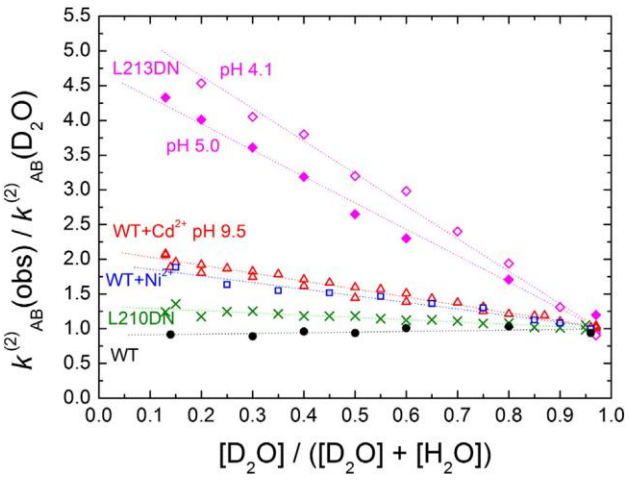

Figure 3.5 Solvent isotope effect of $k^{(2)}_{AB}$ of WT RC (●), L210DN (x) and proton transfer variants WT+Ni^{2+} (□), WT+Cd^{2+} (Δ) and L213DN (◊, pH 4.1 and ♦, pH 5.0) in mixture of water (H_2O) and heavy water (D_2O). Proton ↔ deuterium exchange was carried out by repeated dilution of the RC stock solutions in H_2O or D_2O by D_2O or H_2O, respectively.

The isotope shift due to deuterization of the protonatable groups in the proton delivery pathway occurred "promptly" (i.e., within 2 h, [23]) and no further changes in the rate of the second ET were observed after prolonged (24 h) incubation in D_2O. The reaction mixture was split into two equal parts and they were diluted repeatedly by D_2O and H_2O, respectively. The concentration of the ingradients (detergent, salt and buffers) remained unchanged during the dilution. The D_2O content of the sample could be change between >95% and ~ 10% at the beginning and at the end of the dilution, respectively. The dilution carried out in the reverse direction offered similar results: the observed $k^{(2)}_{AB}$ decreased in a linear manner with increase of the D_2O content of the solvent. The intersections of the best fit straight line to the data at 0% D_2O (H) and 100% D_2O (D) deliver $k^{(2)}_{AB}$(H) and $k^{(2)}_{AB}$(D) and their ratio offers directly the kinetic solvent isotope effect.

As expected, there is no solvent isotope effect in native RC (Fig. 3.5) and the ET mutants show also negligible isotope effect, e.g. 1.11±0.33 for the H173EQ mutant (Fig. 3.3c). In contrast to the wild type and ET mutants, the PT variants demonstrate marked but not very large solvent isotope effects (Fig. 3.3d): 2.11±0.26 (WT+Ni^{2+}), 2.16±0.35 (WT+Cd^{2+}) and 2.34±0.44 (L210DN/M17DN double mutant) and do not depend on pH. The L213DN mutant show unique features: in the strongly acidic pH range (pH ≈ 4), the solvent isotope effect is

large (≈ 6) which drops progressively upon increase of the pH to a low (≈ 1.4) value that approaches the isotope effect of proton/deuterium diffusion in aqueous solution.

Temperature-dependence of $k^{(2)}_{AB}$ in proton transfer variants

The observed large change of the rate of the second ET in different RC variants can be attributed to change of the free energy of activation ($\Delta G^{\#}$). Higher rate corresponds to higher free energy change of activation and the correlation is logarithmic. According to the transition state theory,

$$k_{AB}^{(2)} = \frac{k_B T}{h} \exp\left(\frac{-\Delta G^{\#}}{R\,T} \right), \qquad (3.3)$$

where T is the temperature, h denotes the Planck's constant and k_B and R are the Boltzmann factor and universal gas constant, respectively. The function of $\ln\left(\frac{k_{AB}^2 \cdot h}{k_B T} \right)$ vs. $1/T$ should give a straight line of slope (= $-\Delta H^{\#}/R$) characteristic to the change of activation enthalpy, $\Delta H^{\#}$ and intersection (= $-\Delta S^{\#}/R$) characteristic to the change of activation entropy, $\Delta S^{\#}$ (Eyring plot). The observed activation parameters correspond to the rate limiting step of $k^{(2)}_{AB}$. As the second ET is a combination of electron and proton transfer reactions, the observed activation may correspond to either electron or proton reactions. In PT mutants, the measured change of activation free energy (enthalpy and entropy) relate to the bottle neck of the series of protonation steps in the proton delivery pathway.

Figure 3.6 demonstrates the Eyring plot of the PT variant of the L210DN/M17DN double mutant in the physiological temperature range. The measured points fit to a straight line with $\Delta G^{\#}$ = 15.6 kcal/mol, $\Delta H^{\#}$ = 10.1 kcal/mol and $T \cdot \Delta S^{\#}$ = –5.52 kcal/mol activation free energy, enthalpy and entropic energy, respectively, at room temperature and pH 7.5. As the PT is the rate limiting step of $k^{(2)}_{AB}$, one can expect effect of proton → deuterium exchange in the protein. Indeed, significant modification of the activation parameters is observed after deuteration of the sample. Somewhat less, but still considerable changes can be seen upon isotope (deuterium) exchange in other protonation RC variants investigated in this study: WT+Cd^{2+}, WT+Ni^{2+} and L213DN (Fig. 3.7).

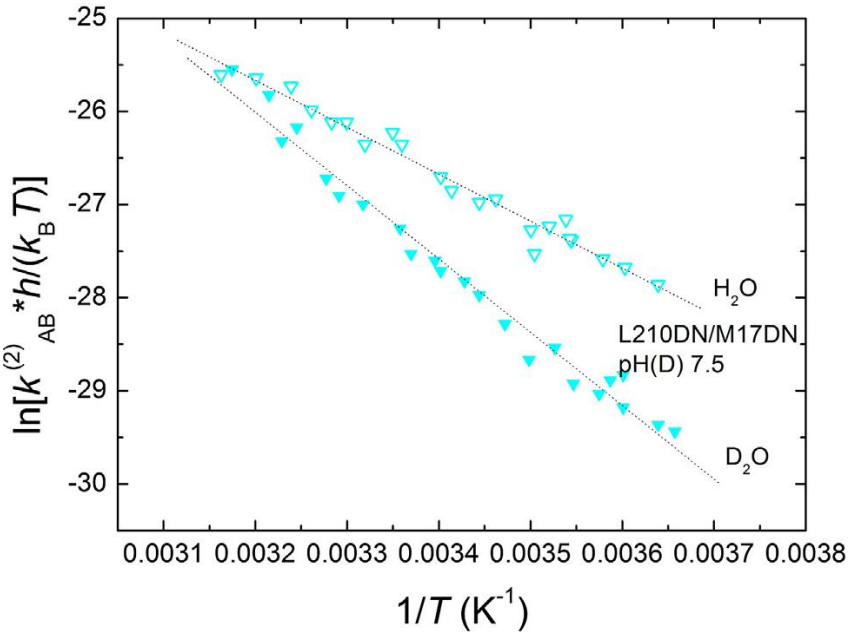

Figure 3.6 Temperature dependence (Eyring plot) of the rates of the second ET ($k^{(2)}_{AB}$) in RC of double mutant L210DN/M17DN in water (H_2O, ∇) and heavy water (D_2O, ▼). Activation enthalpy change (slope): $\Delta H^{\#}$ = 10.1 kcal/mol (H_2O) and 15.6 kcal/mol (D_2O), activation entropy change (intersection): $T{\cdot}\Delta S^{\#}$ = –5.5 kcal/mol (H_2O) and –0.47 kcal/mol (D_2O) and activation free energy change: $\Delta G^{\#}$ = 15.6 kcal/mol (H_2O) and 16.1 kcal/mol (D_2O).
Conditions: 1.0 µM RC, 0.02% Triton X-100, 40 µM UQ_{10}, 5 mM NaCl, 2.5 mM Mops, 2.5 mM Tris, pH(D) 7.50 and 300 µM ethyl ferrocene. Notations: h – Planck's constant and $k_B T$ – Boltzmann term.

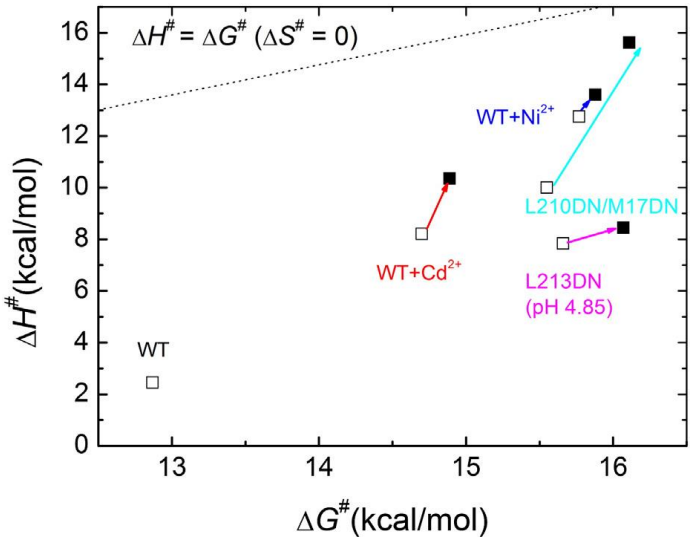

Figure 3.7 Eyring (transition state theory) activation parameters ($\Delta H^{\#}$ vs. $\Delta G^{\#}$) of the second electron transfer of RCs of proton transfer variants (open symbols) and transitions due to deuteration (closed symbols). The states of no entropic changes are indicated by a

In all cases, the activation parameters of the free energy and enthalpy shift to larger values and, in compensation, the entropic contributions become smaller after deuteration. As expected, the WT RC has much less activation free energy and shows no isotope effect.

3.3 Discussion

In native RC, the second interquinone electron transfer occurs after very fast partial proton uptake by Q_B^-. In various proton transfer variants used in this study the proton delivery to Q_B^- can be slowed down dramatically and will become the rate determining step of the electron transfer. Under these conditions, the exchange of hydrogen to deuterium in solvent and RCs imposes reversible isotope effects of $k^{(2)}_{AB}$: upon dilution in H_2O and ultrafiltration of the RCs, the rate can be restored to a value typically measured in H_2O. The discussion will extend on the origin, magnitude and pH dependence of the observed isotope effect found in the various RC variants and will cover the structural and energetic aspects of the possible alternative proton delivery pathways to Q_B^-.

The origin of solvent isotope effect of $k^{(2)}_{AB}$ in RC.

The observed rate of the second electron transfer is the combination of the rates of protonation of the slowest step (the sum of binding and unbinding rates: $k_p = k_{on} + k_{off}$) and the interquinone electron transfer, k_{et}. According to the reaction scheme in Fig. 3.2,

$$k^{(2)}_{AB} = \frac{k_{on} + k_{off} + k_{et} - \sqrt{(k_{on} + k_{off} + k_{et})^2 - 4 \cdot k_{on} \cdot k_{et}}}{2}. \qquad (3.4)$$

In electron transfer limit ($k_p >> k_{et}$), we obtain $k^{(2)}_{AB} = k_{et}/(1+k_{off}/k_{on})$ that is equivalent with Eq. (3.1). No isotope effect is expected unless k_{off}/k_{on} that relates to the proton dissociation constant of the semiquinone Q_B^- might show up equilibrium isotope effect. This effect, however, is negligible ($pK_D - pK_H < 0.1$), as very small if any isotope effect is observed in the electron transfer mutants (Fig. 3.3c).

In proton transfer limit ($k_p << k_{et}$), Eq. (3.4) offers $k^{(2)}_{AB} = k_{on}$ which means that the observed rate is determined by the rate of proton (deuterium) binding only. In this extreme case, $k^{(2)}_{AB}$ might be sensitive to changes due to deuteration (discussed below). In intermediate case, when the rates of protonation and electron transfer are commeasurable, the isotope effect describes transition between the maximum (PT limit) and minimum (ET limit) values. The transition function can be derived from Eq. (3.4).

In proton transfer variants, $k^{(2)}_{AB}$ is significantly (2–3 orders of magnitude) smaller than in native RC. The decreased rate, however, does not include necessarily that the RC

variant should be a PT mutant. In ET limit, $k^{(2)}_{AB}$ decreases if the protonated fraction of Q_B^- decreases (see Eq. (3.1)). This can be achieved by lowering the (operational) pK of Q_B^-/Q_BH. Our results showed that the decrease could be substantial in different ET mutants (Fig. 3.4). Accordingly, the observed rate can be as low as experienced in PT mutants. In H173EQ mutant, $k^{(2)}_{AB}$ is greatly inhibited and drops to a value as low as that of the native RC treated by transition metal ion (Figs. 3.3a and 3.3b). Although H173EQ appears to be borderline in terms of ET vs. PT rate limitation, it remains ET mutant. The effect of mutation on the PT rate is indeterminate and could be essential. This view is supported by independent methods of ET measurements and driving force assay.

The isotope effect on the rate of the second ET exhibits features indicating that the observed kinetics are not caused by an elementary process such as the shift of pK values of the protonatable groups upon solvent deuteration (equilibrium isotope effect) or the unimolecular dissociation of an COO–H bond of an carboxylic group (kinetic isotope effect). Based on our experiments, we are led to conclude that the measured isotope effects in different RC variants may reflect several elementary processes.

Due to severe interruption of the protonation pathway by mutation or by divalent cations at the proton entry point, the Q_B^- semiquinone anion is protonated by any of the much slower alternative pathways controlled by a protonatable amino acid (A) in equilibrium with the aqueous bulk phase: $AH \leftrightarrow A^- + H^+$. The rate of protonation that limits the rate of the second ET $k^{(2)}_{AB}$ is $k_p = k'_{on}\cdot[H^+] + k_{off}$, where k'_{on} is the bimolecular rate constant of proton binding (values of $2–6\cdot10^{10}$ $M^{-1}s^{-1}$ are commonly found for neutralization of strong bases)[22] and k_{off} is the rate constant of proton dissociation. The ratio $K_H = k_{off}/k'_{on}$ gives the proton dissociation constant. If the equilibrium partition between protonatable residue and solvent is sensitive to hydrogen isotopes, then equilibrium isotope effect is observed whose magnitude and pH-dependence can be expressed as

$$\frac{k^{(2)}_{AB}(H^+)}{k^{(2)}_{AB}(D^+)} = \frac{k'_{on}(H^+)}{k'_{on}(D^+)}\cdot\frac{(1+10^{pK_H-pH})}{(1+10^{pK_D-pH})}\cdot 10^{pK_D-pK_H}. \qquad (3.5)$$

The bimolecular rate constants of H^+/D^+ binding are controlled by diffusion, intraprotein electrostatics and/or protein conformation and its sensitivity to H/D exchange should be minor. According to Eq. (3.5), the magnitude of the solvent isotope effect is negligible at low pH (<<

pK_H or pK_D) ($k^{(2)}_{AB}(H^+)$/ $k^{(2)}_{AB}(D^+)$ ≈ 1) and approaches monotonously to the maximum value of $10^{(pK_D - pK_H)}$ at high pH (>> pK_H or pK_D). The transition occurs in two steps at pH ≈ pK_H and pH ≈ pK_D and above these pH values the isotope effect becomes pH-independent. Similar behavior is observed for PT agents M17DN/L210DN double mutant and metal poisoned native RC: the isotope effect is relatively small and pH-independent on the pH range between 5.5 and 9.5 (Fig. 3.3d). Good correspondence with the theory of equilibrium isotope effect is obtained by assumption of highly acidic residue (pK_H << 5.5) and of relatively small increase of pK_H upon deuteration (pK_D – pK_H ≈ 0.3). The intraprotein conditions of the RC are adequate for satisfaction of these assumptions. The Q_B binding pocket is rich of carboxylic acid residues and the members of the acidic cluster can supply proton for the alternative pathways. The validity of the second assumption can be supported by previous experiments. The alkaline protonatable groups responsible for binding of the first proton upon $P^+Q_A^-$ formation demonstrated small increases in the p*K*s (~ 0.2) and a small, pH (pD)-dependent slowing of the binding rate after incubation in D_2O. Although not the same groups participate in the uptake of the first and second protons, the effect of deuteration of RC on binding of the H^+/D^+ ions after the first flash can be informative on the same effect after the second flash.

Large solvent isotope effect was observed in L213DN PT mutant (Fig. 3.3d) that calls for a X–H(D) bond-breaking step characteristic of the kinetic isotope effect. The relatively large isotope effect is due to the large percentage mass change upon replacement of hydrogen with deuterium. The origin of the primary isotope effect is the difference in the frequencies of various vibrational modes of the residue, arising when H is substituted for D (Fig. 3.2). At ambient temperature, the vibrational modes for bond stretches are dominated by the zero-point energy (ZPE). Assuming that the O–H(D) bond of interest is 100% broken at the transition state (not usually the case), we can calculate the maximum possible isotope effect:

$$\frac{k_H}{k_D} = \exp\left(- \frac{h\, c\, \overline{\nu_H} \left(\sqrt{\frac{\mu_{OH}}{\mu_{OD}}} - 1 \right)}{2\, k_B\, T} \right) \qquad (3.6)$$

where c is the speed of light in vacuum, $\overline{\nu_H}$ is the wave number of O-H stretch and μ_{OH} = 1.06 and μ_{OD} = 1.78 are the reduced (atomic) masses. Taking $\overline{\nu_H}$ = 3,200 cm^{-1} for the wave number

of vibration of the O–H bonds of macromolecular association with carboxylic acid, Eq. (3.6) offers $k_H/k_D = 6.0$ for the maximum primary isotope effect at room temperature ($T = 293$ K).

Such a high value was obtained for the L213DN mutant in the highly acidic pH range only and in all other cases the measured isotope effects were smaller. Although the deceleration of the ET in RCs blocked with different transient divalent metal ions (Ni^{2+} and Cd^{2+}) were different (Fig. 3.3b), they gave similar isotope effects ($k_H/k_D \approx 2.1$). This indicates that the observed isotope effects reflect changes upon deuteration in the protein rather than the mode of sealing of the proton entry point. It can occur that the PT reactions do not involve bonds that are completely broken in the transition state (the O–H bond is only partially broken) and/or another is starting to form at the transition state. Both attenuate the isotope effect from that of total homolysis used to approximate the maximum isotope effect.

To understand the pH-dependence of the isotope effects in the L213DN mutant, the ZPE of the various vibrations of the reactant and the activated complex should be compared. Primary kinetic isotope effect is observed if the ZPE difference in the activated complex/transition state is smaller than in the reactants, resulting in a difference in activation energy between O–H and O–D (Fig. 3.2). The magnitude of a primary kinetic isotope effect depends on differences in the ZPE's in the reactant and the activated complex for all the vibrational modes of the reactant and activated complex. In L213DN mutant, the ZPE levels of O–H and O–D vibration profile of the transition state exhibit pH-dependence in a manner of monotonous increase of the ZPE difference at higher pH. The pH-drop of the observed KIE can be formally approximated by a Henderson-Hasselbalch curve centered at pH 5.65 (Fig. 3.3d). It looks like the deprotonation of a protonatable group of pK = 5.65 would control the vibrational energy profile of the rate-determining residue in the PT.

Changes of thermodynamics upon deuteration

Fundamental thermodynamic analysis of the second ET in PT variants can contribute to proper understanding of the PT mechanism. The breakdown of the temperature-dependence into total enthalpy and entropy of activation has proved highly suggestive (Figs. 3.6 and 3.7), although the enthalpy and entropy contributions of the $P^* \rightarrow P^+Q_A^-$ free energy drop seriously challenged existing notions.[23] The wild type shows a rather small activation enthalpy that is not influenced by H/D exchange of the solvent. Any manipulations of the proton pathway by

mutation or by divalent cations result in a larger net enthalpy of activation and less negative entropy. This partial offset is almost certainly not a significant "enthalpy-entropy compensation". The tendency remains the same upon deuteration: the enthalpy increases further and the entropy becomes less negative. The change caused by H/D exchange is small in RC inhibited by Ni^{2+} and large in L210DN/M17DN double mutant where the activation process is almost entirely enthalpic. The small entropy of activation indicates no major conformational changes of the protein upon proton delivery and accounts for slight rearrangement of the hydrogen bonded network, including solvent water, as has been well supported for carbonic anhydrase and superoxide dismutase and almost visualized in bacteriorhodopsin. The L213DN mutant shows somewhat different behavior. The entropic contribution is larger and indicates different kind of limitation. The L213DN is the most drastically PT limited of any known mutant and is blocked at a site nearer the Q_B quinone. Alternate PT pathway directed either to L223S or to L212 behind L213 should be activated that can include H^+/D^+ binding, *per se*, in the rate limiting step.

Alternate proton pathways

As the rates of PT are dramatically decreased in PT mutants compared to that in native RC, the importance of alternate proton pathways should increase.[24] The alternate routes do not satisfy the very strict conditions of fast proton delivery: the H-bond network of protonatable residues and water molecules can be less tightly coupled and can be shorter than the length of the native pathway (~ 20 Å). They can lead directly to O1 of Q_B via L212E/L223S or connect to the main pathway after the site of inhibition (Fig. 3.1). The magnitude and pH-independence of the solvent isotope effect were similar in RCs blocked by divalent cations at the proton entry point and by double mutations at L210D and M17D sites (Fig. 3.3d). This suggests that several (at least two) parallel alternate routes are operational in the pathway regions near the proton entry point that rescue the PT to Q_B^- in inhibited RCs. Other routes in the interior of the protein can also contribute to the PT process where other acidic residues (e.g. H173E) and water molecules become active. The cost of the rescue of proton delivery by alternate pathways is the highly reduced transfer rate.

The L213DN mutant blocks the natural proton pathway at a site closest to the quinone and demonstrates distinct behavior. In this case, the measured $k^{(2)}_{AB}$ is much (by at least 10^4

fold) less than in native RC at pH 7 (Fig. 3.3b). Because $k^{(2)}_{AB}$ is PT limiting, the actual rate of PT is much more strongly (> 10^7 fold) inhibited. The enormous drop of the rate of PT and the close to maximum kinetic isotope effect with strong pH-dependence indicate very limited possibilities of alternate proton pathways. Bridging water molecules and/or L212E can replace L213D but due to loose coupling of the groups, the transfer may include H-bond breaking (or close to this limit) step.

4. PROTONATED RHODOSEMIQUINONE AT THE Q_B BINDING SITE OF M265IT MUTANT REACTION CENTER OF PHOTOSYNTHETIC BACTERIUM *RBA. SPHAEROIDES*

4.1 Background and main idea

It was demonstrated above that coupled electron and proton transfers carry out energy conversion in many living organisms.[25] In reaction center protein of photosynthetic bacterium *Rhodobacter (Rba.) sphaeroides* the light-induced transfer of two electrons to the quinone at the Q_B binding site is accompanied by binding of two protons resulting in fully reduced hydroquinone QH_2. On the first electron transfer (ET) after the first flash, the protein takes up non-stoichiometric amount of H^+ ions reflecting small changes in side chain pK_as due to the novel anionic charge of the semiquinone. Depending on pK_1 of $Q_B^{-\bullet}/Q_BH^\bullet$ and the prevailing pH, the semiquinone itself can also be protonated (Fig. 4.1).

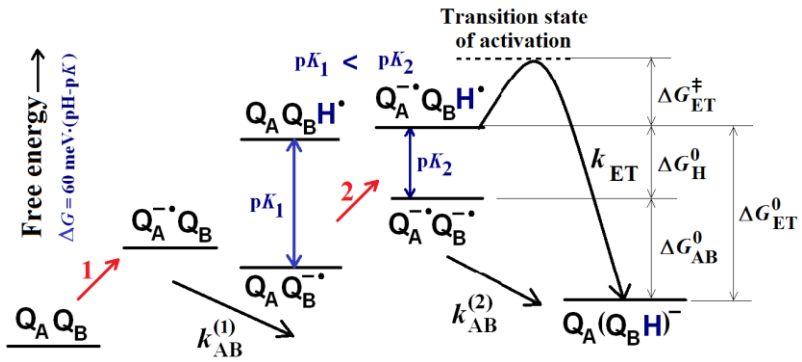

Figure 4.1 The uptake of the first H^+ ion by $Q_B^{-\bullet}$ in one- and two electron states of the acceptor quinone complex of RC after the first and second flashes, respectively. The first electron transfer can be followed by protonation of $Q_B^{-\bullet}$ by pK_1. The second interquinone ET (rate k_{ET}) must be preceded by the proton transfer that should be fast enough to establish $Q_BH^\bullet$ in an equilibrium population determined by pK_2 and the ambient pH. The observed rate of the second ET, $k_{AB}^{(2)}$ is given by Eq. (4.1). The free energy levels of the states involved in the proton-coupled ET are indicated for demonstration.

After the second flash, protons are delivered directly to the quinone head group and the second ET is fully proton-coupled (Fig. 4.2). The analysis of the free energy and pH dependences of the rate has revealed that the reaction mechanism proceeds *via* rapid pre-protonation of the semiquinone in the two-electron state of the acceptor quinone complex ($Q_A^{-\bullet}Q_B^{-\bullet} \leftrightarrow Q_A^{-\bullet}Q_BH^\bullet$) followed by rate-limiting electron transfer ($Q_A^{-\bullet}Q_BH^\bullet \rightarrow Q_AQ_BH^{-\bullet}$). It is now understood to comprise a rate limiting ET that is rate modulated by pH because the protonated semiquinone, $Q_BH^\bullet$, is the actual electron acceptor species.

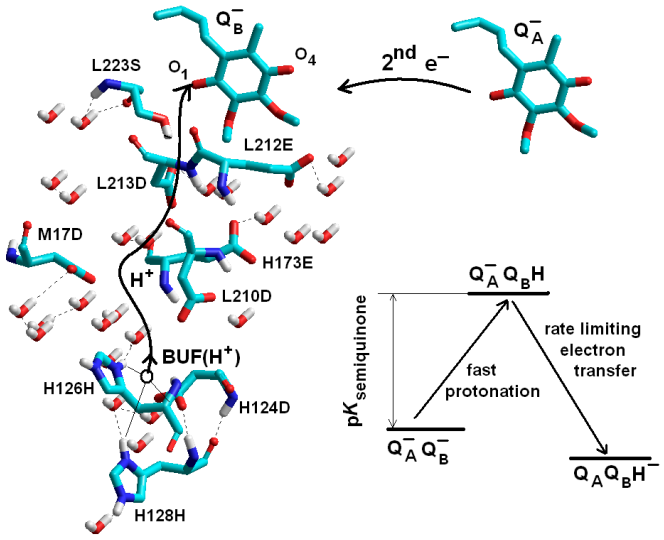

Figure 4.2 Structural (left) and thermodynamic and kinetic (right bottom) view of the sequential proton (H^+) and electron (e^-) uptake by the secondary quinone after the second saturating flash in wild type bacterial RC. The transfer of the second (interquinone) electron from $Q_A^{-\bullet}$ is preceded by a very fast protonation of $Q_B^{-\bullet}$ and followed later by binding of the second proton to $Q_AQ_BH^-$.

The observed rate is

$$k_{AB}^{(2)} = k_{ET} \cdot f(Q_BH^{\bullet}), \tag{4.1}$$

where $f(Q_BH^{\bullet})$ denotes the population of $Q_BH^{\bullet}$. According to a simple (Henderson-Hasselbalch) titration

$$k_{AB}^{(2)} = k_{ET} \cdot \frac{1}{1+10^{pH-pK_2}}. \tag{4.2}$$

The proton transfer equilibrium must be established at least 10 times faster, at all pH. How fast the ET rate is, and therefore how fast the PT rate must be, depends on the functional pK_2 of the Q_B semiquinone. For the native ubiquinone$_{10}$ in RC of *Rba. sphaeroides* the pK_2 should be very low as the Q_B^- semiquinone remains fully anionic at least down to pH 4.5 and therefore the neutral (protonated) semiquinone as the transition intermediate of the 2nd ET cannot be observed.[26]

A straightforward suggestion is to replace the ubiquinone at the Q_B site by other quinone that can forward electrons and protons to quinol formation and its semiquinone form exhibits higher pK value than that of ubisemiquinone. Rhodoquinone (RQ) seems to fulfill these conditions (Fig. 4.3). The rhodoquinone is a required cofactor for anaerobic respiration in *Rhodospirillum rubrum*. RQ is an aminoquinone that is structurally similar to ubiquinone (Q), a ubiquitous lipid component involved in the aerobic respiratory chain. The only

difference between the structures is that RQ has an amino group (NH_2) on the benzoquinone ring in place of a methoxy substituent (OCH_3) in Q.

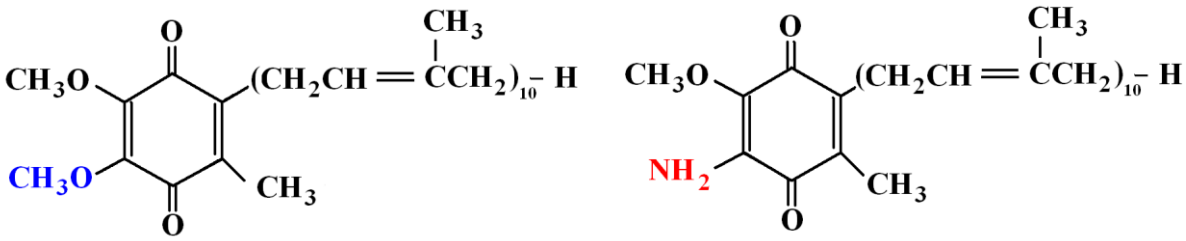

Figure 4.3 Chemical structures of ubiquinone (UQ_{10}) and rhodoquinone (RQ). They can serve as electron acceptors in bacterial RC. The only difference between the structures is that RQ has an amino group (NH_2) on the benzoquinone ring in place of a methoxy substituent (OCH_3) in UQ.

This difference of the structures causes considerable difference of (*i*) the redox midpoint potentials (E_m) measured polarographycally: at pH 7 −63 mV for RQ and +43 mV for UQ (ubiquinone-10) in a mixture of ethanol and water (4:1, v/v) and −30 mV (RQ) and +50 mV (UQ) bound to chromatophores of *Rhodospirillum rubrum* and (*ii*) p*K* of protonation of the semiquinones: in solution, the values of the electron transfer number were $n = 2$ and plots of E_m versus pH formed straight lines with slopes of −30 mV/pH in the neutral pH range offering proton transfer numbers of $m = 1$ for both quinones.[27] When bound, however, to chromatophores, the proton transfer numbers were estimated to $m = 1$ for UQ but $m = 2$ for RQ with apparent p*K* of about 7. Although the quinones were double reduced in these experiments, the results can offer hint for the increased p*K* of the rhodosemiquinone relative to that of ubisemiquinone. The increase of p*K* is probably due to the higher electronegativity of nitrogen in RQ than carbon atom in UQ. The p*K* of $RQ^{-\bullet}/RQH^{\bullet}$ was estimated to 7.3 at the Q_B site of the RC.[28]

The reduction of the low potential rhodoquinone at the Q_B binding site requires the use of low potential analogues of Q_A or direct electron transfer to Q_B along the inactive B branch. Both methods have difficulties. Binding of different (non-native) quinones in the Q_A and Q_B sites calls for great challenge in RC of *Rba. sphaeroides*. The incomplete binding of the quinones results in restricted interquinone electron transfer with a mixture of Q_A^- and Q_B^- states after the first saturating flash. The observation of B branch electron transfer to Q_B needs

heavily modified RC with a total of five mutations and even in that case, the quantum yield of Q_B reduction is very low (about 5%). Because the many modified residues are not located in the region around Q_B, the integrity of the Q_B environment is supposed to be preserved. [29]

In this work, we used a different procedure for reducing rhodoquinone in the Q_B site. The Q_A binding site remained occupied by the native ubiquinone but its redox midpoint potential was lowered by 100–120 mV upon mutation of M265 isoleucine to the smaller, polar residue of threonine in the Q_A binding pocket (Fig. 4.4).

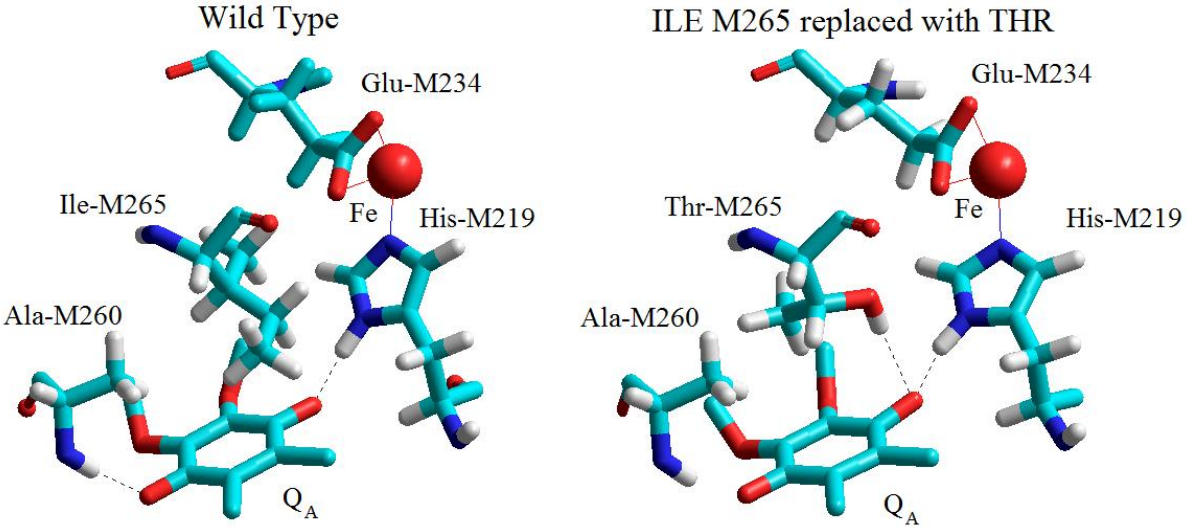

Figure 4.4 The Q_A binding site showing the quinone (Q_A) and three residues (Ala-M260, His-M219 and Ile-M265) of known importance to quinone function in bacterial RC. Ile-M265 above the quinone ring is in van der Waals contact with Q_A that is stabilized by two H-bonds: His-M219 and Ala-M260 form H-bonds with the O4 and O1 carbonyls, respectively (wild type, left). The substitution of isoleucine for threonine (Thr, mutant, right) at position M265 in the Q_A binding pocket has particularly important structural consequences. The H-bond to Ala-M260 at O1 carbonyl is lost (and probably a new H-bond to Thr-M265 at O4 is created) and the redox midpoint potential of QA is modified. Mutation to this residue had shown its importance to quinone redox tuning (from structure 1AIG.pdb).

The H-bond structure and the extensive decrease of the redox midpoint potential of Q_A were studied earlier by delayed fluorescence of the bacteriochlorophyll dimer, FTIR and magnetic resonance spectroscopies and quantum mechanical calculations of the ^{13}C couplings of the 2-methoxy dihedral angle. The large drop in the redox potential of Q_A is attributed to hydrogen bonding of the OH to the peptide C=O of ThrM261, which causes a displacement of the

backbone strand that bears the hydrogen bond donor (AlaM260) to the C1 carbonyl of Q_A, lengthening the hydrogen bond to the semiquinone state, Q_A^-, and thereby destabilizing it. This greatly increases ΔE_m, the driving force for electron transfer. If we combine the two low potential quinones at Q_A (M265IT mutant) and Q_B (RQ substitution) sites, the driving force will remain large enough to get efficient interquinone electron transfer. We will have chance to recognize the protonation of the semiquinone either from the typical light-induced optical absorption spectrum between 400-500 nm or from comparison of the damping of the semiquinone oscillation detected at wavelengths characteristic to the neutral and anionic forms of the semiquinone at the Q_B site of the RC.

4.2 Results

Rate of $P^+Q_A^-$ charge recombination in M265IT mutant RC. The kinetics of P^+ dark decay following a flash were measured at 430 nm in M265IT RC with UQ at the Q_A binding site and empty Q_B binding site (Fig. 4.5).

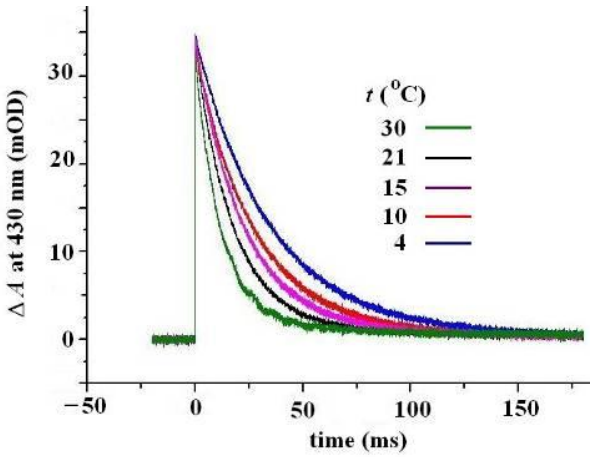

Figure 4.5. The temperature-dependence of the rate constants of $P^+Q_A^- \rightarrow PQ_A$ charge recombination measured by flash-induced absorption change at 430 nm of M265IT mutant RC of *Rba. sphaeroides*. The increasing rate upon higher temperatures is an indication of low potential quinone at the Q_A binding site. Conditions: 1.1 μM RC (Q_B depleted), 0.03% LDAO, 1 mM MOPS buffer, 2.5 mM KCl and pH 7.

The observed rates are 2-3 times faster than those in wild type RC and show temperature dependence. Multiple processes contribute to the observed (net) reaction. The back reaction can occur either directly ($P^+Q_A^- \rightarrow PQ_A$) probably via tunneling or indirectly through the reduced bacteriopheophytine, I, intermediate $P^+I^-Q_A$. In wild type RC, the rate of charge recombination is highly independent on the temperature indicating that the decay occurs exclusively directly. As the bacteriopheophytine is thermally populated in M265IT RC, the observed recombination rate will show temperature-dependence which is a good indication of

the low potential of the quinone at the Q_A binding site. The shift of the midpoint redox potential of Q_A in M265IT relative to that of WT amounts –110 mV at pH 7 (15).

Q_B site of M265IT occupied by RQ. Upon addition of RQ to the Q_B-depleted RC, a slow phase of ~ $(500\ ms)^{-1}$ rate constant appears in the charge recombination kinetics that disappears in the presence of the potent inhibitor terbutryne (data not shown). Subsequent saturating flashes evoke binary oscillation of the semiquinone in the presence of external electron donor to the oxidized dimer, P^+ characteristic of the two-electron gate function of Q_B (Fig. 4.6).

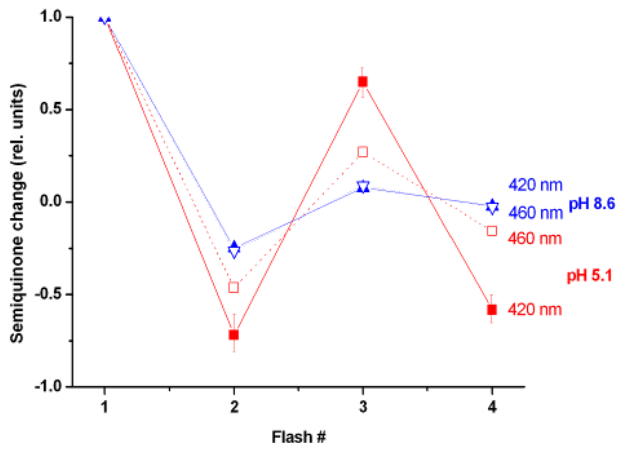

Figure 4.6 Changes of rhodosemiquinone at the Q_B site of M265IT mutant RC upon subsequent saturating flashes measured at two wavelengths: 420 nm (characteristic of protonated RQ, $RQ_BH^{\bullet}$) and 460 nm (characteristic of the anionic form of RQ, $RQ_B^{-\bullet}$) and two pH values (5.1 and 8.6). The magnitudes are normalized to the change evoked by the first flash. The lines were fitted by $\delta = 0.2$ and $\alpha = 0.09$ (pH 5.1 and 420 nm), 0.42 (pH 5.1 and 460 nm), 0.69 (pH 8.6 and 420 nm) and 0.67 (pH 8.6 and 460 nm). Conditions: 1.1 μM RC, 100 μM RQ, 0.02% LDAO, 60 μM ferrocene, 5 mM buffer mix and flash repetition rate 5 Hz.

If UQ occupies the Q_B binding site of the M265IT mutant RC, then the oscillations in Q_B^- semiquinone formation is at least as strong as in wild type RCs, consistent with a large value of electron equilibrium constant and effective transfer of the second electron. If, however, RQ replaces UQ at the Q_B binding site, the magnitude of the semiquinone oscillation is significantly affected and the damping will be larger. The damping of the oscillation of the rhodosemiquinone upon subsequent saturating flashes is determined by *i*) the occupancy of the Q_B site ($1–\delta$), and *ii*) the one-electron equilibrium partition coefficient, $\alpha = [Q_A^-Q_B]/([Q_A^-Q_B] + [Q_AQ_B^-])$ in the acceptor quinone system. The measured semiquinone absorption contains contributions from both Q_A^- and Q_B^- (protonated or deprotonated) and is given after the n^{th} (>0) saturating flash by:

$$\Delta A_n = (1-\delta)\cdot\frac{1-(-1)^n\cdot(1-\alpha)^n}{2-\alpha}+\delta\,. \qquad (4.3)$$

normalized to the absorption change after the first flash, ΔA_1. Figure 4.6 demonstrates the change of the semiquinone content after the n^{th} flash: $\Delta Q^-_n = \Delta A_n - \Delta A_{n-1}$, i.e. the difference between two sequential flashes. By fitting the measured data to the model, we get $\delta = 0.2$ (the occupancy of the Q_B site by RQ is 80% in this experiment) and pH– and wavelength-dependent partition coefficients (Fig. 4.7).

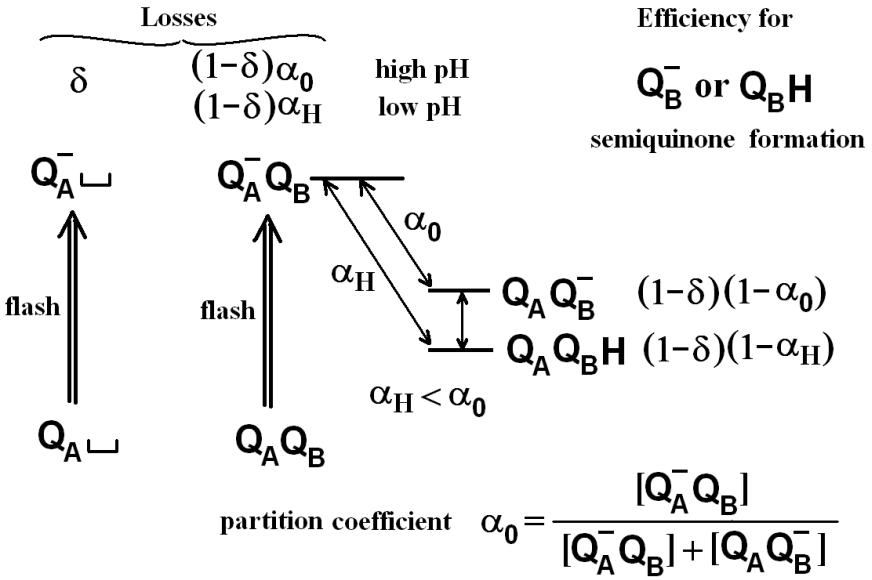

Figure 4.7 Scheme for interpretation of wavelength-dependence of damping of oscillation of rhodosemiquinone upon subsequent saturating flashes. The damping is determined by 1) the occupancy of the QB site (1-δ), and 2) the one-electron equilibrium partition coefficient (α) in the acceptor quinone system. At low pH, the damping is small indicating large Q_B site occupancy and effective electron transfer to Q_B (small δ and α). Additionally, the oscillation at 420 nm (characteristic of protonated RQ, $RQ_BH^{\bullet}$) is larger than at 460 nm (anionic form of RQ, $RQ_B^{-\bullet}$). It is due to higher stabilization (smaller partition coefficient) of the protonated form than that of the anionic form.

At low pH, the damping is small indicating effective electron transfer to Q_B. The oscillation at 420 nm (characteristic of protonated RQ, $RQ_BH^{\bullet}$) is larger than at 460 nm (typical to anionic form of RQ, $RQ_B^{-\bullet}$) expressed by the smaller α at 420 nm than at 460 nm: 0.09 and 0.42, respectively. At low pH (<pK_1), the protonated form of Q_B^- involves lower free energy level than that of the anionic form (Fig. 4.1). Therefore, due to the contribution of $RQ_BH^{\bullet}$, smaller partition coefficient (higher one-electron equilibrium constant) is obtained. Crudely speaking, the protonation stabilizes the semiquinone state. At high pH (= 8.6), the oscillation is strongly damped and no distinctions can be made according to wavelengths: α = 0.69 and 0.67 at 420

nm and at 460 nm, respectively. The rhodosemiquinone is not protonated at all in this pH range.

This indirect statement can be confirmed by direct measurement of the rhodosemiquinone absorption spectra at different pH values (Fig. 4.8).

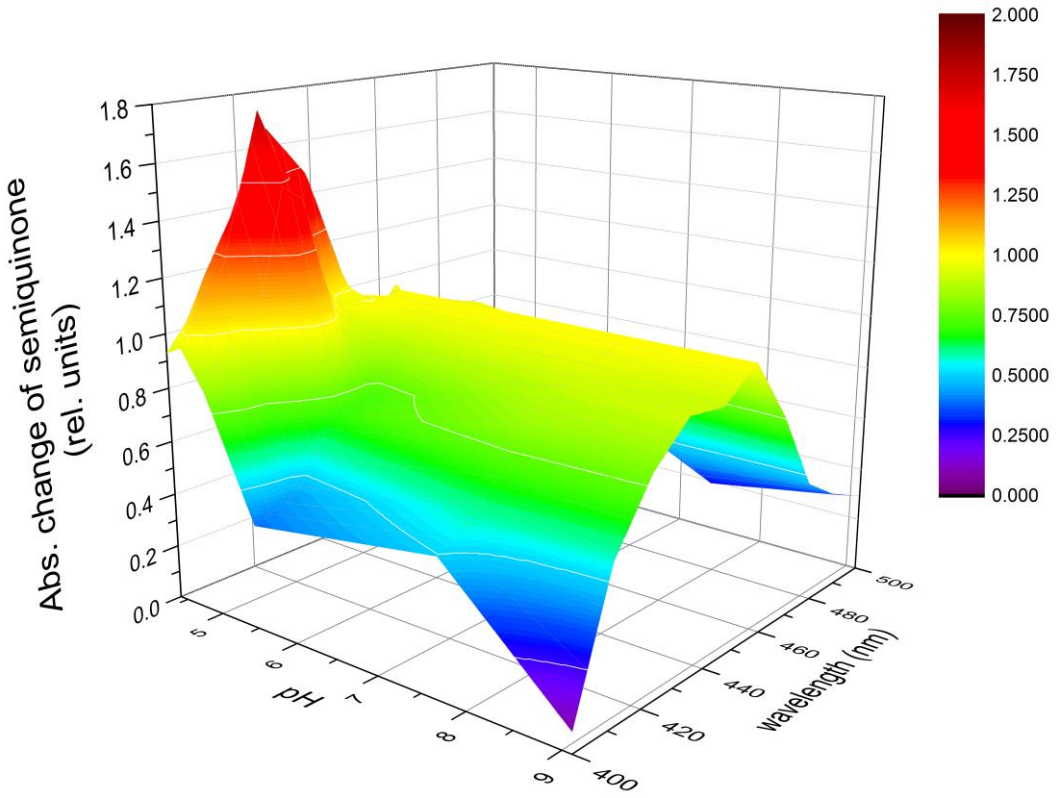

Figure 4.8 Quasi 3D representation of the optical absorption spectra of rhodosemiquinone at the secondary quinone binding site (Q_B) of M265IT mutant RC measured after a saturating flash in the presence of electron donor to the oxidized dimer P^+ at several pH values. The 420 nm band of the spectra at low pH resembles the protonated spectrum of semiquinone in solution. The spectra are normalized to the absorption at 450 nm.

Similar spectra were obtained when the semiquinone appeared (after odd number of flashes) or disappeared (after even number of flashes) indicating that the contribution of RQ_B^- played the determining role. The spectra consisted of components from protonated RQ (characteristic band around 420 nm that appeared below pH 5) and deprotonated (anionic) RQ (characteristic band at 450 nm that dominates above pH 5). Although the appearance and disappearance of the band at 420 nm can be well recognized at low and neutral pH ranges, respectively, it is hard to predict a characteristic p*K* value for protonation of RQ_B^- as its band did not attain

obviously its maximum at the lowest pH value (pH 4.3) used in these measurements. We predict a p$K \leq 5$ that is significantly smaller than 7.3 obtained after a simple titration curve in.

Electron transfer rates. The exchange of UQ for RQ at the Q_B site of M265IT has much larger effect on the energetics of the quinone acceptor system (manifested by variations of the $P^+Q_B^- \rightarrow PQ_B$ charge recombination or semiquinone oscillation) than on the kinetics of the first ($Q_A^-Q_B \rightarrow Q_AQ_B^-$) and second ($Q_A^-Q_B^- \rightarrow Q_AQ_BH$) electron transfers. The rates of the $k^{(1)}_{AB}$ reaction were the same with UQ as with RQ in the Q_B site (data not shown). Since the rate of the first electron transfer is under the control of conformational gating of the Q_B site (31), the result indicates that substitution of RQ does not affect the dynamics of Q_B motion. The rates of the second electron transfer with UQ or RQ at Q_B site show similar and non-integer pH-dependence (Fig. 4.9). They demonstrate highly moderate pH-dependence at low pH but decrease at high pH by a factor of 10 per pH unit. For RQ, the rates are slightly smaller and the crossing point of the lines that approximate the low and high pH behavior, has higher pH value than those for UQ.

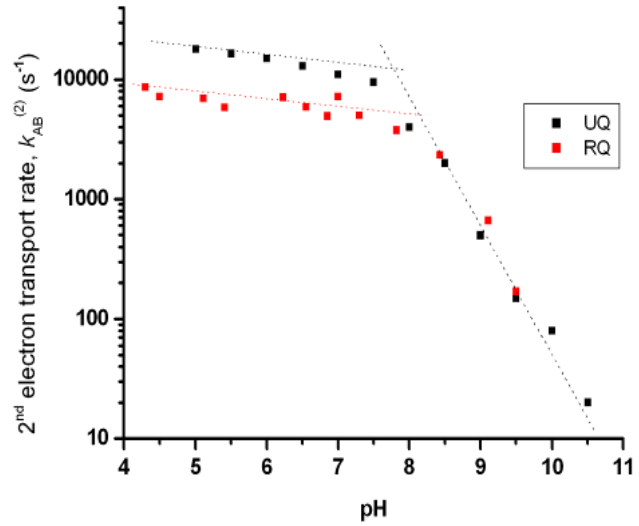

Figure 4.9. pH dependence of the rate of the second electron transfer in M265IT mutant RC whose Q_B is occupied by either native UQ (■) or RQ (■). The rate was measured from the decay of semiquinone absor-bance at 450 nm. The lines represent the approximate small pH-dependence below pH 8 and the theoretical 1 decade/pH unit drop above pH 8. Conditions: 2 μM RC in 2.5 mM KCl, 1 mM buffer mix, 0.02% LDAO, 40 μM UQ_{10} or 100 μM RQ_{10} and 2-200 μM ferrocene (or its derivatives), depending on the rate (or pH).

The rate of the second electron transfer is sensitive to the temperature: it increases upon elevation of the temperature in the physiological range. Figure 4.10 demonstrates this dependence for UQ and RQ at the Q_B site at different pH values in Arrhenius-type representation where the logarithm of the rate is plotted as a function of the reciprocal of the temperature.

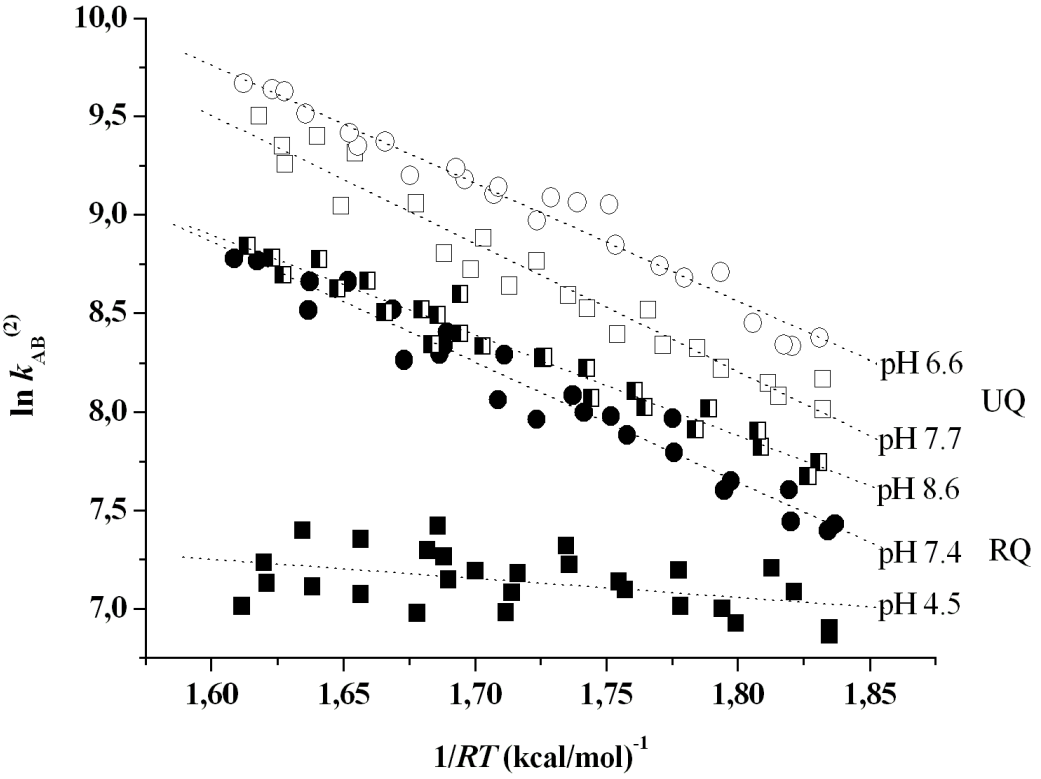

Figure 4.10 Temperature-dependence of the rate of the second electron transfer at the physiological temperature range in M265IT mutant RC with UQ (open symbols) and RQ (closed symbols) at the Q_B binding site at several pH values. According to the transition state theory, the logarithm of the rate constant, ln $k^{(2)}_{AB}$ should show linear relationship with the reciprocal of the temperature, *T* (Eyring plot). Conditions as in Fig. 4.9.

As the measured data fit to straight lines, one can formally introduce observed activation parameters for the temperature-dependence of the 2nd ET:

$$k_{AB}^{(2)} = k_{max} \cdot \exp\left(-\frac{\Delta G^{\neq}_{obs}}{RT}\right), \qquad (4.4)$$

where $k_{max} \approx 3.5 \cdot 10^9$ s^{-1} obtained from the exchange coupling between Q_A^- and Q_B^- in EPR studies, *R* and *T* are the universal gas constant and the absolute temperature, respectively, and $\Delta G^{\ddagger}_{obs}$ is the observed free activation energy that can be decomposed into enthalpy change of activation, $\Delta H^{\ddagger}_{obs}$ and entropic change of activation, $T \cdot \Delta S^{\ddagger}_{obs}$: ($\Delta G^{\ddagger}_{obs} = \Delta H^{\ddagger}_{obs} - T \cdot \Delta S^{\ddagger}_{obs}$). They can be derived from the slope (*Slope*) and intersection (*Int*) of the straight line: $\Delta H^{\ddagger}_{obs}$ =

– *Slope* and $T{\cdot}\Delta S^{\ddagger}_{obs} = RT\ (Int - \ln(k_{max}))$. Their values are tabulated in Table 4.1. As can be seen, neither the rates nor the activation parameters are very much different if UQ is replaced by RQ at the Q_B binding site of the M265IT mutant RC.

Table 4.1 Standard (^{0}) and activation (‡) free energy (ΔG), enthalpy (ΔH) and entropic energy ($T{\cdot}\Delta S$) changes of the second electron transfer in M265IT RC with either UQ or RQ at the Q_B binding site. The observed (obs) activation parameters were obtained from temperature dependence of $k^{(2)}_{AB}$ and the free energies ΔG^0_H, ΔG^0_{ET} and $\Delta G^{\ddagger}_{ET}$ were calculated from Eqs. (4.9), (4.8) and (4.7), respectively. The values of pK_2 and k_{ET} were derived from $\Delta G^0_H = 2.3{\cdot}RT{\cdot}(pH - pK_2)$ and $k_{ET} = k_{max}{\cdot}\exp(-\Delta G^{\ddagger}_{ET}/RT)$, respectively. For the maximum electron transfer rate $k_{max} = 3.5{\cdot}10^9\ s^{-1}$, for the reorganization energy $\lambda = 1.2$ eV and for the free energy gap between the quinones in two-electron states $\Delta G^0_{AB} = -60$ meV (UQ in WT and RQ in M265IT) and $\Delta G^0_{AB} = -160$ meV (UQ in M265IT) were taken.

RC	Q_B site	pH	$\Delta H^{\ddagger}_{obs}$ (kcal/mol)	$T{\cdot}\Delta S^{\ddagger}_{obs}$ (kcal/mol)	$\Delta G^{\ddagger}_{obs}$ (kcal/mol)	ΔG^0_H (kcal/mol)	pK_2	ΔG^0_{ET} (kcal/mol)	$\Delta G^{\ddagger}_{ET}$ (kcal/mol)	k_{ET} $(\mu s)^{-1}$
	UQ	6.6	6.0	-1.52	7.52	3.28	3.81	-6.98	3.87	4.43
	UQ	7.7	6.1	-1.95	8.05	4.15	4.31	-7.85	3.56	7.56
M265IT	RQ	4.5	6.5	-1.20	7.70	2.25	2.60	-3.64	5.22	0.43
	RQ	7.4	5.09	-2.85	7.94	2.69	5.20	-4.08	5.03	0.60
	RQ	8.6	0.97	-7.63	8.60	3.85	5.58	-5.24	4.55	1.37
WT	UQ	7.8	4.17	-4.80	8.97	4.78	4.34	-6.17	4.18	2.6

4.3 Discussion

The results confirmed the incorporation of RQ into the Q_B site (~ 80%) and the reconstitution of the Q_B activity. It was demonstrated that the drop of the midpoint potential of Q_A in M265IT mutant was high enough to compensate largely the similar shift of midpoint potential of Q_B when UQ is replaced by the low potential RQ. Although the driving force and the electron equilibrium constants in the quinone complex became smaller, effective interquinone electron transfer and turnover of the RC could be measured. The discussion will focus on the pH-dependent p*K* values of the Q_B^- semiquinones and the decomposition of the observed activation free energy of the second electron transfer into contributions of both proton and electron transfer steps.

pK values of semiquinone at the Q_B site. The p*K* of the ubisemiquinone has been estimated at p$K_1 \approx 3.8$ for $(Q_A)Q_B^-/Q_BH$ one-electron equilibrium and p$K_2 \approx 4.5$ for $(Q_A^-)Q_B^-/Q_BH$ two-electron equilibrium valid at pH 7.5. These are mildly suppressed from the value in aqueous solution (p$K_a \approx 4.9$) but, more importantly, the RC value appears to be pH dependent due to changing charge distribution, and possibly sensitive to the nature of the environment, i.e., detergent vs. native membrane. Several acidic groups with Q_B^- constitute a cluster of strongly interacting components resulting in remarkable and unexpected pH-dependence of flash-induced proton uptake. The protonation of the semiquinone does not follow a simple titration curve and, to preserve the formalism, pH-dependent p*K* values should be introduced. The weak pH dependence of the rate of the 2nd ET up to pH 8 suggests that the p*K* of the semiquinone is not constant but is continuously modulated by interactions with a changing electrostatic environment. Recently, a molecular probe (stigmatellin) was introduced to measure the electrostatic potential at the Q_B site.[30] The apparent p*K* of the semiquinone at a definite pH depends on minor changes in the intrinsic pK_a values of Q_B^- and the amino acids involved, and on their strengths of interaction. By measuring the decrease of the rate constant of the second electron transfer in several mutants, considerable decrease of the operational p*K* of Q_B^-/Q_BH was observed upon change of a single amino acid at key positions: the estimated p*K* 4.5 (native) dropped to 3.9 (L210DN), 3.7 (M17DN) and 3.1 (H173EQ) at pH 7. The results may simply suggest that the point at which p*K* approaches and exceeds the ambient pH (thereby allowing significant levels of $Q_BH^{\bullet}$) will depend on interaction with components of the acidic cluster.

While the values of p*K* of ubisemiquinone fall in the lower part, the p*K* for rhodosemiquinone lies at the upper limit of the range of those of carboxylates (4–5), where the protein electrostatics are most complex. Similar type of interactions as discussed above for UQ may be responsible for increase of the operational p*K* of rhodosemiquinone that was large enough to be able to measure the protonated rhodosemiquinone below pH 5.5. The estimated p*K*, however, was much smaller in our study than reported earlier. The lower p*K* value was supported by recent low-temperature EPR and ENDOR investigations where no changes of the spectra were found by decreasing the pH from the alkaline to the acidic range as low as pH 4.5.

In chromatophores, the protonation of the stable Q_B ubisemiquinone ($Q_AQ_BH^{\bullet}$) was readily observable, with a functional pK = 6. This also suggests slight changes of interactions in RC embedded in chromatophores relative to isolated RC. In addition to the functional pK for Q_B^-, other differences may exist between isolated RCs and chromatophores. The midpoint redox potential of the primary quinone, $E_m(Q_A^-/Q_A)$ is strongly pH-dependent in chromatophores but not in isolated RCs. However, determinations of the free energy gap between P* and $P^+Q_A^-$ in chromatophores reveal an identical pH dependence to that seen in isolated RCs and cast serious doubt on the potentiometric determinations of $E_m(Q_A^-/Q_A)$ probably because of poor mediation of the Q_A binding site of the protein. It was suggested that Q_A may actually be titrated through the Q_B site, reflecting titration of the quinone pool or perhaps a redox mediator in the Q_B site. Nevertheless, this remained an open question whose answer is critical to our understanding of the acceptor quinones.

The semiquinone has two different pK values in one- (pK_1) and two (pK_2) electron states of the quinone acceptor complex (Fig. 4.1).We were able to determine pK_1 from the oscillation of the flash induced absorption changes of the stable semiquinone, when Q_A was oxidized. The determination of pK_2 of the transient semiquinone important in the 2nd ET is not straightforward but a realistic estimate can be offered. The difference between pK_1 and pK_2 is due to the extra (electrostatic) interaction of Q_A^- with Q_B^- that can be deduced from equilibrium and kinetic electron transfer and proton uptake measurements and electrostatic calculations. The long range interactions between the two quinone sites prepare the Q_B site for the subsequent electron transfer from Q_A. The electrostatic influence of Q_A^- on the apparent pK_a of the acidic cluster that controls the pH-dependence of electron equilibrium in the quinone complex causes a difference of 0.5–1 units between pKs in states Q_AQ_B and $Q_A^-Q_B$. This result is consistent with the conclusions drawn from pH dependence of the H^+/Q_A^- and H^+/Q_B^- stoichiometries. Light activation causes proton uptake as the acid cluster reprotonates in accordance with the pK shifts induced by the semiquinone anions. The pH dependence of the H^+-uptake stoichiometries, H^+/Q_A^- and H^+/Q_B^-, can be deconvoluted into discrete contributions. Q_A^- causes pK shifts of 0.7–0.8 pH units estimated for the pK_2 of the Q_B semiquinone in the 2-electron state $Q_A^-Q_B^-$, and for the first pK of the quinol, QH^-, in the 3-electron state $Q_A^-Q_BH^-$. The 0.7–0.8 unit upshift in pK of the normal ubiquinone in the $Q_A^-Q_B^-$ state was similar to that inferred for the rhodoquinone occupant. In this work, the

protonation of the rhodosemiquinone was observed in the one electron state, $Q_AQ_B^-$ ‹–› Q_AQ_BH with pK_1 = 7.3. On the second electron transfer, $k_{AB}^{(2)}$ displayed a well-behaved pH dependence (see Eq. (4.2) with pH independent pK): it was constant below pH 7 and decelerated 10-fold per pH unit above a pK of 8.0 in the $Q_A^-Q_B^-$ state. In contrast, our kinetic and thermodynamic data were consistent with significantly smaller and pH-dependent functional pK_1 of the rhodosemiquinone.

Activation analysis of the 2nd ET. The fast proton-pre-equilibrium is followed by a rate-limiting ET. The states involved in the $k^{(2)}_{AB}$ reaction are shown in Figure 4.1. The observed activation parameters are characteristic to both the proton equilibrium and the subsequent electron transfer step. On one hand, the rate of the 2nd ET increases upon decrease of the activation barrier, $\Delta G^{\ddagger}_{ET}$, on the other hand, decreases due to increase of the free energy to protonate the semiquinone, $\Delta G^0_H = 2.3 \cdot RT \cdot (\text{pH} - \text{p}K_2)$ that results in smaller population of the $Q_B^{-\bullet}$ state. The connected proton and electron transfer steps give complex behavior of the apparent activation. Whatever rate model is used for the ET, the proton pre-equilibrium (acid association) parameters (ΔG^0_H, etc) combine with those of the true activations step ($\Delta G^{\ddagger}_{ET}$, etc) to give the observed activation energies ($\Delta G^{\ddagger}_{obs}$, etc) that will not be, however, the simply the sum of the components.

The rate limiting step is a non-adiabatic ET and the Marcus formalism should be used.

$$k_{AB}^{(2)} = \frac{k_{max} \cdot \exp\left(-\frac{\Delta G_{ET}^{\neq}}{RT}\right)}{1 + \exp\left(\frac{\Delta G_H^0}{RT}\right)}. \qquad (4.5)$$

If Eqs. (4.4) and (4.5) are compared, then

$$\Delta G_{obs}^{\neq} = \Delta G_{ET}^{\neq} + RT \cdot \ln\left(1 + \exp\left(\frac{\Delta G_H^0}{RT}\right)\right). \qquad (4.6)$$

Here, the activation free energy of ET, $\Delta G^{\ddagger}_{ET}$ can be expressed from the free energy of the ET (defined as the free energy of the final minus the initial state), ΔG^0_{ET} and the reorganization energy, λ:

$$\Delta G_{\mathrm{ET}}^{\neq} = \frac{\left(\Delta G_{\mathrm{ET}}^{0} + \lambda\right)^2}{4\lambda}. \qquad (4.7)$$

The standard free energy levels follow a simple summation rule. The free energy for electron transfer, ΔG^0_{ET} is the difference of the free energy between initial and final states, ΔG^0_{AB} and the free energy to protonate $Q_B^{-\bullet}$, ΔG^0_{H}:

$$\Delta G_{\mathrm{ET}}^{0} = \Delta G_{\mathrm{AB}}^{0} - \Delta G_{\mathrm{H}}^{0}. \qquad (4.8)$$

Replacing Eq (4.8) into Eq (4.7) and inserting Eq (4.7) into Eq (4.6) we obtain

$$\Delta G_{\mathrm{obs}}^{\neq} = \frac{\left(\Delta G_{\mathrm{AB}}^{0} - \Delta G_{\mathrm{H}}^{0} + \lambda\right)^2}{4\lambda} + RT \cdot \ln\left(1 + \exp\left(\frac{\Delta G_{\mathrm{H}}^{0}}{RT}\right)\right). \qquad (4.9)$$

ΔG^0_{H} and pK_2 at a definite pH can be obtained by solution of Eq. (4.9) with λ = 1.2 eV (= 27.7 kcal/mol) and ΔG^0_{AB} = –160 meV for UQ and ΔG^0_{AB} = –60 meV for RQ at the Q_B site. Although the latter values refer to the free energy differences between the semiquinones in one-electron states, similar values can be taken for the two-electron states. In WT RC, very small (β < 0.05) partition coefficient was found for the two-electron equilibrium in the acceptor quinone system at pH < 8. The measured and calculated values are summarized in Table 4.1. The functional (pH-dependent) pK_2 values are somewhat higher for RQ than for UQ. Although the increase is not as large as reported earlier, a fraction of protonated RQ could be detected in our experiments at low pH range (see Fig. 4.8). This observation is in good agreement with conclusions of recent EPR and ENDOR studies.

The $T{\cdot}\Delta S^{\ddagger}_{\mathrm{obs}}$ entropy change is small and negative. The negative value makes sense as an activation parameter. By our estimates, the entropic component from the electron transfer, $T{\cdot}\Delta S^{\ddagger}_{\mathrm{ET}}$ is quite small and pH-independent. Most of the observed activation entropy is due to the protonation equilibrium, i.e. entropy of mixing. Accordingly, it should have an increasingly negative entropy contribution with pH. Indeed, the entropy of activation

decreases (becomes more negative) since H^+ ions are being brought from an increasingly dilute solution as the pH is raised.

4.4 Conclusions

The secondary quinone activity of the M265IT mutant RC could be reconstituted by binding low potential RQ to the Q_B site. The 2nd electron transfer reaction followed the mechanism of proton activated electron transfer. The flash-induced rhodosemiquinone showed partly neutral (protonated) character below pH 5 and was completely anionic above pH 5.5. Kinetic and thermodynamic assays of the second ET supported the low value of the functional p*K* of RQ at the Q_B site that was slightly higher than that of the native ubiquinone. The p*K* is pH-dependent due to pH-dependent local potential whose main contributor is the cluster of acidic residues around Q_B. The complex deprotonation of the cluster makes the positive local potential at low pH gradually more and more negative at high pH. The pH-dependence of the p*K* is responsible for the fact that the 2nd ET rate has a non-integer pH dependence below pH 8.

5. OUTLOOK

In free energy converting biomembranes with bioenergetic proteins of living organisms, a transmembrane gradient of electrons, protons and/or other species is created that covers the costs of energy consuming physiological processes including communication, growth or division. The triggering mechanism can play essential role. Usually, the biochemical processes are initiated by substrate (e.g. ATP) binding that is slow and kinetically less well defined. If, however, the pumping mechanism across the membrane is triggered and driven by light, then the entire process will be set under optical control with much better defined time resolution. Some members of the microbial opsin family are membrane-bound and light-activated pumps that transport proton (bacteriorhodopsin) and various ions (halorhodopsins and channelrhodopsins) in response to light. This opens the stage for numerous applications in bio- and medical sciences by integration of optics and genetics (optogenetics) to achieve gain (excitation) or loss (inhibition) of function of well-defined events within specific cells of living tissue.[31,32] Microbial opsin genes can be introduced to get optical control of defined action potential patterns in specific targeted neuronal populations within freely moving mammals or other intact-system preparations. By inserting opsin genes into the cells of the brain, flashes of light may trigger (or block) specific neurons on command. This technology permits the conducting of extremely precise and targeted experiments in the brains of living, freely moving animals, which electrodes and other traditional methods do not allow. These optogenetic approaches are already yielding potentially useful insights into the neuroscience of psychiatric disorders such as depression or schizophrenia. The reaction center protein of photosynthetic bacterium studied here should be a perspective candidate for optogenetic and/or bioenergetic purposes.

Additionally, the bacterial RC is a robust redox protein that can preserve the ability of light-induced charge separation under wide range of conditions for long time.[33] Bound to porous silicon microcavities, new types of biomaterials can be created which are useful for optoelectronics. The nanoscale circuits integrated into solid-state electronics are attractive biotechnological applications and the development of biodevices has become a challenging new field.[34] Understanding what happens at the nanoscale could allow us to tailor-design materials to build better solar cells, batteries, nanoscale (electron or proton) wires and more. The stage is set for widespread bionanotechnical applications of bacterial RC.

6. SUMMARY

The photosynthetic purple bacterium *Rhodobacter sphaeroides* uses reaction center protein to convert light into protonmotive force (proton electrochemical potential). Light absorption by the reaction center results in electron transfer through a series of cofactors coupled to proton binding of the protein and finally of the secondary ubiquinone Q_B. The protonation of Q_B was studied for wild type and a mutant reaction centers.

The 2nd electron transfer in reaction center of photosynthetic bacterium *Rba. sphaeroides* is a two step process in which protonation of Q_B^- precedes interquinone electron transfer. The thermal activation and pH dependence of the overall rate constants of different RC variants were measured and compared in solvents of water (H_2O) and heavy water (D_2O). The electron transfer variants where the electron transfer was rate limiting (wild type and M17DN, L210DN and H173EQ mutants) did not show solvent isotope effect and the significant decrease of the rate constant of the second electron transfer in these mutants was due to the drop of the operational pK_a of Q_B^-/Q_BH: 4.5 (native), 3.9 (L210DN), 3.7 (M17DN) and 3.1 (H173EQ) at pH 7.). In contrast, the PT variants where the PT was rate limiting demonstrated solvent isotope effect of pH-independent moderate magnitude (2.11±0.26 (WT+Ni^{2+}), 2.16±0.35 (WT+Cd^{2+}) and 2.34±0.44 (L210DN/M17DN)) or pH-dependent large magnitude (5.7 at pH 4 (L213DN)). Upon deuteration, the free energy and the enthalpy of activation increased in all PT variants by about 1 kcal/mol and the entropy of activation becomes negligible in L210DN/M17DN mutant. The results indicated the manifestation of equilibrium and kinetic solvent isotope effects and the structural possibility of alternate proton delivery pathways.

The 2nd electron transfer from the primary ubiquinone Q_A to the secondary ubiquinone Q_B in the reaction center from *Rhodobacter sphaeroides* involves protonated Q_B^- intermediate state whose low pK_a makes the direct observation impossible. We replaced the native ubiquinone by low potential rhodoquinone at the Q_B binding site of the M265IT mutant RC. As the in situ midpoint redox potential of Q_A of this mutant was lowered about the same extent (≈ 100 mV) as that of Q_B upon UQ→RQ exchange, the Q_B activity could be reconstituted. After subsequent saturating flash excitations, a period of two damped oscillation of the protonated rhodosemiquinone was observed. The $Q_BH^{\bullet}$ was identified by the characteristic band at 420 nm of the absorption spectrum and smaller damping of the

oscillation detected at 420 nm (due to the neutral form) than at 460 nm (attributed to the anionic form). The appearance of the neutral semiquinone was restricted to the acidic pH range indicating a functional pK_a of less than 5.5, slightly higher than that of the native ubisemiquinone (pK_a < 4.5) at pH 7. The analysis of the pH- and temperature dependences of the rates of the 2nd electron transfer supports the concept of pH-dependent pK_a of the semiquinone at the Q_B binding site. The local electrostatic potential is severely modified by the strongly interacting neighboring acidic cluster and the pK_a of the semiquinone is in the middle of the pH range of the complex titration. The kinetic and thermodynamic data are interpreted in frame of the electron-activated proton transfer mechanism combined with pH-dependent functional pK_a of the semiquinone at the Q_B site of the RC.

7. REFERENCES

1. Mitchell P. *Chemiosmotic Coupling in Oxidative and Photosynthetic Phosphorylation* (Glynn Research Ltd., Bodmin, UK, 1966)
2. Mitchell P. Coupling of phosphorylation to electron and hydrogen transfer by a chemi-osmotic type of mechanism. *Nature* 191, 141–148 (1961)
3. Nagle J.F. and Tristam-Nagle S. Hydrogen Bonded Chain Mechanisms for Proton Conduction and Proton Pumping. *J. Membrane Biol.* 74, 1-14 (1983)
4. Silverman D.N. and Lindskog S. The Catalytic Mechanism of Carbonic Anhydrase: Implications of a Rate-Limiting Protolysis of Water. *Acc. Chem. Res.* 21, 30-36 (1988)
5. Morii M., Yamauchi M., Ichikawa T., Fujii T., Takahashi Y., Asano S., Takeguchi N. and Sakai H. Involvement of the H_3O^+-Lys-164 -Gln-161-Glu-345 Charge Transfer Pathway in Proton Transport of Gastric H^+,K^+-ATPase. *The Journal of Biological Chemistry*, 283, 16876-16884 (2008)
6. Lanyi J.K. A structural view of proton transport by bacteriorhodopsin, in: M. Wikström (Ed.), Biophysical and Structural Aspects of Bioenergetics, Royal Society of Chemistry, Cambridge, UK, pp. 227–248 (2005)
7. Gennis R.B. Principles of molecular bioenergetics and the proton pump of cytochrome oxidase, in: M. Wikstrom (Ed.), Biophysical and Structural Aspects of Bioenergetics, Royal Society of Chemistry, Cambridge, UK, pp. 1–25 (2005)
8. Wraight C.A. Proton and electron transfer in the acceptor quinone complex of bacterial photosynthetic reaction centers. *Frontiers Biosciences* 9, 309-327 (2004)
9. Stowell M.H.B., McPhillips T.M., Rees D.C., Soltis S.M., Abresch E. and Feher G. Light-Induced Structural Changes in Photosynthetic Reaction Center: Implications for Mechanism of Electron-Proton Transfer. *Science* 276, 812-816 (1997)
10. Takahashi E. and Wraight C.A. Small weak acids reactivate proton transfer in reaction centers from *Rhodobacter sphaeroides* mutated at Asp^{L210} and Asp^{M17}. *J. Biol. Chem.* 281, 4413-4422 (2006)
11. Marcus R.A. and Sutin N. Electron transfers in chemistry and biology. *Biochim Biophys Acta* 811, 265-322 (1985)

12. Feher G. and Okamura M. Y. Chemical composition an properties of reaction centers, In *The Photosynthetic Bacteria* (Clayton R. K. and Sistrom W.R.. Eds.), Plenum Press, New York, pp 349-386 (1978)
13. Maróti P. and Wraight C.A. Flash-induced H^+ binding by bacterial photosynthetic reaction centers: comparison of spectrophotometric and conductimetric methods. *Biochim. Biophys. Acta* 934, 314-328 (1988)
14. Takahashi E., Maróti P. and Wraight C.A. In *Current Research in Photosynthesis* (Baltscheffsky M., Ed.), Kluwer Academic Publishers, Boston, pp 169-172 (1990)
15. Takahashi E. and Wraight C.A. Proton and electron transfer in the acceptor quinone complex of *Rhodobacter sphaeroides* reaction centers: characterization of site-directed mutants of the two ionizable residues, GluL212 and AspL213, in the Q_B binding site. *Biochemistry* 31, 855-866 (1992)
16. Goldsmith J.O. and Boxer S.G. Rapid isolation of bacterial photosynthetic reaction centers with an engineered poly-histidine tag. *Biochim.Biophys. Acta* 1276, 171-175 (1996)
17. Graige M.S., Paddock M.L., Bruce J.M., Feher G., Okamura M.Y. Mechanism of proton-coupled electron transfer for quinone (Q_B) reduction in reaction centers of *Rb. sphaeroides*. *J. Am. Chem. Soc*. 118, 9005–9016 (1996)
18. Okamura M.Y., Paddock M.L., Graige M.S., Feher G. Proton and electron transfer in bacterial reaction centers. *Biochim. Biophys. Acta* 1458, 148-163 (2000)
19. Maróti P. and Wraight C.A. Kinetics of H^+-ion binding by the $P^+Q_A^-$ state of the bacterial photosynthetic reaction centers: Rate limitation within the protein. *Biophys. J*. 73, 367-381 (1997)
20. Paddock M.L., Adelroth P., Chang C., Abresch E.C., Feher G., Okamura M.Y. Identification of the Proton Pathway in Bacterial Reaction Centers: Cooperation between Asp-M17 and Asp-L210 Facilitates Proton Transfer to the Secondary Quinone (Q_B). *Biochemistry* 40, 6893-6902 (2001)
21. Wraight C.A. and Maróti P. Temperature dependence of the 2^{nd} electron transfer in bacterial reaction centers. *Biophys. J.* 86(1), 148A Part 2. (2004)
22. Eigen M. Proton transfer, acid-base catalysis, and enzymatic hydrolysis, Part I. Elementary processes. *Angew. Chem. Int.* Ed. Engl. 3, 1-72 (1964)

23. Cooper A., Johnson C.M., Lakey J.H., Nöllmann M. Heat does not come in different colours: entropy-enthalpy compensation, free energy windows, quantum confinement, pressure perturbation calorimetry, solvation and the multiple causes of heat capacity effects in biomolecular interactions. *Biophys. Chem*. 93, 215-230 (2002)
24. Cheap H., Bernad S., Derrien V., Gerencsér L., Tandori J., de Oliveira P., Hanson D.K., Maróti P., Sebban P. M234Glu is a component of the proton sponge in the reaction center from photosynthetic bacteria. *Biochim. Biophys. Acta* 1787, 1505–1515 (2009)
25. Wraight C.A. Intraprotein proton transfer - Concepts and realities from the bacterial photosynthetic reaction center. In: Wikström M (ed) Biophysical and Structural Aspects of Bioenergetics, Royal Society of Chemistry, Cambridge, U.K. pp 273-313 (2005)
26. Maróti Á., Wraight C.A. and Maróti P. The rate of second electron transfer to Q_B^- in bacterial reaction center of impaired proton delivery shows hydrogen-isotope effect. *Biochim. Biophys. Acta* 1847, 223–230 (2015)
27. Erabi T., Higuti T., Kakuno T., Yamashita J., Tanaka M., Horio, T. Polarographic studies on ubiquinone-10 and rhodoquinone bound with chromatophores from Rhodospirillum rubrum. J. Biochem. (Tokyo) 78(4), 795-801 (1975)
28. Graige M. S., Paddock M. L., Feher G., Okamura M.Y. Observation of the protonated semiquinone intermediate in isolated reaction centers from *Rhodobacter sphaeroides*: Implications for the mechanism of electron and proton transfer in proteins. *Biochemistry* 38, 11465-11473 (1999)
29. Paddock M.L., Flores M., Isaacson R., Shepherd J.N., Okamura M.Y. EPR and ENDOR investigation of rhodosemiquinone in bacterial reaction centers formed by B-branch electron transfer. *Appl. Magn. Reson.* 37(1-4), 39-48 (2010)
30. Gerencsér L., Boros B., Derrien V., Hanson D.K. Wraight C.A., Sebban P., Maróti P. Stigmatellin probes the electrostatic potential in the Q_B site of photosynthetic reaction center. *Biophys. J.* 108(2) 379-395 (2015)
31. Yizhar O, Fenno L.E., Davidson T.J., Mogri M., Deisseroth K. Optogenetics in Neural Systems. *Neuron* 71, 9-34 (2011)
32. Leifer A.M., Fang-Yen Ch., Gershow M., Alkema M.J., Samuel A.D.T. Optogenetic manipulation of neural activity in freely moving *Caenorhabditis elegans. Nature methods* 1-8 (2011)

33. den Hollander M.J., Magis J.G., Fuchsenberger P., Aartsma T.J., Jones M.R., Frese R.N. Enhanced Photocurrent Generation by Photosynthetic Bacterial Reaction Centers through Molecular Relays, Light-Harvesting Complexes, and Direct Protein-Gold Interactions. *Langmuir* 27, 10282–10294 (2011)
34. Kondo M., Iida K., Dewa T., Tanaka H., Ogawa T., Nagashima S., Nagashima K.V.P, Shimada K., Hashimoto H., Gardiner A.T., Cogdell R.J., Nango M. Photocurrent and Electronic Activities of Oriented-His-Tagged Photosynthetic Light-Harvesting/Reaction Center Core Complexes Assembled onto a Gold Electrode. *Biomacromolecules*, *13*(2), 432–438 (2012)

8. ATTACHMENTS

PROTON TRANSFER IN BIOENERGETIC PROTEINS

by

ÁGNES MARÓTI MD

Ph.D. Thesis

Submitted in partial fulfilment of the requirements
for the degree of Doctor of Philosophy in Clinical Medicine Sciences
in the Graduate School of the University of Szeged, Hungary

Supervisor: Csaba Bereczki MD, PhD

Head of the Department of Paediatrics

University of Szeged, Hungary

Szeged

2015.

INTRODUCTION

The external energy sources (food) and stimulations (sound, light, etc) are converting to metabolic energy forms and neural responses, respectively, almost exclusively by chemiosmotic mechanisms in which oxidation-reduction (redox) free energy is changed into transmembrane proton (H^+ ion) and electrical gradients (Mitchell's chemiosmotic theory, Nobel Prize 1978) (1). The vast majority of these reactions occur not in solution but in proteins bound to membranes. About one third of all proteins are redox active and an overlapping one third are membrane proteins. The chemistry is performed by various redox and photobiological cofactors (hemes, metal clusters, quinones, flavins, pterins, etc) that are invested with extraordinary properties by the proteins that bind them. The protein-cofactor interactions are the same as those that operate on a substrate in an enzyme active site. The membrane proteins of respiration, photosynthesis, methanogenesis, etc provide ideal systems for studying the catalysis with astonishing specificity and revealing concepts, realities and design that can be related to similar systems of higher complexity. The present dissertation is inspired by that concept and will demonstrate the abundance of this approach.

The transfer of protons in living organisms can be classified into two (not fundamentally different) categories: reactions of 1) acid-base catalysis and 2) proton transport. In the former, the proton transfer events are highly localized and occur generally pair wise between adjacent groups (e.g. an amino acid and a substrate) in the active site. The importance of acid-base catalysis in enzyme activity is well known and documented in several fields of medical sciences including the control of pH balance of blood or gastric juice. In the latter, the transport of protons is usually coupled to electron transfer or conformational changes induced by light (e.g. vision) or hydrolysis of ATP (e.g. gastric proton pump). It is effective over long distance and typical in bioenergetics. The primary purpose of the proton transfer is to translocate protons into and across the membrane, e.g., of the mitochondrion or cells. The transport necessarily involves many elementary proton transfer steps constituting proton delivery pathway in permanent or transiently formed structure of the protein where proton donors and acceptors line up and form bucket-brigade mechanism to transport H^+ ions (2). There are not only energetic constraints (e.g. pathway should be formed) but also kinetic limitations, because usually high rate of proton delivery is needed to reduce the dissipation (losses) of the available free energy by competing additional processes. Below, the transfer of

protons in some selected channels and bioenergetic proteins will be introduced to demonstrate the design of functionality of long distance proton transport of medical (biological) interest (3,4). The criteria of natural design of long distance proton transfer pathways include the need to provide kinetic competence, high selectivity and also the overarching criterion of evolutionary stability or robustness. A comparison of diverse proton conducting materials, from gramicidin to cytochrome oxidase, led to the conclusion that rotationally mobile water is a major constituent of proton pathways, for energetic (especially entropic) reasons, and because it provides substantial immunity to mutational catastrophe.

There are numerous examples for proton transport in bioenergetic proteins of medical interest. *Human carbonic anhydrase* catalyzes the rapid interconversion of carbon dioxide and water to bicarbonate and protons to maintain acid-base balance in blood and other tissues, and to help the transport of carbon dioxide out of the tissues (5). *The H^+/K^+ ATPase proton pump* causes the exchange of a proton against a potassium ion through the membrane (6). This pump is present in the colon, the kidney, but especially the stomach where it is particularly active: controls the secretion of protons into the gastric fluid which becomes acid. It generates a gradient of pH of more than 6 pH units: whereas the blood pH is 7.3 that of the gastric fluid is about 1. The protein *bacteriorhodopsin* relates to vertebrate rhodopsins that sense light in the retina. Although rhodopsins also contain retinal, the functions of rhodopsin and bacteriorhodopsin are different. Bacteriorhodopsin captures light energy and uses it to move protons across the membrane out of the cell (7). The *respiratory cytochrome oxidase* catalyses the reduction of the oxygen molecule in cell respiration and pumps hydrogen ions simultaneously out of the mitochondrion. The overall process leads to generation of an electrical membrane potential and a pH gradient across the membrane, which may be used to form ATP by another enzyme in the same membrane (8).

Bacterial reaction center protein as model system for proton transport

In bacterial reaction center (RC), the H^+ ions are taken up from solution by long range proton transfer over a distance of about 15 Å, and a cluster of ionizable residues near the secondary quinone binding site is known to be involved in this delivery pathway. The bacterial RC provides a unique system to understand the principles of long distance proton transfer. The proton-coupled multielectron reactions, i.e., reactions with intermediate redox states like Q_B (but also others including the water oxidizing complex of Photosystem II and hydrogenases),

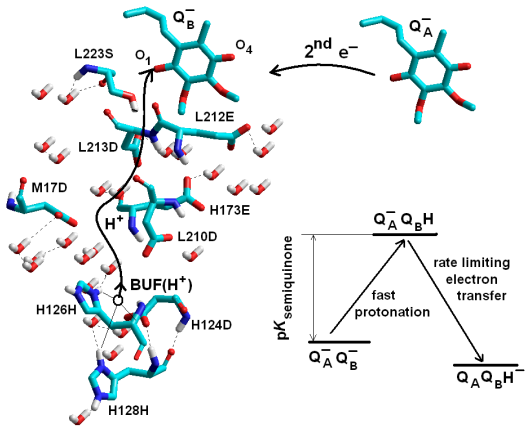

need to protect the cofactors from adventitious electron scavenging reactions. A minimum depth of about 10 Å can be estimated from simple Marcus theory. If the electron transfer is intermolecular, then the Moser-Dutton rule suggests that the distance should not be greater than 15Å, which limits the depth at which the charge accumulating site can be buried. However, if the electron transfer is intramolecular (as for Q_B), the depth is limited only by biosynthetic cost and functional adequacy. This necessitates long distance proton transfer if H^+ ions are involved in the reactions.

Aims

The RC is ideally suited for studying how protein-cofactor interactions induce unique properties in bound cofactors and substrates. We should like to capitalize on these features to investigate how the protein environment controls proton (and electron) transfer and tunes the functional properties of the cofactors with special interest on Q_B. The rich sructural and functional information about the RC provides a unique (model) system for studying the intraprotein proton transport and dielectric responses of proteins. The kinetics of proton transport if it is the rate limiting step, should be sensitive to deuterization i.e. to change of H^+ ions to D^+ ions in the aqueous cytoplasmic phase and to modification of the p*K* value of the quinone at the Q_B binding site. We hope the results will shed some more light to the principles of electron transport coupled proton uptake in bioenergetic proteins.

Materials and methods

Depending on the particular mutation, the mode of growth of photosynthetic non-sulphur purple bacteria *Rhodobacter sphaeroides* varied between anaerobic, semiaerobic and aerobic conditions. In all cases, the basis of the growth medium was Sistrom's minimal medium but with malate used as the carbon source, in place of succinate. The RC protein was isolated and purified by standard biochemical techniques (9-12).

The flash induced electron and proton transfer steps were tracked by optical kinetic absorption spectroscopy. The characteristic optical changes of the individual processes were

detected at the following wavelengths: P^+Q^- → PQ charge recombination (P denotes the bacteriochlorophyll dimer of the RC) at 430 nm (or 860 nm), $Q_A^-Q_B$ → $Q_AQ_B^-$ first interquinone electron transfer at 398 nm and $Q_A^-Q_B^-$ ↔ Q_AQ_B production/disappearance of semiquinones at 450 nm (if the semiquinone is deprotonated (ionic)) and at 420 nm (if the semiquinone is protonated (neutral). Ferricenium/ferrocene redox pair was used as external electron donor to P^+ that showed no spectral disturbance to the semiquinone spectrum in the 400-500 nm spectral range.

Thesis

1. Rhodoquinone bound to the secondary quinone binding site Q_B ceases the physiological activity of the RC. However, the secondary quinine activity can be re-established by single site mutation of isoleucine to threonine at M265 in the primary quinone binding site Q_A. (II. and IV.)

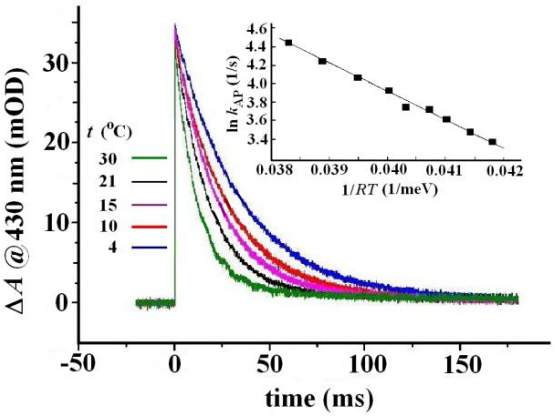

In wild type RC, the midpoint redox potential of the ubiquinone at the Q_B binding site is about 60 mV higher that that of the ubiquinone at the Q_A binding site (pH 8). This potential difference drives the Q_A → Q_B (interquinone) electron transfer. If, however, the native ubiquinone at Q_B is replaced by the low potential rhodoquinone, then no interquinone electron transfer would occur. As the midpoint redox potential of the rhodoquinone is 80-100 mV lower than that of the ubiquinone, the electron transfer from Q_A to Q_B becomes energetically unfavourable. The electron transfer can be reconstituted if the isoleucine at M265 in the Q_A binding pocket is replaced by threonine. The mutation causes a slight conformation change of the alanine at M260 position that reduces the electronegativity and therefore the midpoint potential of the quinone ring of Q_A. The drop is 110 mV (pH 8), that was determined from the temperature-dependence of the $P^+Q_A^-$ → PQ_A charge recombination. In contrast to the wild type RC, the rate of the back reaction of the M265IT mutant demonstrated substantial temperature-dependence in the physiological temperature range which proved that the midpoint potential of Q_A became lower. The $P^+Q_A^-$ → PQ_A charge recombination did not occur directly (via tunnelling as in wild type RC) but indirectly through one of the relaxed

states of P^+I^- (I denotes the bacteriopheophytine in the RC). The drop of the midpoint redox potential generated by mutation at the Q_A site is able to compensate the similar decrease of the midpoint redox potential of Q_B produced by replacement of the native ubiquinone by rhodoquinone at the Q_B binding site. This is the reason why the modified molecular construction can reconstitute the original enzyme activity. Indeed, we could observe all assays that are characteristics of the proper function of the secondary quinone: 1) the $P^+Q_B^-$ → PQ_B charge recombination from the secondary quinone becomes slower than that of the $P^+Q_A^-$ → PQ_A back reaction and shows characteristic pH-dependence, 2) the semiquinone demonstrates binary oscillation upon a series of saturating exciting flashes. From the damping of the binary oscillation, we could derive the degree of reconstitution of the Q_B activity and the one-electron equilibrium constant in the quinone acceptor complex. The reconstitution of the Q_B activity was complete, it was very close (practically identical) to that experienced in wild type RC.

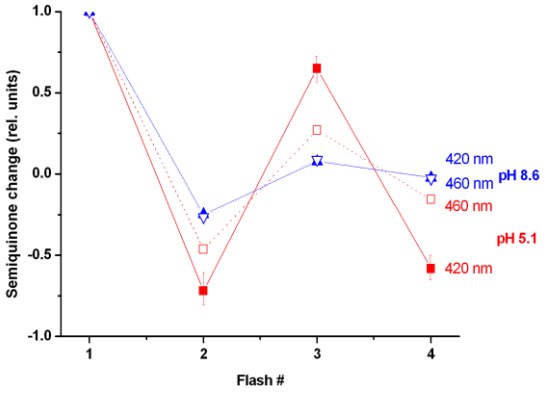

2. The rate of the second electron transfer shows kinetic and equilibrium solvent isotope effects in proton transfer mutants of RC. (I. és III.)

In wild type RC, the transfer of the first proton is much faster than the transfer of the second electron to Q_B i.e. the electron transfer is the rate limiting step in the electron/proton coupled 2^{nd} electron transfer. Therefore, all phenomena that effect the proton transfer only have not influence on the observed 2^{nd} electron transfer. In wild type or electron transfer mutant RCs where the electron transfer is the bottleneck, no solvent isotope effect (change of H_2O to D_2O) can be experienced. However, in proton transfer mutants, where the rate of proton transfer is significantly reduced (even below that of the electron transfer) by mutations, solvent isotope effects can be expected.

We found that the rate of the proton transfer was particularly sensitive 1) to the intactness of the proton gate at the entrance and 2) to the amino acids of the acidic cluster in the vicinity of the secondary quinine. Accordingly, proton transfer mutants can be created by inhibition of the histidine ligand of the proton gate by divalent cations (Cd^{2+} or Ni^{2+}) and/or

by exchange of some key protonatable amino acids (e.g. Glu L212 or Asp L213) to non-protonatable amino acids of similar size in the proton delivery pathway. In these proton transfer mutants, kinetic and equilibrium isotope effects could be observed which were dependent on the prevailing pH and of the location of the mutations. The rate of uptake of the deuterium ions demonstrated particularly large drop in the L213DN mutant relative to that of H^+ ions. The experimentally obtained kinetic solvent isotope effect (the ratio of the rates of proton and deuterium delivery, respectively) approached the theoretical limit (k_H/k_D ~ 6) determined based on a simplified model of the H/D bond vibrations. In addition to the kinetic isotope effect, an equilibrium isotope effect (the shift of the pK values of the protonatable amino acids upon $H^+ \leftrightarrow D^+$ exchange) was also observed with $\Delta pK = pK_D - pK_H < 0.8$ pH unit magnitude.

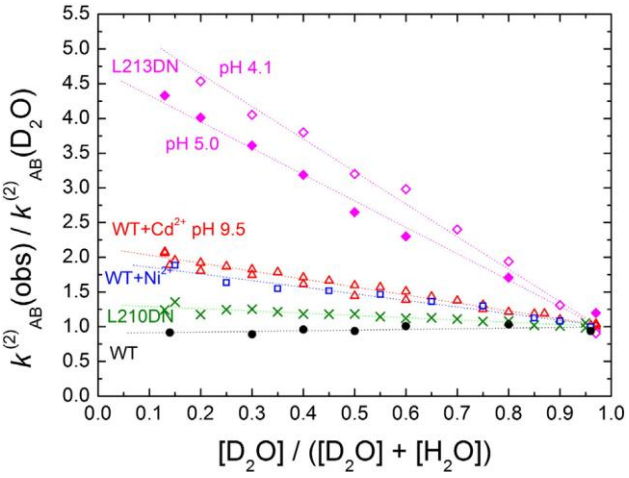

3. The native secondary ubiquinone bound to the Q_B site is strongly acidic (pK<4.5) and the proton affinity of the semiquinone depends on the prevailing pH of the solution and can be modified by exchange of some key protonatable amino acids of the RC to nonprotonatable ones. (I. és III.)

The pK value of the UQ/UQH$^\bullet$ redox pair in mixtures of aqueous or organic solvents is low (p$K \approx 4.0$) and similarly low proton affinity can be predicted in the Q_B binding site of the RC protein. As the standard polarographic or radiolytic measurements do not offer firm results, we applied kinetic spectroscopy combined with solvent isotope and mutational methods to estimate the apparent pK value of the $UQ_B/UQ_BH^\bullet$ redox pair. We came to the conclusion, that the UQ/UQH$^\bullet$ redox partners did not follow a simple Henderson-Hasselbalch type pH-titration as commonly used for acid/base titration in aqueous solutions but the titration is complex. To preserve the Henderson-Hasselbalch equation formally even in this case, a pH-dependent pK value should be assumed. The extension of the concept of the proton equilibrium constant includes that the protonatable group is located in an environment whose structure and electrostatics is not constant but changes upon pH. Our experiments indicate that

the UQ/UQH$^{\bullet}$ redox couple is located in a similar surrounding in the Q_B binding site. It is in strong and pH-dependent interaction with the amino acids of the neighbouring acidic cluster and its formal consequence is the pH-dependent p*K* value in the Henderson-Hasselbalch equation. The mainly carboxyl residues of the amino acids in the cluster become more and more negative upon increase of the pH that causes the extension of the pH-titration of the quinine/semiquinone couple. This rationalizes the slight increase of the p*K* of the $UQ_B/UQ_BH^{\bullet}$ redox pair (~4.5) relative to that of 1,4-benzoquinone reported in solution (4.0).

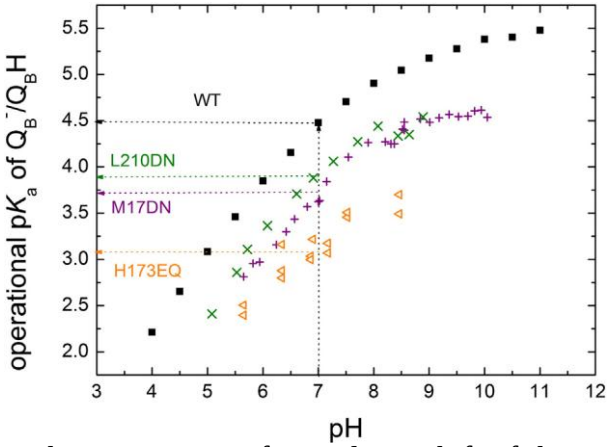

We were able to demonstrate the strong dependence of the p*K* value of the $UQ_B/UQ_BH^{\bullet}$ redox couple on the internal electrostatics the RC modified by mutations. By neutralizing well located negative charge in the protein, significant down-shift of the p*K* values could be detected at pH 7: 4.5 (WT), 3.9 (L210DN), 3.7 (M17DN) and 3.1 (H173EQ).

4. In spite of the very low proton affinity (small p*K*), we were able to observe the stable protonated semiquinone state of the rhodoquinone bound to the Q_B site of the RC. (II. és IV.)

The second electron transfer from Q_A^- to $Q_B^{-\bullet}$ after the second flash will take place only after the $Q_B^{-\bullet}$ semiquinone produced by the first flash has been protonated to $Q_BH^{\bullet}$. In wild type RC, the proton uptake occurs at least one order of magnitude faster (rate $>10^7$ s, pH 8), than the subsequent electron transfer (~10^6 s). However, the proton uptake by the semiquinone is a free energy demanding process (ΔG = 60 meV·(pH−p*K*)), and therefore the entire protonation of $Q_B^{-\bullet}$ can be never achieved. Although the proton equilibrium between the protonated and unprotonated forms is completed within very short time, the protonation equilibrium is shifted toward the unprotonated form, therefore the observed rate of the second electron transfer is much (orders of magnitude) smaller than the that of the "net" electron transfer (without protonation, i.e. at very low pH).

The principal assumption of the mechanism of the proton activated electron transfer is the establishment of protonated semiquinone. Its observation is a great challenge because of

the low p*K* of $Q_B^{-\bullet}/Q_BH^{\bullet}$. By replacement of the native ubiquinone by rhodoquinone at the Q_B site of the M265IT mutant, we managed to detect the protonated (neutral) form of rhodosemiquinone. The spectra of the optical absorption change of the semiquinone produced after even number of flashes (disappeared after odd number of flashes) were recorded in the 400-500 nm spectral range. Two absorption bands with maxima 420 nm (protonated semiquinone) and 450 (deprotonated semiquinone) could be distinguished below pH 5. The neutral species disappeared completely above pH 5.5. The observation of protonated rhodosemiquinone is a direct proof of the proton-activated electron transfer mechanism of the second electron transfer. This is a nice manifestation of the interaction of the electron and proton transfers occurring in many channel mechanisms and bioenergetic proteins of medical interest.

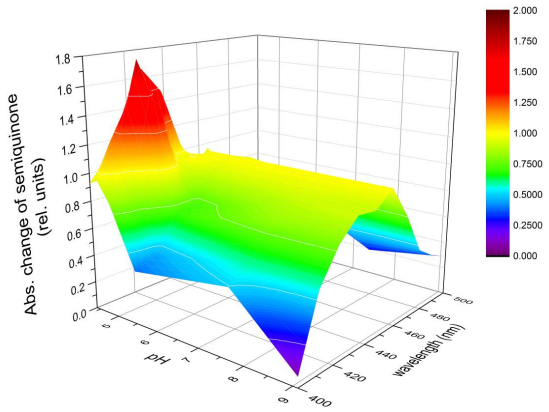

References

1. Mitchell P. *Chemiosmotic Coupling in Oxidative and Photosynthetic Phosphorylation,* Glynn Research Ltd., Bodmin, UK, 1966.
2. Nagle J.F. and Tristam-Nagle S. Hydrogen Bonded Chain Mechanisms for Proton Conduction and Proton Pumping. *J. Membrane Biol.* 74, 1-14 (1983)
3. Wraight C.A. Intraprotein proton transfer - Concepts and realities from the bacterial photosynthetic reaction center. In: Wikström M (ed) Biophysical and Structural Aspects of Bioenergetics, Royal Society of Chemistry, Cambridge, U.K. pp 273-313 (2005)
4. Wraight C. A. Chance and design—proton transfer in water, channels and bioenergetic proteins. *Biochim. Biophys. Acta 1757*, 886–912 (2006)
5. Silverman D.N. and Lindskog S. The Catalytic Mechanism of Carbonic Anhydrase: Implications of a Rate-Limiting Protolysis of Water. *Acc. Chem. Res.* 21, 30-36 (1988)
6. Morii M., Yamauchi M., Ichikawa T., Fujii T., Takahashi Y., Asano S., Takeguchi N. and Sakai H. Involvement of the H_3O^+-Lys-164 -Gln-161-Glu-345 Charge Transfer Pathway in Proton Transport of Gastric H^+,K^+-ATPase. *The Journal of Biological Chemistry*, 283, 16876-16884 (2008)

7. Lanyi J.K. A structural view of proton transport by bacteriorhodopsin, in: M. Wikström (Ed.), Biophysical and Structural Aspects of Bioenergetics, Royal Society of Chemistry, Cambridge, UK, pp. 227–248 (2005)
8. Gennis R.B. Principles of molecular bioenergetics and the proton pump of cytochrome oxidase, in: M. Wikstrom (Ed.), Biophysical and Structural Aspects of Bioenergetics, Royal Society of Chemistry, Cambridge, UK, pp. 1–25 (2005)
9. Maróti P. and Wraight C.A. Flash-induced H^+ binding by bacterial photosynthetic reaction centers: comparison of spectrophotometric and conductimetric methods. *Biochim. Biophys. Acta* 934, 314-328 (1988)
10. Takahashi E., Maróti P. and Wraight C.A. In *Current Research in Photosynthesis* (Baltscheffsky M., Ed.), Kluwer Academic Publishers, Boston, pp 169-172 (1990)
11. Takahashi E. and Wraight C.A. Proton and electron transfer in the acceptor quinone complex of *Rhodobacter sphaeroides* reaction centers: characterization of site-directed mutants of the two ionizable residues, GluL212 and AspL213, in the Q_B binding site. *Biochemistry* 31, 855-866 (1992)
12. Goldsmith J.O. and Boxer S.G. Rapid isolation of bacterial photosynthetic reaction centers with an engineered poly-histidine tag. *Biochim.Biophys. Acta* 1276, 171-175 (1996)

Self publications used in the dissertation

I. Ágnes Maróti, Colin A. Wraight and Péter Maróti: The rate of second electron transfer to Q_B^- in bacterial reaction center of impaired proton delivery shows hydrogen-isotope effect. *Biochim. Biophys. Acta, Bioenergetics,* 1847 (2015) 223–230.
Impact factor: 4.829.

II. Ágnes Maróti, Colin A. Wraight and Péter Maróti: Protonated rhodosemiquinone at the Q_B binding site of M265IT mutant reaction center of photosynthetic bacterium *Rhodobacter sphaeroides. Biochemistry,* American Chemical Society (2015) DOI: 10.1021/bi501553t.
Impact factor: 3.194.

III. Ágnes Maróti, Colin A. Wraight and Péter Maróti: Equilibrium- and kinetic isotope effects of electron transfer in bacterial reaction center of photosynthetic bacteria. COST conference, Visegrád (2014) talk.

IV. Ágnes Maróti, Colin A. Wraight and Péter Maróti: Spectroscopic evidence for protonated semiquinone in reaction center protein of photosynthetic bacteria. Molecular Machines Conference, Ringberg, Germany (2014) poster.

Other scientific activities not strictly connected to the dissertation

Zita Gyurkovits, Ágnes Maróti, Lóránd Rénes, Gábor Németh, Attila Pál, and Hajnalka Orvos: Adrenal haemorrhage in term neonates: a retrospective study from the period 2001–2013

The Journal of Maternal-Fetal Neonatal Medicine, Early Online: 1–4, 2014. DOI: 10.3109/14767058.2014.976550

Impact factor: 1.21

Maróti Ágnes: Inzulinpumpa kezelése és alkalmazása gyermekkorban. *Gyermekorvos Továbbképzés. 2014.*

Cumulativ impact factor: 9.23

Training courses

2007-2011 American – Austrian Foundation, Open Medical Institute, member of the society and coordinator of the Hungarian society.

Seminar in Pediatric Anesthesiology / Critical Care, Salzburg, Austria

Seminar in Pediatric Emergency Medicine, Salzburg, Austria

Seminar in Pediatric Endocrinology and Diabetes, Salzburg, Austria

2010. Andlinger fellowship, Childrens Hospital of Philadelphia, USA

Emergency Medicine, Pediatric Endocrinology and Diabetes

2010. 49th Annual Meeting of the European Society for Paediatric Endocrinology (ESPE), Praha

2013. Graz, University Hospital, Intensive Care Unit, Austria

2013. Great Ormond Street Childerens Hospital, Hiperinsulinaemia Group, London

2014. 50th Annual Meeting of European Association for the Study of Diabetes (EASD), Vienna

PROTONTRANSZFER ENERGIAÁTALAKÍTÓ FEHÉRJÉKBEN

MARÓTI ÁGNES MD

TÉZISEK

a doktori tudományos fokozat (Ph. D.) megszerzésére.

Témavezető: Dr. Bereczki Csaba
az SZTE Gyermekklinika igazgatója

SZTE Doktori Iskola
Klinikai Tudományok Doktori Iskolája
Szegedi Tudományegyetem Gyermekklinika

Szeged
2015.

Bevezetés

A külső energiaforrás (élelem) metabolikus energiaformává vagy a külső inger (hang, fény stb.) neurális válasszá szinte kizárólagosan csak kemiozmotikus mechanizmussal alakul át. Ennek során az oxidációs/redukciós szabadenergia átváltozik membránon keresztüli (transzmembrán) proton (H^+ ion) és elektromos gradienssé (Mitchell-féle kemiozmotikus elmélet, Nobel díj 1978) (1). Az energetikai reakciók döntő többsége nem oldatokban, hanem biomembránokhoz kötött fehérjékben zajlik le. Az összes fehérje kb. harmada redoxi aktív, és ezek harmada membránfehérje. A fizikai és kémiai reakciók azokban a fehérjéhez kötött és fotobiológiai kofaktorokban (hem csoportokban, fémklaszterekben, kinonokban, flavinokban, stb.) játszódnak le, amelyeket a fehérjekörnyezet különleges tulajdonságokkal ruház fel. A légzés, a fotoszintézis, a metántermelés stb. membránfehérjéi ideális rendszerek a nagy bonyolultságú, de részleteiben csodálatraméltóan egyszerű és specifikus katalízis tanulmányozására. Ezt a doktori munkát az a koncepció hozta létre, hogy azt itt megismerhető elvek más hasonló, esetleg még összetettebb (pl. humán) rendszerekben is működnek, és ezáltal ezek-ben tervezhető változtatásokat hajthatunk végre.

Élőlényekben a H^+ ionok (protonok) vándorlásának (egyik csoportról egy másik csoportra való átadásának) két (lényegét tekintve kevéssé különböző) lehetősége merül fel: 1) sav-bázis katalízis és 2) protontranszport. Az első esetben a protonátadás erősen lokalizált, és általában szomszédos párok (pl. egy aminosav és egy szubsztrát) között jön létre a fehérje aktív helyén. A sav-bázis katalízisnek és az enzimek aktivitásában meghatározó szerepének jól dokumentált irodalma van az orvostudományban. Gondoljunk csak a vér vagy a gyomorsav pH értékeinek beállítására és stabilizálására. A hatásmechanizmus felismerése, szabályozása és betegre szabott eredményes alkalmazása több tudományterület közös erőfeszítését feltételezi. A másik esetben, a protontranszporthoz általában elektrontranszport (pl. légzés), konformációváltozás (pl. látás) vagy az ATP hidrolízise (pl. a gyomorsav protonpumpája) kapcsolódik. A protontranszfer nagy hatótávolságú, és a bioener-getikai folyamatokra jellemző mechanizmus. Elsődleges jelentősége abban áll, hogy képes a protonokat a sejtek, mitokondriumok vagy más sejtalkotók memb-ránjainak egyik oldaláról a másikra továbbítani. A protonok az állandósult vagy csak időlegesen felépülő elemek (proton donorok és akceptorok) láncolatán, mint futószalagon haladnak végig (2). A protontranszfer útjában nem csupán energetikai akadályok állhatnak (pl. a lánc szakadozhat, struktúrális

vízmolekulák eshet ki, a protonálható aminosavak a hidrogen-híd kötéstávolságánál messzebbre kerülhet-nek, stb.), hanem kinetikai nehézségek is felmerülhetnek, ha a protontranszfer annyira lelassul, hogy a vele versenyző veszteségi (disszipációs) folyamatok ér-vényre tudnak jutni (3,4).

Az orvos- és élettudományokban számos esetet említhetünk a szabadenergia-átalakító membránfehérjékben vagy membráncsatornákban megvalósuló nagy hatótávolságú protontranszferre. A *human szén-anhidráz enzim* a széndioxidnak és víznek bikarbonáttá való gyors és szabályozott átalakítását katalizálja proton közreműködésével, amivel beállítja a kívánatos sav-bázis egyensúlyt a vérben és más szövetekben (5). A H^+/K^+ *ATPáz protonpumpa* kálium iont cserél proton ellenében a membránon keresztül (6). Ilyen pumpa működik a vastagbélben, a vesében és különösen a gyomorban, ahol több mint 6 pH egység protongrádienst épít ki a vér (pH 7,3) és a gyomorsav (pH 1) között. *Bakteriorodopszin* az emlősök retiná-jában előforduló rodopszinnal ill. a benne levő retinállal hozható kapcsolatba, amely a szem fényérzékenységéért, végső soron a látásért felelős. A bakterio-rodopszin az elnyelt fényenergiát arra használja, hogy a membránon keresztül protonokat pumpáljon ki a sejtből. A protontranszfer protonelektrokémiai grádienst épít ki (7). A légzési *citokróm oxidáz* az oxigénmolekula redukálását katalizálja a sejtlégzés során, és egyidejűleg H^+ ionokat pumpál ki a mitokondriumból (8). A folyamat transzmembrán pH grádienst és elektromos potenciált kelt, amely szabad-energiát egy másik enzim ugyanebben a membránban ATP szintetizálásra használ.

Modell-membránfehérje: bakteriális reakciócentrum-fehérje

A fotoszintetizáló bíborbaktériumok reakciócentruma (RC) ideális membránfehérje a nagy hatótávolságú protontranszfer tanulmányozására, valamint az itt megálla-pított elveknek és következtetéseknek más fehérjékre való alkalmazására. Elsődleges előnyei közé tartozik, hogy a protontranszfer 1) fényimpulzussal (flash-sel) indítható, ami nagy időfelbontást tesz lehetővé, 2) hosszútávú (~ 15 Å), 3) elektron-transzferhez kapcsolható, 4) nyomonkövetésére rutin-szerűvé vált kinetikai, (optikai) spektroszkópiai, és biokémiai mérési módszerek

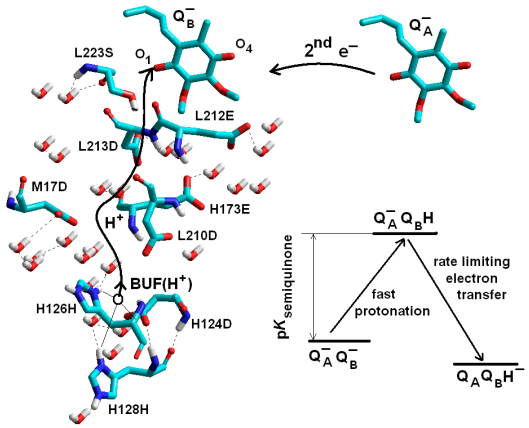

alkalmazhatók és 5) mind a kinetikai, mind a termodinamikai (energetikai) jellem-zői jól kidolgozott mutációs technikákkal tervezhető módon változtathatók.

Célkitűzések

Célul tűztük ki a RC-ban a második fényfelvillanással kiváltott első H^+ ion útjának nyomonkövetését a vizes fázisból a protonkapun belépve a protonálható amino-savak futószalagján keresztül a másodlagos kinonkötőhelyen (Q_B) levő szemi-kinonig. Feladatunk olyan alapkérdések megválaszolása, mint 1) a lánc végi H^+ akceptornak ($Q_B^{-\bullet}$) milyen affinitása van a protonokhoz (mekkora a p*K*-ja), 2) hogyan változik a transzfer sebessége, ha a H^+ iont deuterium ionra cseréljük (oldószer izotóp hatás), és 3) a külső feltételek közül az oldatbeli pH és a szállításban résztvevő aminosavak hogyan határozzák meg a protontranszfert.

Anyagok és módszerek

A *Rhodobacter sphaeroides* nem-kén bíbor baktériumokat vagy fényben és anaerob (levegőtől elzárt) körülmények között szukcináton, mint szénforráson (vad típus) vagy sötétben, rázógépen és szemiaerob körülmények között maláton, mint szénforráson (mutánsok esetén még antibiotikumokon) neveltük (9-11). Az egész sejtekből standard biokémiai fehérje-tisztítási eljárásokkal nyertük ki a reakció-centrum-fehérjét (9,12).

Fényfelvillanással az izolált RC-ban kiváltott elektron- és protontranszfer egyes lépéseit optikai spektroszkópiai eljárásokkal követtük. Az egyes folyamatok jellegzetes abszorpció-változásait az alábbi hullámhosszaknál figyeltük meg: $P^+Q^- \rightarrow PQ$ töltésrekombináció (P a bakterioklorofill dimért jelöli) 430 nm (vagy 860 nm), $Q_A^-Q_B \rightarrow Q_AQ_B^-$ kinonok közötti első elektrontranszfer 398 nm és $Q_A^-Q_B^- \leftrightarrow Q_AQ_B$ (kettős) szemikinon keletkezés/eltűnés 450 nm (ha deprotonált (ionikus) a szemikinon) ill. 420 nm (ha a protonált (semleges) a szemikinon). Ebben a spektrális tartományban más formák is mutathatnak abszorpció-változást, amelyek átlapolva a szemikinon jelét, annak meghatározását nagyban meg-nehezíthetik. A dimér redoxi pár (P/P^+) és az oxidált dimért (P^+) visszaredukáló külső elektron donor redoxi pár (D/D^+, pl. citokróm c^{2+}/c^{3+}) mutatnak különösen zavaró abszorpcióváltozást. Emiatt olyan elektron donort (ferrocén/ferricénium) és olyan koncentrációban alkalmaztunk, amelynek nincs abszorpció-változása a 400-500 nm hullámhossz-tartományban, ill. igazodik a RC-ban lezajló reakciók kineti-kájához és a gerjesztő flash-sorozat által meghatározott feltételekhez.

Tézisek

1. A másodlagos (természetes) ubikinon helyére bekötött rhodokinon megszünteti a RC fiziológiai aktivitását, de helyreállítható az elsődleges kinonkötőhelyen végrehajtott M265IT pontmutációval. (II. és IV.)

Vad típusú RC-ban a Q_B kötőhelyen az ubikinon középponti potenciálja ~60 mV-tal magasabb, mint a Q_A kötőhelyen levő, (kémiailag) ugyanolyan ubikinon potenciálja (pH 8). Ez az energia-különbség a hajtóereje a $Q_A \rightarrow Q_B$ elektrontranszfernek. Ha azonban a Q_B kötőhelyen az ubikinont rhodokinonnal helyettesítjük, akkor megszűnik a két kinon közti elektrontranszfer. Ennek az az oka, hogy a rhodokinon középponti potenciálja 80-100 mV-tal alacsonyabb, mint az ubikinoné, ezzel energetikailag kedvezőtlenné teszi a Q_A-ról a Q_B-ra való elektronátadást. Az elektrontranszfer azonban helyreállítható, ha a Q_A kötőhelyen az M265 izoleucin aminosavat treoninra cseréljük. A mutáció a Q_A-hoz közeli 260-as alanin helyzetét úgy változtatja meg, hogy csökken a kinon gyűrű elektronegativitása és ezzel együtt a középponti potenciálja. A csökkenés 110 mV (pH 8), amelyet a $P^+Q_A^-$ → PQ_A töltésrekombináció sebességének hőmérséklet-függéséből határoz-tunk meg. A vad típustól eltérően, az M265IT mutáns esetén a visszreakció sebes-sége számottevő hőmérsékletfüggést mutatott, amely annak a bizonyítéka, hogy a kinon potenciálja alacsonyabb lett, és a $P^+Q_A^-$ → PQ_A töltésrekombináció már nem direkt (alagutazással, mint a vad típusban), hanem indirekt úton (relaxált P^+I^- állapoton keresztül) megy végbe. Ez a mutációval a Q_A oldalon létrehozott középponti potenciál csökkenés kompenzálni tudja a másik (Q_B) oldalon a rhodokinonnal való helyettesítés miatt bekövetkezett középponti redoxi potenciál csökkenést. Ezzel magyarázható, hogy ez a molekuláris rendszer alkalmas az elektrontranszfer visszaállítására. Valóban, megfigyelhetjük mindazokat a jelensé-geket, amelyek a RC másodlagos kinonjának működésére jellemzők:

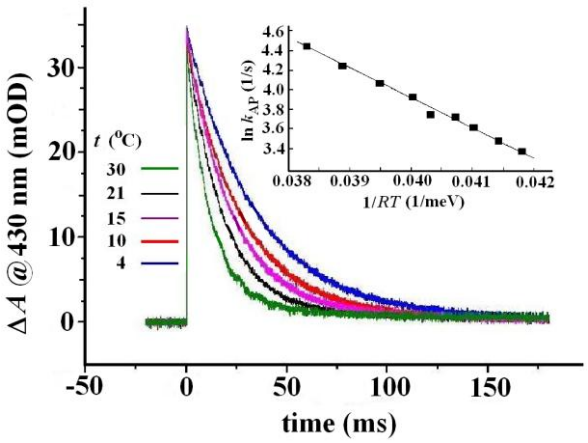

1) a $P^+Q_B^-$ → PQ_B másodlagos kinontól származó töltésrekombináció a $P^+Q_A^-$ → PQ_A visszreakcióhoz képest lelassul, sebessége jellegzetes pH-függést mutat, 2) ismételt fény-

gerjesztésekkel a szemikinon binárisan oszcillál. Az oszcilláció csillapodásából egyrészt a Q_B aktivitás helyreállításának mértékére, másrészt a kinonok közötti egy-elektron egyensúlyi állandóra következtethettünk. Azt tapasztaltuk, hogy a RC másodlagos kinonjához köthető funkciók a vad típuséval megegyező szintre álltak vissza, azaz a rekonstrukció teljes volt.

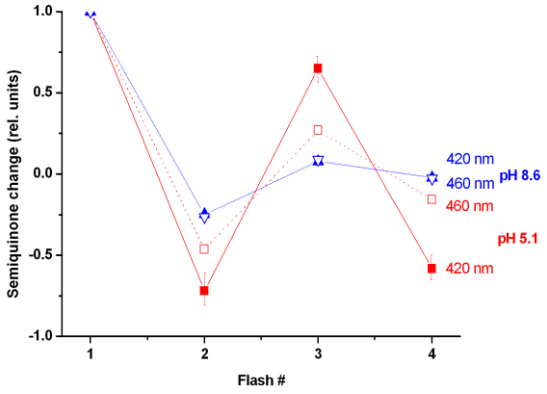

2. A második elektrontranszfer sebessége oldószer izotóp effektust mutat a RC proton-transzfer mutánsaiban. (I. és III.)

Vad típusú RC-ban a második flash után a proton transzfer sokkal gyorsabb, mint az elektron transzfer, azaz az elektron átadás a sebességmeghatározó lépés. Emiatt olyan hatások, amelyek a protontranszfer sebességét érintik, nem mutatkoznak a megfigyelt transzfersebességben. Oldószer izotóp-effektus, azaz a természetes víznek (H_2O) nehézvízre (D_2O) cserélése a vad típusú RC-ban (ill. az olyan (ú.n. elektrontranszfer)-mutánsokban, ahol az elektrontranszfer továbbra is (a proton-transzferéhez képest) lassú marad) semmiféle hatást nem fejt ki. Ha ellenben olyan mutánsokat hozunk létre, amelyek a protonátadás sebességét jelentősen (jóval az elektrontranszfer sebessége alá) csökkentik, akkor már várható izotóp oldószer-hatás.

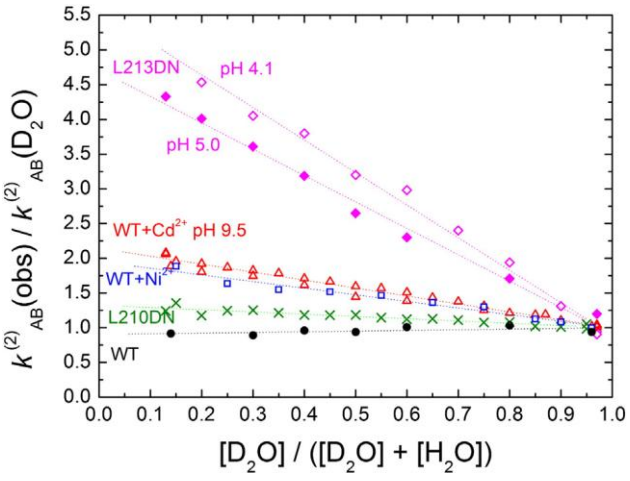

Azt találtuk, hogy a protontranszfer sebessége különösen érzékeny egyrészt az ú.n. protonkapu összetételére, másrészt a Q_B körüli savas klaszter egyes protonálható aminosavjaira. A protonkapunak diva-lens kationokkal (Cd^{2+} ionnal vagy Ni^{2+} ionnal) való blokkolása és/vagy a protonútba eső aminosavaknak (az L212 glutaminsavnak vagy az L213 aszparaginsavnak) nem protonálható aminosavakra való kicserélése protontranszfer mutánsokat hozott létre. Az így módosított RC-ban a protontranszfer mutáció típusától és a pH-től függő oldószer izotóp hatás lépett fel. A deutériumfelvétel sebessége az

L213DN mutánsban különösen nagy esést mutatott a protonfelvétel sebességéhez képest. A kísérletileg meghatározott oldószer izotóp effektus (a H^+ és D^+ ionok megfigyelt transzfer-sebességeinek aránya) egy egyszerűsített modellel kiszámítható elméleti határt ($k_H/k_D \sim 6$) megközelítette. A kinetikai izotóp effektus mellett egyensúlyi izotóp hatást (a protonálható csoportok p*K* értékeiben való eltolódást, $pK_D - pK_H$) < 0,8 pH egység nagyságrendben is megfigyeltünk.

3. A másodlagos ubikinon erősen savas jellegű (p*K*<4.5), p*K*-ja az oldat pH-jával és a fehérje egyes kitüntetett aminosavjainak cseréjével változtatható. (I. és III.)

Az UQ/UQH$^\bullet$ redoxi pár (szerves és vizes) oldatbeli p*K* értéke igen alacsony (p*K* ≈ 4,0), és hasonlóan csekély proton affinitást mutat a RC fehérje Q_B kötőhelyén. Ennek megállapítására a szokásos polarografikus vagy radiolitikus mérések vagy nem alkalmazhatók vagy csak kevéssé megbízható eredményeket adnak. Mi az $UQ_B/UQ_BH^\bullet$ redoxi pár pK értékére ill. annak változására a különböző mutánsokon elvégzett kinetikai, spektroszkópiai és izotóphelyettesítési méréseinkből következtettünk. A legfontosabb megállapításunk szerint a UQ/UQH$^\bullet$ redoxi pár nem egy egyszerű Henderson-Hasselbalch egyenlet szerint titrálódik, mint ahogy azt a közönséges savak (bázisok) esetén azok vizes oldataiban megszoktuk, hanem a titrálási görbe összetett. Ha mégis formálisan meg szeretnénk tartani a Henderson-Hasselbalch egyenletet a pH-titrálás leírására, akkor ezt csak annak árán tehetjük meg, hogy a protonálható csoport p*K* értékét pH-függőnek vesszük. Ez az általánosítás azt veszi figyelembe, hogy a protonálható csoport egy olyan kör-nyezetben van, amelynek térbeli és legfőképp elektrosztatikai szerkezete nem állandó, hanem a pH változásával folyamatosan változik. A UQ/UQH$^\bullet$ redoxi pár ilyen helyen van a RC Q_B kötőhelyén, hiszen vele a környező savas klaszter erősen pH-függő kölcsönhatást létesít, amelynek formális következménye a pH-függő p*K* érték. Mivel a főleg karboxil csoportot tartalmazó klaszterbeli aminosavak a növekvő pH-val egyre inkább negatív töltésűekké válnak, ezek hatása kvalitatívan a kinon/szemikinon pár p*K* értékének megemelését, ezzel a pH-titrálás „elnyújtását” okozzák. Emiatt (is) mérhetünk a $UQ_B/UQ_BH^\bullet$ redoxi pár p*K* értékére egy kissé magasabb (~4,5) értéket, mint amit pl. az 1,4-benzokinon esetén oldatban megfigyelhetünk (4,0). Bemutattuk, hogy a $UQ_B/UQ_BH^\bullet$ redoxi pár p*K* értéke erősen függ a RC fehérje szerkezetétől. A szerkezet (esetünkben elsősorban az elektrosztatikus térkép) megváltoztatását azonban nem csak a pH változtatásával, hanem néhány kulcsfontosságú aminosav jól

irányzott cseréjével (mutációjával) is előállíthatjuk. Azt kaptuk, hogy a vad típusban mért 4,5 p*K* érték egy-egy negatív töltésű amino-savnak semleges (és közel azonos térigényű) társra való cseréjével 3,9 (L210DN), 3,7 (M17DN) vagy 3,1 (H173EQ) értékre csökkenhet pH 7-nél. (Ne feledjük, hogy itt látszólagos p*K* értékekről beszélünk, amely adatok a pH 7-nél mért fehérje konfigurációra vonatkoznak).

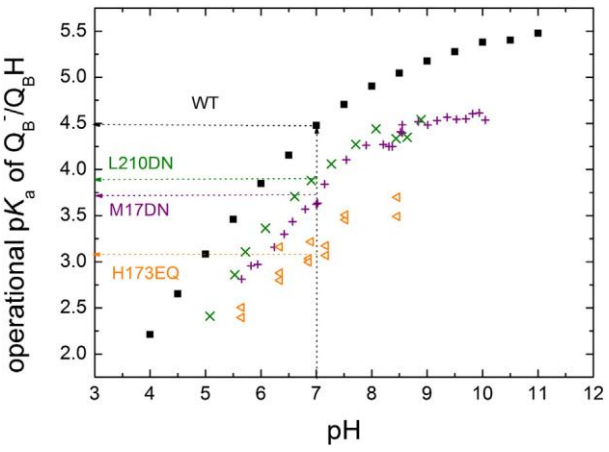

4. A kis protonaffinitás (alacsony p*K*) ellenére sikerült stabil és protonált rhodoszemikinont a másodlagos kinonkötőhelyen megfigyelni. (II. és IV.)

A Q_A és Q_B kinonok között a második elektron (a második flash után) csak akkor adódik át, ha ezt megelőzően az első fényfelvillanással létrehozott Q_B^- szemikinon protont vesz fel. Vad típus esetén a H^+ ion bekötése legalább egy nagyságrenddel gyorsabban következik be (>10^7 s, pH 8), mint az ezt követő elektrontranszfer (~10^6 s). A szemikinon protonációja azonban szabadenergia igényes folyamat (ΔG = 60 meV·(pH−p*K*)), és emiatt messze nem teljes mértékű, noha a mindenkori egyensúlyi helyzet a protontált és a deprotonált formák között nagyon gyorsan beáll. Az elektrontranszfer megfigyelhető sebességét (az általában igen alacsony a protonegyensúlyi állandó jelentékenyen csökkenti a „tiszta" elektronátadás sebességéhez képest.

Az ilyen proton-aktivált elektrontranszfer mechanizmus érvényesülése szempontjából kruciális jelentőségű a protonált szemikinon forma kísérletes megfigyelése, mert ez az elektrontranszfer kiindulási anyaga (prekurzora). A detektálás elsősorban azért nehéz, mert az ubikinon/ubiszemikinon redoxi pár p*K*-ja a fehérje Q_B kötőhelyén igen alacsony (<4.5), és az erősen savas tartományban az izolált RC könnyen instabillá válik. Megbízható mérést akkor várhatunk, ha a natív ubikinont olyan kinon-származékkal helyettesítjük a RC Q_B kötőhelyén, amelynek magasabb a p*K*-ja. Erre a célra rhodokinont választottunk, és sikerült annak protonált formáját megfigyelni. Felvettük az első (és minden további páratlan számú) flash után *keletkező* ill. a második (és minden további páros számú flash után *eltűnő*) szemirhodokinon optikai abszorpciós spektrumát a 400-500 nm közötti hullámhossz-

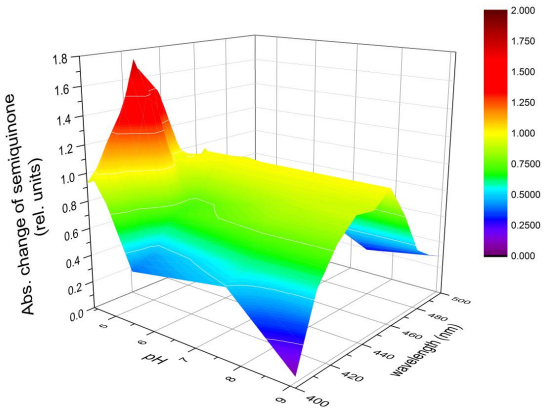

tartományban. A spektrumban két abszorpciós sáv különült el 420 nm és 450 nm körüli maximumokkal, amely komponensek a protonált (anionikus) ill. a deprotonált (ionikus) rhodoszemikinonra jellemzők. A proto-nált forma jól felismerhető volt a pH<5 tartományban, és teljesen eltűnt pH>5.5 értékeknél. A protonált rhodoszemikinon megfigyelése egyértelmű kísérleti bizonyítéka annak, hogy proton-aktiváció előzi meg, és teszi lehetővé a második elektron átadását. Ez eklatáns példája a fehérjéken belüli proton- és elektron-transzferek kölcsönös feltételezésének.

Irodalom

1. Mitchell P. *Chemiosmotic Coupling in Oxidative and Photosynthetic Phosphorylation*, Glynn Research Ltd., Bodmin, UK, 1966.
2. Nagle J.F. and Tristam-Nagle S. Hydrogen Bonded Chain Mechanisms for Proton Conduction and Proton Pumping. *J. Membrane Biol.* 74, 1-14 (1983)
3. Wraight C.A. Intraprotein proton transfer - Concepts and realities from the bacterial photosynthetic reaction center. In: Wikström M (ed) Biophysical and Structural Aspects of Bioenergetics, Royal Society of Chemistry, Cambridge, U.K. pp 273-313 (2005)
4. Wraight C. A. Chance and design—proton transfer in water, channels and bioenergetic proteins. *Biochim. Biophys. Acta 1757*, 886–912 (2006)
5. Silverman D.N. and Lindskog S. The Catalytic Mechanism of Carbonic Anhydrase: Implications of a Rate-Limiting Protolysis of Water. *Acc. Chem. Res.* 21, 30-36 (1988)
6. Morii M., Yamauchi M., Ichikawa T., Fujii T., Takahashi Y., Asano S., Takeguchi N. and Sakai H. Involvement of the H_3O^+-Lys-164 -Gln-161-Glu-345 Charge Transfer Pathway in Proton Transport of Gastric H^+,K^+-ATPase. *The Journal of Biological Chemistry*, 283, 16876-16884 (2008)
7. Lanyi J.K. A structural view of proton transport by bacteriorhodopsin, in: M. Wikström (Ed.), Biophysical and Structural Aspects of Bioenergetics, Royal Society of Chemistry, Cambridge, UK, pp. 227–248 (2005)

8. Gennis R.B. Principles of molecular bioenergetics and the proton pump of cytochrome oxidase, in: M. Wikstrom (Ed.), Biophysical and Structural Aspects of Bioenergetics, Royal Society of Chemistry, Cambridge, UK, pp. 1–25 (2005)
9. Maróti P. and Wraight C.A. Flash-induced H^+ binding by bacterial photosynthetic reaction centers: comparison of spectrophotometric and conductimetric methods. *Biochim. Biophys. Acta* 934, 314-328 (1988)
10. Takahashi E., Maróti P. and Wraight C.A. In *Current Research in Photosynthesis* (Baltscheffsky M., Ed.), Kluwer Academic Publishers, Boston, pp 169-172 (1990)
11. Takahashi E. and Wraight C.A. Proton and electron transfer in the acceptor quinone complex of *Rhodobacter sphaeroides* reaction centers: characterization of site-directed mutants of the two ionizable residues, GluL212 and AspL213, in the Q_B binding site. *Biochemistry* 31, 855-866 (1992)
12. Goldsmith J.O. and Boxer S.G. Rapid isolation of bacterial photosynthetic reaction centers with an engineered poly-histidine tag. *Biochim.Biophys. Acta* 1276, 171-175 (1996)

A tézisekben felhasznált saját publikációk

I. Ágnes Maróti, Colin A. Wraight and Péter Maróti: The rate of second electron transfer to Q_B^- in bacterial reaction center of impaired proton delivery shows hydrogen-isotope effect. *Biochim. Biophys. Acta, Bioenergetics,* 1847 (2015) 223–230.
Impakt faktor: 4.829.

II. Ágnes Maróti, Colin A. Wraight and Péter Maróti: Protonated rhodosemiquinone at the Q_B binding site of M265IT mutant reaction center of photosynthetic bacterium *Rhodobacter sphaeroides. Biochemistry,* American Chemical Society (2015) DOI: 10.1021/bi501553t.
Impakt faktor: 3.194.

III. Ágnes Maróti, Colin A. Wraight and Péter Maróti: Equilibrium- and kinetic isotope effects of electron transfer in bacterial reaction center of photosynthetic bacteria. COST konferencia, Visegrád, 2014. előadás.

IV. Ágnes Maróti, Colin A. Wraight and Péter Maróti: Spectroscopic evidence for protonated semiquinone in reaction center protein of photosynthetic bacteria. Molecular Machines Conference, Ringberg, Germany, 2014. poszter.

Az eddigi egyéb (nem szorosan a tézisekhez tartozó) tudományos tevékenységem

Zita Gyurkovits, Ágnes Maróti, Lóránd Rénes, Gábor Németh, Attila Pál, and Hajnalka Orvos: Adrenal haemorrhage in term neonates: a retrospective study from the period 2001–2013

The Journal of Maternal-Fetal Neonatal Medicine, Early Online: 1–4, 2014. DOI: 10.3109/14767058.2014.976550

Impakt faktor: 1.21

Maróti Ágnes: Inzulinpumpa kezelése és alkalmazása gyermekkorban. *Gyermekorvos Továbbképzés. 2014.*

Összesített impakt faktor: 9.23

Külföldi tanulmányutak

2007-2011 American – Austrian Foundation, Open Medical Institute, tag és a szervezet magyar koordinátora, az alábbi szemináriumokon való részvétel (előadásokkal):

Seminar in Pediatric Anesthesiology / Critical Care, Salzburg, Ausztria

Seminar in Pediatric Emergency Medicine, Salzburg, Ausztria

Seminar in Pediatric Endocrinology and Diabetes, Salzburg, Ausztria

2010. Andlinger ösztöndíj, Childrens Hospital of Philadelphia, USA

Emergency Medicine, Pediatric Endocrinology and Diabetes

2010. 49th Annual Meeting of the European Society for Paediatric Endocrinology (ESPE), Prága

2013. Graz, University Hospital, Intensive Care Unit, Ausztria

2013. Great Ormond Street Childerens Hospital, Hiperinsulinaemia Group, London

2014. 50th Annual Meeting of European Association for the Study of Diabetes (EASD), Bécs

Full text publications of the candidate

I.

Ágnes Maróti, Colin A. Wraight and Péter Maróti:

The rate of second electron transfer to Q_B^- in bacterial reaction center of impaired proton delivery shows hydrogen-isotope effect.

Biochim. Biophys. Acta, Bioenergetics, 1847 (2015) 223–230.

Impact factor: 4.829

Biochimica et Biophysica Acta 1847 (2015) 223–230

Contents lists available at ScienceDirect

Biochimica et Biophysica Acta

journal homepage: www.elsevier.com/locate/bbabio

The rate of second electron transfer to Q_B^- in bacterial reaction center of impaired proton delivery shows hydrogen-isotope effect

Ágnes Maróti [a], Colin A. Wraight [b,c,1], Péter Maróti [d,*]

[a] Department of Pediatrics, University of Szeged, Hungary
[b] Center for Biophysics and Computational Biology, University of Illinois, Urbana, IL 61801-3838, USA
[c] Department of Plant Biology, University of Illinois, Urbana, IL 61801-3838, USA
[d] Department of Medical Physics, University of Szeged, Hungary

ARTICLE INFO

Article history:
Received 2 September 2014
Received in revised form 31 October 2014
Accepted 5 November 2014
Available online 13 November 2014

Keywords:
Bacterial photosynthesis
Reaction center protein
Flash-induced proton delivery
Protonation mutant
Solvent isotope effect

ABSTRACT

The 2nd electron transfer in reaction center of photosynthetic bacterium *Rhodobacter sphaeroides* is a two step process in which protonation of Q_B^- precedes interquinone electron transfer. The thermal activation and pH dependence of the overall rate constants of different RC variants were measured and compared in solvents of water (H_2O) and heavy water (D_2O). The electron transfer variants where the electron transfer is rate limiting (wild type and M17DN, L210DN and H173EQ mutants) do not show solvent isotope effect and the significant decrease of the rate constant of the second electron transfer in these mutants is due to lowering the operational pK_a of Q_B^-/Q_BH: 4.5 (native), 3.9 (L210DN), 3.7 (M17DN) and 3.1 (H173EQ) at pH 7. On the other hand, the proton transfer variants where the proton transfer is rate limiting demonstrate solvent isotope effect of pH-independent moderate magnitude (2.11 ± 0.26 (WT + Ni^{2+}), 2.16 ± 0.35 (WT + Cd^{2+}) and 2.34 ± 0.44 (L210DN/M17DN)) or pH-dependent large magnitude (5.7 at pH 4 (L213DN)). Upon deuteration, the free energy and the enthalpy of activation increase in all proton transfer variants by about 1 kcal/mol and the entropy of activation becomes negligible in L210DN/M17DN mutant. The results are interpreted as manifestation of equilibrium and kinetic solvent isotope effects and the structural, energetic and kinetic possibility of alternate proton delivery pathways are discussed.

1. Introduction

Proton transfer reactions (acid-base catalysis in enzyme activity [1] or transport of protons over large distances in bioenergetics [2]) are of crucial significance in biology [3]. They need well defined atomic structure (gramicidin [4] and carbonic anhydrase [5]), substantial energetic constraints (aquaporin [6]) and, in many cases, are coupled to conformation changes (bacteriorhodopsin [7]) or electron transfer [8] (cytochrome oxidase [9] and oxygen evolution [10] and quinone reduction cycle of photosynthesis [11]) in the protein. In photosynthetic reaction center (RC) from purple bacteria, the proton coupled electron transfer is evoked by two subsequent saturating flashes and results in full reduction of quinone (Q) at the secondary quinone binding site Q_B: $Q + 2e^- + 2H^+ \rightarrow QH_2$ [12]. The same proton path, formed by acidic cluster around Q_B is used to deliver protons both on the first and on the second electron transfers (Fig. 1, [13,14]). The nature of the proton accepting group(s), however, is quite different. On the first flash, the protons are accepted by an array of ionizable residues in the cluster as their pK_a values increase in response to the Q_B^- formation [15–17]. On the second flash, the proton is trapped at any pH by Q_B^- itself. The rate of the $Q_A^-Q_B^- + H^+ \rightarrow Q_AQ_BH^-$ second electron transfer depends on the free energy gap $\Delta G_{AB}^{(2)}$, as has been shown by driving force assay using RC preparations with Q_A replaced by low-potential quinones [18]. This finding has been interpreted as an evidence of a fast, non-rate-limiting protonation of a semiquinone anion ($Q_B^- + H^+ \rightarrow Q_BH$) followed by a rate-limiting nonadiabatic ET reaction ($Q_BH \rightarrow Q_BH^-$) with rate constant $k_{et}^{(2)}$ (Fig. 2, [13,18]). Thus, the 2nd electron transfer proceeds with an observed rate of

$$k_{AB}^{(2)} = k_{et}^{(2)} \cdot f(Q_BH), \quad (1)$$

where $f(Q_BH)$ is the fraction of the semiquinone in the protonated state.

In contrast to the first electron transfer, there is no conformational control on the second electron transfer. It is not surprising, because both Q_B^- and the ubiquinol-anion Q_BH^- are likely to be fixed in similar positions [19]. However, the contribution of the protonic relaxation to the kinetics of the 2nd electron transfer is an open question. Due to the low pK_a value of the Q_B^-/Q_BH couple, the absence of a notable protonic relaxation can be expected in wild type and in mutants where

Abbreviations: ET, electron transfer; PT, proton transfer; P, bacteriochlorophyll dimer; Q_A and Q_B, primary and secondary quinone acceptors, respectively; RC, (bacterial) reaction center

* Corresponding author at: Department of Medical Physics, University of Szeged, Rerrich Béla tér 1, Szeged, H-6720 Hungary. Tel.: +36 62 544 120; fax: +36 62 544 121.
E-mail address: pmaroti@sol.cc.u-szeged.hu (P. Maróti).

[1] Passed away on 10 July 2014. This work is dedicated to his memory.

http://dx.doi.org/10.1016/j.bbabio.2014.11.002
0005-2728/

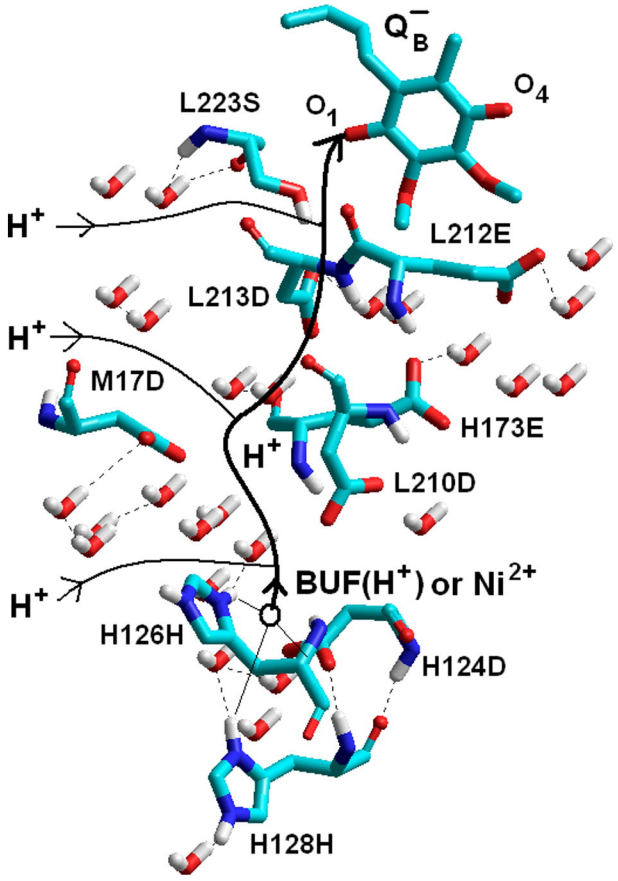

Fig. 1. Key protonatable amino acids and water molecules of the proton delivery pathway from the proton entry point BUF(H^+) to Q_B^- semiquinone after the second flash in native RC of *R. sphaeroides*. The proton transport is severely impaired by ligation of divalent transition metal ions (e.g. Ni^{2+}) to the H126H/H128H/H124D cluster or by replacement of the protonatable amino acids to nonprotonatable residues by single (or double) mutations. The alternative (by-pass) proton pathways are connected to the main pathway above the deletion sites.
The structure was taken from Brookhaven Protein Databank 3I4D (www.rcsb.org).

the electron transfer is the rate limiting step. On the other hand, in mutants of PT limitation, the rate becomes independent of $\Delta G_{AB}^{(2)}$ [20] and thereby the proton relaxation control over the second electron transfer might be imposed.

The recognition of protonic relaxation modes could be facilitated by the notion that the protonic component should depend on the H/D isotope substitution as shown below by two examples: 1) The slow (1–30 μs) phase of the reduction of the photo-oxidized primary donor of the photosystem II ($P680^+$) by a redox-active tyrosine Y_Z is sensitive to the H/D substitution and has been attributed to the protonic relaxation [21]. 2) The two hydrogen-bonded protons associated with Q_A of reaction centers from *Rhodobacter sphaeroides* can be exchanged with deuterons from solvent D_2O. The rate of $P^+Q_A^- \rightarrow PQ_A$ electron-transfer, k_{PA} was found to increase slightly with deuterium exchange up to a maximum $k_{PA}(D^+)/k_{PA}(H^+) = 1.06$ [22]. The solvent isotope effect indicates that these protons play a role in the vibronic coupling associated with electron transfer of charge recombination.

These examples indicate that there seems to be great potential in H/D exchange experiments while light-induced proton binding/unbinding is taking place in bacterial RC. Incubation in D_2O caused pH (pD)-dependent slowing of the H^+/D^+ binding rate after the first flash [23]. A maximum isotope effect of the apparent proton binding rate constant $k_{on}(H)/k_{on}(D) = 3.0$ was found. It is worth to carry out similar isotope measurements with the 2nd ET of various proton transfer RC variants. These RCs impede the normal fast function of the bucket brigade mechanism of PT at well defined locations: native RC treated with divalent metal ions at the proton entry point [24,25], L210DN/M17DN double mutation between L210D and M17D [26,27] and L213DN single mutation at L213 close (<5 Å) to Q_B [20,28]. The proton delivery with significantly increased free energy of activation will be the bottle neck of the observed 2nd ET (Fig. 2). The proton equilibrium partitioning (see Eq. (1)), and therefore the fraction of protonated sites of Q_B^- may be affected by H/D exchange (equilibrium isotope effect). Additionally, if proton pathways are limited by bond-breaking steps, the observed rate will be sensitive to deuteration of the RC (kinetic isotope effect). These effects can be used to elucidate the PT mechanisms including rate limiting steps, transition states and alternate pathways.

2. Materials and methods

2.1. Reagents and reaction centers

Ethanolic solutions of ferrocene, ethyl ferrocene and DAD (diaminodurene) were prepared fresh prior use. Cytochrome-*c* (horse heart grade VI) was reduced (>95%) by hydrogen gas on platinum black and filtered (0.2 μm pore size acetate filter). Experiments were carried out in mixture (2–2 mM) of buffers (citric acid, Mes, Mops, Pipes, Tris, Ches and Caps) whose pK_a values are close to the pH value of the solution.

Details of the molecular biological techniques in generating *Rhodobacter (R.) sphaeroides* with mutant RCs have been described earlier [28]. Reaction centers from *R. sphaeroides*, strain R-26, wild type and mutants were isolated in LDAO (lauryldimethylamine *N*-oxide) as described earlier [29]. The RC was concentrated to ~100 μM by centrifugation (Amicon Centricon-30) and dialyzed 1–2 days at 4 °C against 1 mM Tris buffer (pH 8.0) and 0.03% Triton X-l00 detergent before use. As RCs isolated this way showed little secondary quinone activity, it was reconstituted by addition of ubiquinone-10 solubilized in ethanol in large excess ([UQ]/[RC] >10) to RC prior to use.

2.2. Electron transfer measurements

Kinetics of flash-induced ET was measured by absorption changes using a single beam spectrophotometer of local design [29]. The rates of charge recombination ($P^+Q_B^- \rightarrow PQ_B$) were obtained by monitoring the recovery of the dimer (P) absorbance at 430 nm, following a saturating exciting flash. The concentration of RCs was determined using an extinction coefficient of 26 $mM^{-1}\,cm^{-1}$. The occupancy of the Q_B site (typically ~90% at pH 8.0) was determined from the relative amplitudes of the slow and fast kinetic phases of charge recombination [30].

The rate constants of the second ET to Q_B^- were determined by monitoring the decay of absorbance of the semiquinones (Q_A^- and Q_B^-) at wavelength 450 nm following a second saturating flash in RC solution containing an exogenous reductant to reduce the oxidized dimer P^+. Depending on the magnitude of $k^{(2)}{}_{AB}$, different donors were applied to reduce P^+: mammalian cytochrome *c* or cytochrome c_2 (fast donation) and ferrocene (slow donation at low (2–10 μM) concentrations and fast donation at high (400 μM) concentration) [31]. With the use of different donors, their disadvantages were tried to minimize. A small fraction of cytochrome c^{2+} under our conditions did follow a relatively slow photo-oxidation (in the range of several hundreds of microseconds) after the second flash, and it could have kinetic contribution to the observed absorption change at 450 nm. To avoid the overlap in the (sub) millisecond range, ferrocene, a much slower donor than the cytochrome c^{2+} was also applied. Although the redox changes of ferrocene do not have contribution in this optical range, the observed kinetics includes the large absorption change from P/P^+ and its separation from that of Q/Q^- needs careful multiexponential peeling of the traces carried out by Marquardt's least square method.

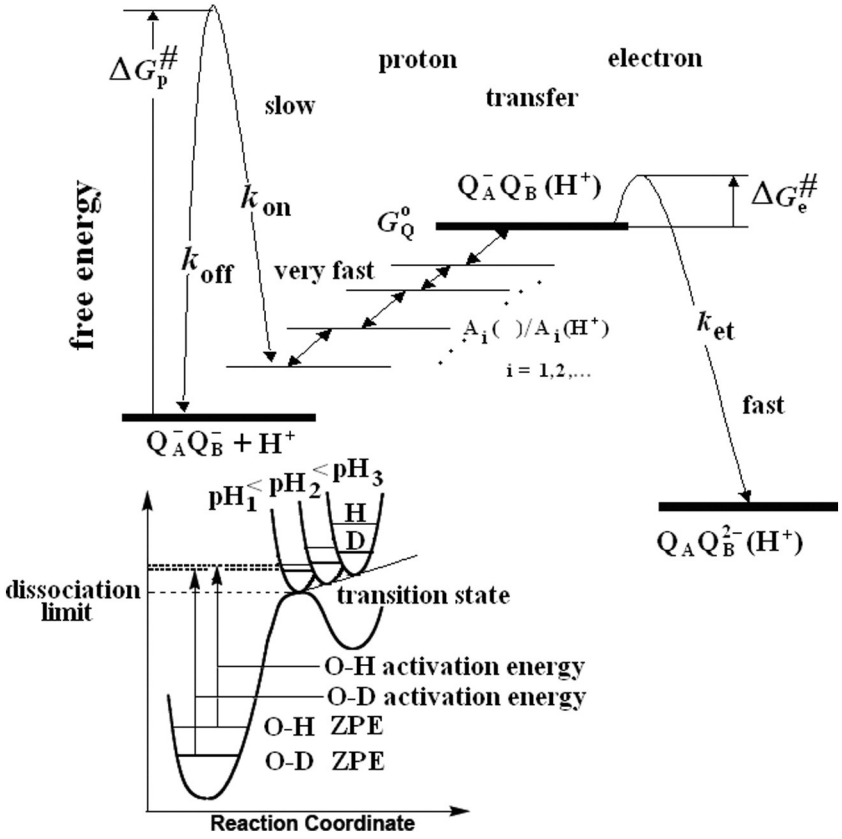

Fig. 2. Proton coupled second ET in bacterial RC. The fast interquinone ET (k_{et}) is preceded by faster (WT) or slower (PT variants) proton equilibration with Q_B^-. The rate limiting step of proton delivery to Q_B^- is attributed to enhanced proton free energy of activation ($\Delta G_p{}^{\#}$) with k_{on} and k_{off} forward and back PT rate constants, respectively. Depending on mutations and ways of impedance in the proton pathway, the bottle neck can occur in different locations (amino acids, A_i) of the proton delivery network. Kinetic solvent isotope effect is attributed to difference of the zero point energies in the reactant and transition states that can show pH-dependence. Notations: G^o_Q — standard free energy level of semiquinone at Q_B, A_i — intermediate protonatable residue (amino acid or water) in the chain and ZPE — zero point energy of O – H(D) vibration.

The PT mutants (e.g. L213DN) can trap Q_B^- very effectively and the relaxation to the PQ_AQ_B state is very long [20,28]. Therefore, most measurements were performed with a fresh sample for each measurements.

2.3. Hydrogen isotope measurements

The rate constants of $k^{(2)}_{AB}$ are sensitive to measurement conditions (RC preparation, pH, detergent concentration, etc.) and their standard deviation can be commeasurable to the isotope effect, i.e. the difference between rates measured in water and heavy water. Instead of comparative measurements on two separately prepared samples, the RCs from a highly concentrated stock (>300 μM) in H_2O (or D_2O) were diluted into D_2O (or H_2O) gradually while the salt and detergent concentrations were held constant. The observed rates were plotted as a function of dilution and a linear fit to the measured rates offered $k^{(2)}_{AB}(D)$ and $k^{(2)}_{AB}(H)$ as interception at heavy water ($[D_2O] / ([D_2O] + [H_2O]) = 1$) and normal water ($[D_2O] / ([D_2O] + [H_2O]) = 0$), respectively. The isotope effect is characterized by the negative slope of the straight line, i.e. $k^{(2)}_{AB}(H)/k^{(2)}_{AB}(D)$.

All pH(D) measurements were made with a glass electrode (Radiometer, Copenhagen, Denmark) and were reported in D_2O as pD = apparent pH + 0.40, to indicate the corrected D^+-ion concentration for the glass electrode solvent isotope artifact [32,33]. The "apparent pH" means the actual pH meter reading. Deuterated acid (DCl) and base (NaOD) were used for pD adjustment. The glass electrode had been standardized with conventional buffer mixtures (in H_2O) at pH 7.0 and 11.0 (alkaline range) or 4.0 (acidic range).

3. Results

3.1. Rate constant of second electron transfer, $k^{(2)}_{AB}$ and operational pK_a of Q_B^-/Q_BH

The proton-coupled ET rate constant $k^{(2)}_{AB}$ ($Q_A^-Q_B^- + H^+ \rightarrow Q_AQ_BH^-$) was measured by monitoring the absorption changes at 450 nm due to the simultaneous disappearance of two semiquinones (Q_A^- and Q_B^-) after the second saturating flash in the presence of an exogenous donor. The donor was selected to make the electron donation to the RC either faster (cytochrome c^{2+}) or slower (various ferrocene compounds at low concentrations) than the second ET because of kinetic separation of the second ET from P^+ donation (cyt c^{2+} $P^+ \rightarrow$ cyt c^{3+}P) and/or elimination of the charge recombination ($P^+Q_A^-Q_B^- \rightarrow PQ_AQ_B^-$). The rate constant $k^{(2)}_{AB}$ measured in native RC was not dramatically affected in L210DN, M17DN and H173EQ electron transfer mutants (Fig. 3a). The decrease from the native value was small (about 3-fold) in L210DN and M17DN mutants but significantly larger (about 200-fold) in H173EQ mutant. In contrast, the PT mutants (L213DN single mutant and L210DN/M17DN double mutant together with native RC poisoned by transient divalent ions) show much larger (up to 4 orders of magnitude) decrease relative to that of the native value (Fig. 3b) in nice agreement with earlier measurements [20,26].

The pH profiles of $k^{(2)}_{AB}$ of electron and proton transfer limited RCs show marked differences. The logarithms of $k^{(2)}_{AB}$ of PT variants display (with good approximation) linear pH dependence throughout the entire pH range from 4 to 9. The electron transfer RC mutants, however, describe monotonously decreasing function with gradually increasing slope: it is

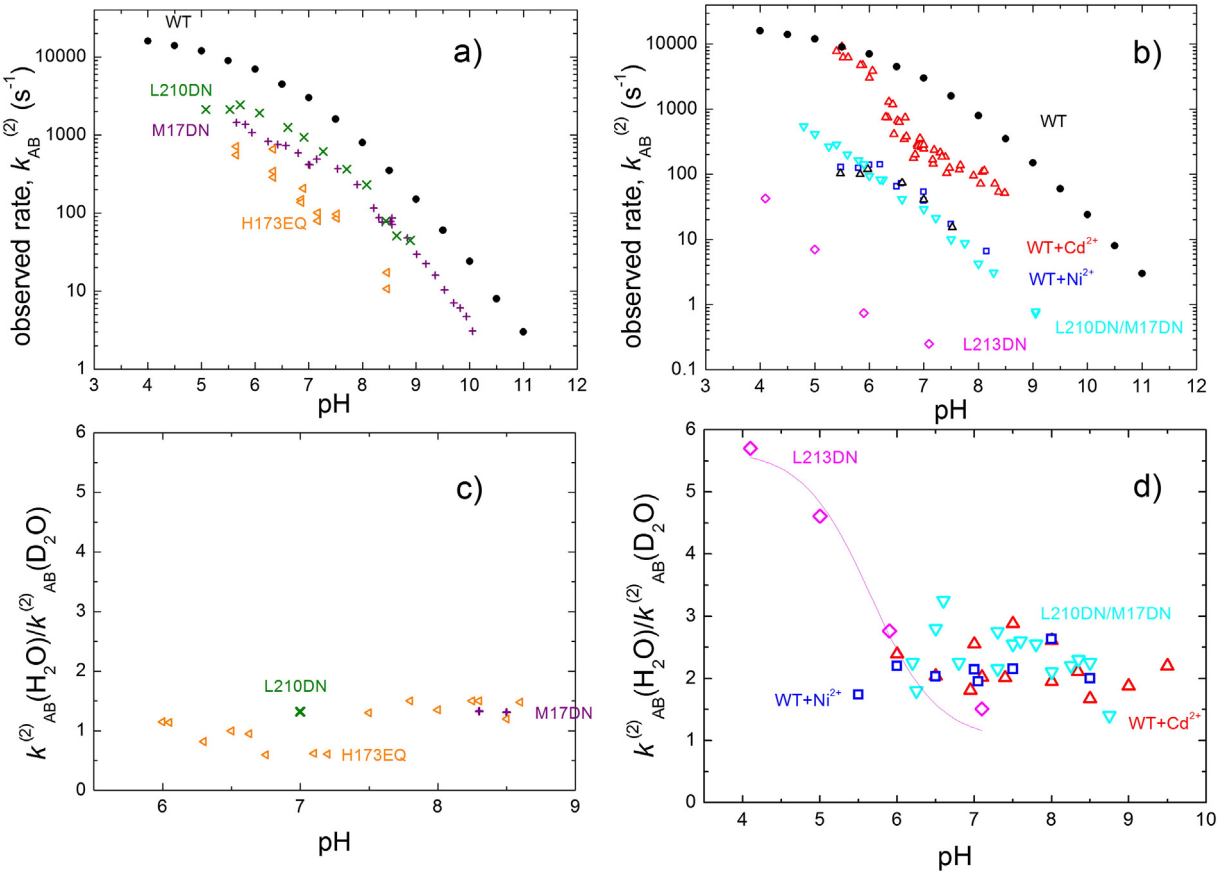

Fig. 3. pH dependence of the observed rate constants ($k^{(2)}_{AB}$, panels a and b) and solvent isotope effect ($k^{(2)}_{AB}(H)/k^{(2)}_{AB}(D)$, panels c and d) of second ET for various RC strains of ET (panels a and c) and PT (panels b and d) limitation. The pH-dependence of the isotope effect in the L213DN mutant is approximated by a Henderson–Hasselbalch function with amplitude of 5.7 and pK_a = 5.65 (panel d). Symbols: ● (WT), □ (WT + Ni^{2+}), △ (WT + Cd^{2+}), ◊ (L213DN), × (L210DN), + (M17DN), ◁ (H173EQ) and ▽ (L210DN/M17DN). Conditions: 1.0–4.0 μM RC, 0.02% Triton X-100, 40 μM UQ_{10}, 5 mM KCl, T = 293 K, 2–2 mM buffer mix, 20 μM cyt c^{2+} or 2–8 μM/300–500 μM (ethyl-, methyl)ferrocene (depending on $k^{(2)}_{AB}$, see Materials and methods) and 100 μM $CdCl_2$ or 1 mM $NiCl_2$ in metal treated WT RC.

small in the acidic pH range, becomes more pronounced in the neutral and slightly alkaline pH regions and approaches the limiting value of −1 in the highly alkaline pH range. The measured rates are pH-dependent because the population of Q_BH is pH dependent. In native (and other ET mutant) RCs, the rate limiting ET is preceded by very fast proton equilibrium $Q_A^- Q_B^- + H^+ \leftrightarrow Q_A^- Q_BH$. In the simplest case, the protonated fraction, $f(Q_BH)$ follows the Henderson–Hasselbalch equation, but the complex electrostatics of the protein interior results in an extended pH-dependence [17] that can be formally approximated by a Henderson–Hasselbalch function with pH-dependent (operational) pK_a values:

$$f(Q_BH) = \frac{10^{pK_a(pH)-pH}}{1+10^{pK_a(pH)-pH}} \quad (2)$$

By inserting Eq. (2) into Eq. (1) and taking $k^{(2)}_{et} = 1 \cdot 10^6\ s^{-1}$ [34], the pH-dependence of the operational pK_a of Q_BH can be derived from the measured $k^{(2)}_{AB}$ values in wild type and some other ET mutant RCs (Fig. 4). At pH 7, the operational pK_a values of the native semiubiquinone-10 are 4.5 (WT) [34–36], 3.9 (L210DN), 3.7 (M17DN) and 3.1 (H173EQ) which are in good accordance with values obtained from temperature dependence of the second ET [37]. In absence of any electrostatic interactions between RC and Q_B^-, one would expect a constant pK_a value throughout the pH scale. This is clearly not the case. In the acidic pH range, the increase of the operational pK_a is steep (close to 1) and levels off in the alkaline pH region.

3.2. Solvent isotope effect of $k^{(2)}_{AB}$

The solvent isotope effect was studied by comparison of $k^{(2)}_{AB}$ measured in water (H_2O) and in heavy water (D_2O) under otherwise identical conditions. The proton → deuterium exchange in the protein was initiated at t = 0 by injecting the concentrated stock of RC into

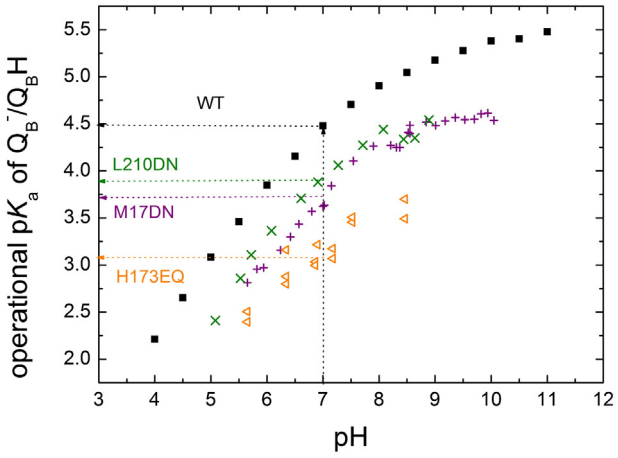

Fig. 4. pH-dependence of the operational pK_a values of Q_B^-/Q_BH calculated from the rate constants of the second ET limited by ET (Fig. 3a) according to Eqs. (1) and (2). The rate constant of intrinsic ET was taken $k^{(2)}_{et} = 1 \cdot 10^6\ s^{-1}$ [34]. The operational pK_a values for some ET mutants at pH 7 are indicated by arrows.

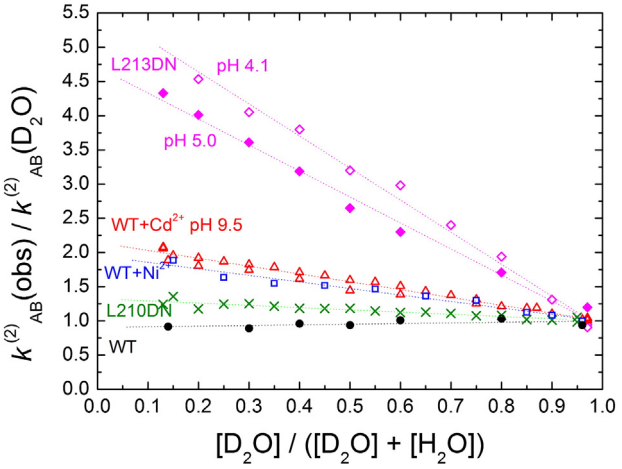

Fig 5. Solvent isotope effect of $k^{(2)}_{AB}$ of WT RC (●), L210DN (×) and proton transfer variants WT+Ni^{2+} (□), WT+Cd^{2+} (△) and L213DN (◊, pH 4.1 and ◆, pH 5.0) in mixture of water (H_2O) and heavy water (D_2O). Proton ↔ deuterium exchange was carried out by repeated dilution of the RC stock solutions in H_2O or D_2O by D_2O or H_2O, respectively.

D_2O (Fig. 5). The isotope shift due to deuteration of the protonatable groups in the proton delivery pathway occurred "promptly" (i.e., within 2 h [23]) and no further changes in the rate of the second ET were observed after prolonged (24 h) incubation in D_2O. The reaction mixture was split into two equal parts and they were diluted repeatedly by D_2O and H_2O, respectively. The concentration of the ingredients (detergent, salt and buffers) remained unchanged during the dilution. The D_2O content of the sample could change between >95% and ~10% at the beginning and at the end of the dilution, respectively. The dilution carried out in the reverse direction offered similar results: the observed $k^{(2)}_{AB}$ decreased in a linear manner with increase of the D_2O content of the solvent. The intersections of the best fit straight line to the data at 0% D_2O (H) and 100% D_2O (D) deliver $k^{(2)}_{AB}$(H) and $k^{(2)}_{AB}$(D) and their ratio measures directly the solvent isotope effect.

As expected, there is no solvent isotope effect in native RC (Fig. 5) and the ET mutants show also negligible isotope effect, e.g. 1.11 ± 0.33 for the H173EQ mutant (Fig. 3c). In contrast to the wild type and ET mutants, the PT variants demonstrate marked but moderately large solvent isotope effects (Fig. 3d): 2.11 ± 0.26 (WT + Ni^{2+}), 2.16 ± 0.35 (WT + Cd^{2+}) and 2.34 ± 0.44 (L210DN/M17DN double mutant) and do not depend on pH. The L213DN mutant shows unique features: in the strongly acidic pH range (pH ≈ 4), the solvent isotope effect is large (≈6) which drops progressively upon increase of the pH to a low (≈1.4) value that approaches the isotope effect of proton/deuterium diffusion in aqueous solution.

3.3. Temperature-dependence of $k^{(2)}_{AB}$ in proton transfer variants

The observed large change of the rate constant of the second ET in different RC variants can be attributed to change of the free energy of activation ($\Delta G^{\#}$). Lower rate corresponds to higher free energy change of activation and the correlation is logarithmic. According to the transition state theory (TST [38]),

$$k^{(2)}_{AB} = \frac{k_B T}{h} \exp\left(\frac{-\Delta G^{\#}}{RT}\right), \quad (3)$$

where T is the temperature, h denotes the Planck's constant and k_B and R are the Boltzmann factor and universal gas constant, respectively. (The transmission coefficient is taken 1.) The function of $\ln\left(\frac{k^2_{AB} \cdot h}{k_B T}\right)$ vs. $1/T$ should give a straight line of slope ($=-\Delta H^{\#}/R$) characteristic to the change of activation enthalpy, $\Delta H^{\#}$ and intersection ($=-\Delta S^{\#}/R$) characteristic to the change of activation entropy, $\Delta S^{\#}$ (Eyring plot). The observed activation parameters relate to the rate limiting step of $k^{(2)}_{AB}$. As the second ET is a combination of electron and proton transfer reactions, the observed activation may correspond to either electron or proton reactions. In PT mutants, the analysis is simplified as the measured change of activation free energy (enthalpy and entropy) relates to the bottle neck of the series of protonation steps in the proton delivery pathway.

Fig. 6 demonstrates the Eyring plot of the PT variant of the L210DN/M17DN double mutant in the physiological temperature range. The measured points fit to a straight line with $\Delta G^{\#} = 15.6$ kcal/mol, $\Delta H^{\#} = 10.1$ kcal/mol and $T \cdot \Delta S^{\#} = -5.52$ kcal/mol activation free energy, enthalpy and entropic energy, respectively, at room temperature and pH 7.5. As the PT is the rate limiting step of $k^{(2)}_{AB}$, one can expect effect of proton → deuterium exchange in the protein. Indeed, significant modification of the activation parameters is observed after deuteration of the sample. Somewhat less, but still considerable changes can be seen upon isotope (deuterium) exchange in other protonation RC variants investigated in this study: WT + Cd^{2+}, WT + Ni^{2+} and L213DN (Fig. 7). In all cases, the activation parameters of the free energy and enthalpy shift to larger values and the entropic contributions become smaller after deuteration. As expected, the WT RC has much less free energy and enthalpy of activation and shows no isotope effect.

4. Discussion

In native RC, the second interquinone ET occurs after very fast partial proton uptake by Q_B^-. In various PT variants used in this study the proton delivery to Q_B^- can be slowed down dramatically and will become the rate determining step of the ET. Under these conditions, the exchange of hydrogen to deuterium in solvent and RCs imposes reversible isotope effects of $k^{(2)}_{AB}$: upon dilution in H_2O and ultrafiltration of the RCs, the rate constant can be restored to a value typically measured in H_2O. The discussion will extend on the origin, magnitude and pH dependence of the observed isotope effect found in the various RC variants and will cover the structural and energetic aspects of the possible alternative proton delivery pathways to Q_B^-.

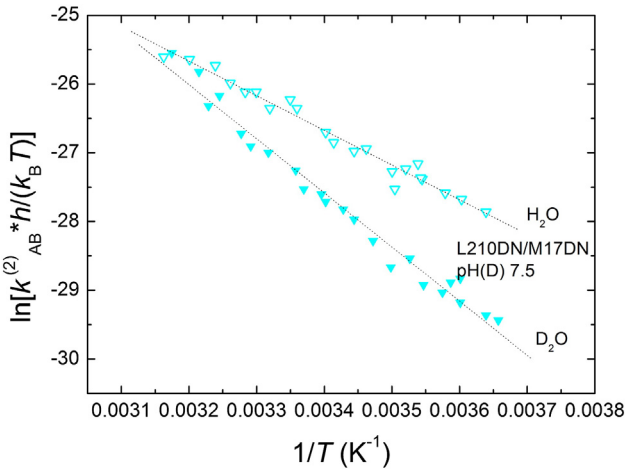

Fig. 6. Temperature dependence (Eyring plot) of the rate constants of the second ET ($k^{(2)}_{AB}$) in RC of double mutant L210DN/M17DN in water (H_2O, ▽) and heavy water (D_2O, ▼). Activation enthalpy change (slope): $\Delta H^{\#} = 10.1$ kcal/mol (H_2O) and 15.6 kcal/mol (D_2O), activation entropy change (intersection): $T \cdot \Delta S^{\#} = -5.5$ kcal/mol (H_2O) and −0.47 kcal/mol (D_2O) and activation free energy change: $\Delta G^{\#} = 15.6$ kcal/mol (H_2O) and 16.1 kcal/mol (D_2O). Conditions: 1.0 μM RC, 0.02% Triton X-100, 40 μM UQ_{10}, 5 mM NaCl, 2.5 mM Mops, 2.5 mM Tris, pH(D) 7.50 and 300 μM ethyl ferrocene. Notations: h — Planck's constant and k_BT — Boltzmann term.

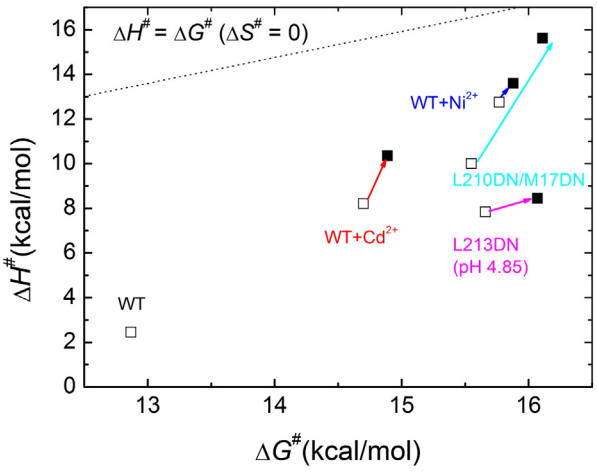

Fig. 7. Eyring (transition state theory) activation parameters ($\Delta H^{\#}$ vs. $\Delta G^{\#}$) of the second ET of RCs of PT variants (open symbols) and transitions due to deuteration (closed symbols). The states of no entropic changes are indicated by a straight line.

4.1. The origin of solvent isotope effect of $k^{(2)}_{AB}$ in RC

The observed rate of the second ET is the combination of the rates of protonation of the slowest step (the sum of binding and unbinding rates: $k_p = k_{on} + k_{off}$) and the interquinone ET, k_{et}. According to the reaction scheme in Fig. 2,

$$k^{(2)}_{AB} = \frac{k_{on} + k_{off} + k_{et} - \sqrt{(k_{on} + k_{off} + k_{et})^2 - 4 \cdot k_{on} \cdot k_{et}}}{2}. \quad (4)$$

In ET limit ($k_p \gg k_{et}$), we obtain $k^{(2)}_{AB} = k_{et}/(1 + k_{off}/k_{on})$ that is equivalent with Eq. (1). No isotope effect is expected unless k_{off}/k_{on} that relates to the proton dissociation constant of the semiquinone Q_B^- might show up equilibrium isotope effect. This effect, however, is negligible ($pK_D - pK_H < 0.1$), as very small if any isotope effect is observed in the ET mutants (Fig. 3c).

In PT limit ($k_p \ll k_{et}$), Eq. (4) offers $k^{(2)}_{AB} = k_{on}$ which means that the observed rate is determined by the rate constant of proton (deuterium) binding only. In this extreme case, $k^{(2)}_{AB}$ might be sensitive to changes due to deuteration (discussed below). In intermediate case, when the rates of protonation and ET are commeasurable, the isotope effect describes transition between the maximum (PT limit) and minimum (ET limit) values. The transition function can be derived from Eq. (4).

In PT variants, $k^{(2)}_{AB}$ is significantly (2–3 orders of magnitude) smaller than in native RC. The decreased rate, however, does not include necessarily that the RC variant should be a PT mutant. In ET limit, $k^{(2)}_{AB}$ decreases if the protonated fraction of Q_B^- decreases (see Eq. (1)). This can be achieved by lowering the (operational) pK_a of Q_B^-/Q_BH. Our results showed that the decrease could be substantial in different ET mutants (Fig. 4). Accordingly, the observed rate can be as low as experienced in PT mutants. In H173EQ mutant, $k^{(2)}_{AB}$ is greatly inhibited and drops to a value as low as that of the native RC treated by transition metal ion (Figs. 3a and b). Although H173EQ appears to be a borderline in terms of ET vs. PT rate limitation, it remains ET mutant [3]. The effect of mutation on the PT rate is indeterminate and could be essential. This view is supported by independent methods of ET measurements [39] and driving force assay [13,18].

The solvent isotope effect on the rate constant of the second ET exhibits features indicating that the observed kinetics are not caused by an elementary process such as the shift of pK_a values of the protonatable groups upon solvent deuteration (equilibrium isotope effect) or the unimolecular dissociation of an COO – H bond of an carboxylic group (kinetic isotope effect). Based on our experiments, we are led to conclude that the measured isotope effects in different RC variants may reflect several elementary processes.

Due to severe interruption of the protonation pathway by mutation or by divalent cations at the proton entry point, the Q_B^- semiquinone anion is protonated by any of the much slower alternative pathways controlled by a protonatable amino acid (A) in equilibrium with the aqueous bulk phase: $AH \leftrightarrow A^- + H^+$. The rate of protonation that limits the rate of the second ET $k^{(2)}_{AB}$ is $k_p = k'_{on} \cdot [H^+] + k_{off}$, where k'_{on} is the bimolecular rate constant of proton binding (values of $2–6 \cdot 10^{10}$ M^{-1} s^{-1} are commonly found for neutralization of strong bases [40]) and k_{off} is the rate constant of proton dissociation. The ratio $K_H = k_{off}/k'_{on}$ gives the proton dissociation constant. If the equilibrium partition between protonatable residue and solvent is sensitive to hydrogen isotopes, then equilibrium isotope effect is observed whose magnitude and pH-dependence can be expressed as

$$\frac{k^{(2)}_{AB}(H^+)}{k^{(2)}_{AB}(D^+)} = \frac{k'_{on}(H^+)}{k'_{on}(D^+)} \cdot \frac{\left(1 + 10^{pK_H - pH}\right)}{\left(1 + 10^{pK_D - pH}\right)} \cdot 10^{pK_D - pK_H}. \quad (5)$$

The bimolecular rate constants of H^+/D^+ binding are controlled by diffusion, intraprotein electrostatics and/or protein conformation and its sensitivity to H/D exchange should be minor [23]. According to Eq. (5), the magnitude of the solvent isotope effect is negligible ($k^{(2)}_{AB}(H^+)/k^{(2)}_{AB}(D^+) \approx 1$) at low pH ($\ll pK_H$ or pK_D) and approaches monotonously to the maximum value of $10^{(pK_D - pK)_H}$ at high pH ($\gg pK_H$ or pK_D). The transition occurs in two steps at pH ≈ pK_H and pH ≈ pK_D and above these pH values the isotope effect becomes pH-independent. Similar behavior is observed for PT agents M17DN/L210DN double mutant and metal poisoned native RC: the isotope effect is relatively small and pH-independent on the pH range between 5.5 and 9.5 (Fig. 3d). Good correspondence with the theory of equilibrium isotope effect is obtained by assumption of highly acidic residue ($pK_H \ll 5.5$) and of relatively small increase of pK_H upon deuteration ($pK_D - pK_H \approx 0.3$). The intraprotein conditions of the RC are adequate to satisfy these assumptions. The Q_B binding pocket is rich of carboxylic acid residues and the members of the acidic cluster can supply proton for the alternative pathways. The validity of the second assumption can be supported by previous experiments. The alkaline protonatable groups responsible for binding of the first proton upon $P^+Q_A^-$ formation demonstrated small increases in the p*K*a (~0.2) and a small, pH (pD)-dependent slowing of the binding rate after incubation in D_2O [23]. Although not the same groups participate in the uptake of the first and second protons, the effect of deuteration of RC on binding of the H^+/D^+ ions after the first flash can be informative on the same effect after the second flash.

Large solvent isotope effect was observed in L213DN PT mutant (Fig. 3d) that calls for a X-H(D) bond-breaking step characteristic of the kinetic isotope effect. The origin of the primary isotope effect is the difference in the frequencies of various vibrational modes of the residue, arising when H is substituted for D (Fig. 2). The large kinetic isotope effect is due to the large percentage mass change upon replacement of hydrogen with deuterium. At ambient temperature, the vibrational modes for bond stretches are dominated by the zero-point energy (ZPE). The O – H(D) bond of interest is 100% broken at the dissociation limit. In this case, the maximum possible isotope effect can be calculated from the difference of the ZPE values of the OD and OH vibrations:

$$\frac{k_H}{k_D} = \exp\left(-\frac{h\ c\ \overline{\nu_H}\left(\sqrt{\frac{\mu_{OH}}{\mu_{OD}}} - 1\right)}{2\ k_B\ T}\right) \quad (6)$$

where h is the Planck constant, c is the speed of light in vacuum, $\overline{\nu_H}$ is the wave number of O – H stretch and $\mu_{OH} = 1.06$ and $\mu_{OD} = 1.78$ are the

reduced (atomic) masses. The actual k_H/k_D ratio depends also on the ZPE values of the intermediate protonation states of the proton delivery pathway from the bulk to Q_B^-. If the transition state is very close to the dissociation limit, i.e. the O – H(D) bond breaks upon proton transfer nearly completely, then Eq. (6) would give a reasonable approximation to the upper limit of the kinetic isotope effect. Taking $\overline{\nu_H} = 3200\ cm^{-1}$ for the wave number of vibration of the O – H bonds of macromolecular association with carboxylic acid, Eq. (6) offers $k_H/k_D = 6.0$ for the maximum primary isotope effect at room temperature ($T = 293$ K).

Such a high value was obtained for the L213DN mutant in the highly acidic pH range only and in all other cases the measured isotope effects were smaller. Although the deceleration of the ET in RCs blocked with different transient divalent metal ions (Ni^{2+} and Cd^{2+}) were different (Fig. 3b), they gave similar solvent isotope effects ($k_H/k_D \approx 2.1$). This indicates that the observed isotope effects reflect changes upon deuteration in the protein rather than the mode of sealing of the proton entry point. It can occur that the PT reactions do not involve bonds that are completely broken in the transition state (the O – H bond is only partially broken) and/or another is starting to form at the transition state. Both attenuate the isotope effect from that of total homolysis used to approximate the maximum isotope effect.

To understand the pH-dependence of the isotope effects in the L213DN mutant, the ZPE of the various vibrations of the reactant and the activated complex should be compared. Primary kinetic isotope effect is observed if the ZPE difference in the activated complex/transition state is smaller than in the reactants, resulting in a difference in activation energy between O – H and O – D (Fig. 2). The magnitude of a primary kinetic isotope effect depends on differences in the ZPE's in the reactant and the activated complex for all the vibrational modes of the reactant and activated complex. In L213DN mutant, the ZPE levels of O – H and O – D vibration profile of the transition state exhibit pH-dependence in a manner of monotonous increase of the ZPE difference at higher pH. The pH-drop of the observed kinetic isotope effect can be formally approximated by a Henderson–Hasselbalch curve centered at pH 5.65 (Fig. 3d). It looks like the deprotonation of a protonatable group of $pK_a = 5.65$ would control the vibrational energy profile of the rate-determining residue in the PT. The identification of this residue and characteristics of the interaction are beyond the capacity of our work.

4.2. Changes of thermodynamics upon deuteration

Fundamental thermodynamic analysis of the second ET in PT variants can contribute to deeper understanding of the PT mechanism. The breakdown of the temperature-dependence into total enthalpy and entropy of activation has proved highly suggestive (Figs. 6 and 7), although the enthalpy and entropy contributions of the $P^* \rightarrow P^+Q_A^-$ free energy drop seriously challenged existing notions [41,42]. The wild type shows a rather small activation enthalpy that is not influenced by H/D exchange of the solvent. Any manipulations of the proton pathway by mutation or by divalent cations result in a larger net enthalpy of activation and less negative entropy. This partial offset is almost certainly not a significant "enthalpy–entropy compensation" [43,44]. The tendency remains the same upon deuteration: the enthalpy increases further and the entropy becomes less negative. The change caused by H/D exchange is small in RC inhibited by Ni^{2+} and large in L210DN/M17DN double mutant where the activation process is almost entirely enthalpic. The small entropy of activation indicates no major conformational changes of the protein upon proton delivery and accounts for slight rearrangement of the hydrogen bonded network, including solvent water, as has been well supported for carbonic anhydrase [45] and superoxide dismutase [46] and almost visualized in bacteriorhodopsin [7]. The L213DN mutant shows somewhat different behavior. The entropic contribution is larger and indicates different kinds of limitation. The L213DN is the most drastically PT limited of any known mutant and is blocked at a site nearer the Q_B quinone. Alternate PT pathway directed either to L223S or to L212 behind L213 should be activated that can include H^+/D^+ binding, per se, in the rate limiting step.

4.3. Alternate proton pathways

As the rates of PT are dramatically decreased in PT mutants compared to that in native RC, the importance of alternate proton pathways should increase [15–17]. The alternate routes do not satisfy the very strict conditions of fast proton delivery operating in native RC. The H-bond network of protonatable residues and water molecules can be less tightly coupled and can be shorter than the length of the native pathway (~20 Å). They can lead directly to O1 of Q_B via L212E/L223S or connect to the main pathway after the site of inhibition (Fig. 1). The magnitude and pH-independence of the solvent isotope effect were similar in RCs blocked by divalent cations at the proton entry point and by double mutations at L210D and M17D sites (Fig. 3d). This suggests that several (at least two) parallel alternate routes are operational in the pathway regions near the proton entry point that rescue the PT to Q_B^- in inhibited RCs. Other routes in the interior of the protein can also contribute to the PT process where other acidic residues (e.g. H173E) and water molecules become active. The cost of the rescue of proton delivery by alternate pathways is the highly reduced transfer rate.

The L213DN mutant blocks the natural proton pathway at a site closest to the quinone and demonstrates distinct behavior. In this case, the measured $k^{(2)}_{AB}$ is much (by at least 10^4 fold) less than in native RC at pH 7 (Fig. 3b). Because $k^{(2)}_{AB}$ is PT limiting, the actual rate of PT is much more strongly ($>10^7$ fold) inhibited. The enormous drop of the rate of PT and the close to maximum kinetic isotope effect with strong pH-dependence indicate very limited possibilities of alternate proton pathways. Bridging water molecules and/or L212E can replace L213D but due to loose coupling of the groups, the transfer may include H-bond breaking (or close to this limit) step.

Acknowledgements

Thanks to TÁMOP 4.2.2.A-11/1KONV-2012-0060, TÁMOP 4.2.2.B and COST Action on "Understanding Movement and Mechanism in Molecular Machines" (CM1306) programs for financial support.

References

[1] C.A. Wraight, Intraprotein proton transfer — concepts and realities from the bacterial photosynthetic reaction center, biophysical and structural aspects of bioenergetics-Chapter 12 in: M. Wikstrom (Ed.), RSC Biomolecular Science Series, Royal Society of Chemistry, Cambridge, U.K., 2005
[2] M.R. Gunner, M. Amin, X. Zhu, J. Lu, Molecular mechanisms for generating transmembrane proton gradients, Biochim. Biophys. Acta 1827 (8–9) (2013) 892–913.
[3] C.A. Wraight, Chance and design — proton transfer in water, channels and bioenergetic proteins, Biochim. Biophys. Acta 1757 (2006) 886–912.
[4] A. Chernyshev, S. Cukierman, Thermodynamic view of activation energies of proton transfer in various gramicidin A channels, Biophys. J. 82 (2002) 182–192.
[5] R. Mikulski, D. West, K.H. Sippel, B.S. Avvaru, M. Aggarwal, C. Tu, R. McKenna, D.N. Silverman, Water networks in fast proton transfer during catalysis by human carbonic anhydrase II, Biochemistry 52 (1) (2013) 125–131.
[6] B.L. de Groot, H. Grubmüller, The dynamics and energetics of water permeation and proton exclusion in aquaporins, Curr. Opin. Struct. Biol. 15 (2005) 176–183.
[7] J.K. Lányi, Crystallographic studies of the conformational changes that drive directional transmembrane ion movement in bacteriorhodopsin, Biochim. Biophys. Acta 1459 (2000) 339–345.
[8] A. Migliore, N.F. Polizzi, M.J. Therien, D.N. Beratan, Biochemistry and theory of proton-coupled electron transfer, Chem. Rev. 114 (7) (2014) 3381–3465.
[9] V.R.I. Kaila, M.I. Verkhovsky, M. Wikström, Proton-coupled electron transfer in cytochrome oxidase, Chem. Rev. 110 (12) (2010) 7062–7081.
[10] G. Renger, Mechanism of light induced water splitting in photosystem II of oxygen evolving photosynthetic organisms, Biochim. Biophys. Acta 1817 (2012) 1164–1176.
[11] P. Maróti, M. Trotta, Artificial photosynthetic systems, in: A. Griesbeck, M. Oelgemöller, F. Ghetti (Eds.), CRC Handbook of Organic Photochemistry and Photobiology, Third edition, vol.1, CRC Press, 2012, pp. 1289–1324 (Chapter 55, Third Edition).
[12] C.A. Wraight, M.R. Gunner, The acceptor quinones of purple photosynthetic bacteria — structure and spectroscopy, in: C.N. Hunter, F. Daldal, M. Thurnauer, J.T. Beatty (Eds.),

Advances in Photosynthesis and Respiration: The Purple Phototrophic Bacteria, Springer, Dordrecht, The Netherlands, 2009, pp. 379–405.
[13] M.Y. Okamura, M.L. Paddock, M.S. Graige, G. Feher, Proton and electron transfer in bacterial reaction centers, Biochim. Biophys. Acta 1458 (2000) 148–163.
[14] M.L. Paddock, G. Feher, M.Y. Okamura, Proton transfer pathways and mechanism in bacterial reaction centers, FEBS Lett. 555 (2003) 45–50.
[15] H. Cheap, S. Bernad, V. Derrien, L. Gerencsér, J. Tandori, P. de Oliveira, D.K. Hanson, P. Maróti, P. Sebban, M234Glu is a component of the proton sponge in the reaction center from photosynthetic bacteria, Biochim. Biophys. Acta 1787 (2009) 1505–1515.
[16] J. Tandori, L. Baciou, E. Alexov, P. Maróti, M. Schiffer, D.K. Hanson, P. Sebban, Revealing the involvement of extended hydrogen-bond networks in the cooperative function between distant sites in bacterial reaction centres, J. Biol. Chem. 276 (49) (2001) 45513–45515.
[17] H. Cheap, J. Tandori, V. Derrien, M. Benoit, P. de Oliveira, J. Köpke, J. Lavergne, P. Maróti, P. Sebban, Evidence for delocalized anticooperative flash induced proton bindings as revealed by mutants at M266His iron ligand in bacterial reaction centers, Biochemistry 46 (2007) 4510–4521.
[18] M.S. Graige, M.L. Paddock, J.M. Bruce, G. Feher, M.Y. Okamura, Mechanism of proton-coupled electron transfer for quinone (Q_B) reduction in reaction centers of *Rb. sphaeroides*, J. Am. Chem. Soc. 118 (1996) 9005–9016.
[19] C.R.D. Lancaster, H. Michel, The coupling of light-induced electron transfer and proton uptake as derived from crystal structures of reaction centres from *Rhodopseudomonas viridis* modified at the binding site of the secondary quinone, QB, Structure 5 (1997) 1–22.
[20] M.L. Paddock, M.E. Senft, M.S. Graige, S.H. Rongey, T. Turanchik, G. Feher, M.Y. Okamura, Characterization of second site mutations show that fast proton transfer to Q_B^- is restored in bacterial reaction centers of *Rhodobacter sphaeroides* containing the Asp-L213 → Asn lesion, Photosynth. Res. 55 (1998) 281–291.
[21] M.J. Schilstra, F. Rappaport, J.H. Nugent, C.J. Barnett, D.R. Klug, Proton/hydrogen transfer affects the S-state-dependent microsecond phases of P6801 reduction during water splitting, Biochemistry 37 (1998) 3974–3981.
[22] M.Y. Okamura, G. Feher, Isotope effect on electron transfer in reaction centers from *Rhodopseudomonas sphaeroides*, Proc. Natl. Acad. Sci. U. S. A. 83 (1986) 8152–8156.
[23] P. Maróti, C.A. Wraight, Kinetics of H^+-ion binding by the $P^+Q_A^-$ state of the bacterial photosynthetic reaction centers: rate limitation within the protein, Biophys. J. 73 (1997) 367–381.
[24] M.L. Paddock, M.S. Graige, G. Feher, M.Y. Okamura, Identification of the proton pathway in bacterial reaction centers: inhibition of proton transfer by binding of Zn^{2+} or Cd^{2+}, Proc. Natl. Acad. Sci. U. S. A. 96 (1999) 6183–6188.
[25] L. Gerencsér, P. Maróti, Retardation of proton transfer caused by binding of transition metal ion to bacterial reaction center is due to pK_a-shifts of key protonatable residues, Biochemistry 40 (2001) 1850–1860.
[26] M.L. Paddock, P. Adelroth, C. Chang, E.C. Abresch, G. Feher, M.Y. Okamura, Identification of the proton pathway in bacterial reaction centers: cooperation between Asp-M17 and Asp-L210 facilitates proton transfer to the secondary quinone (Q_B), Biochemistry 40 (2001) 6893–6902.
[27] E. Takahashi, C.A. Wraight, Small weak acids reactivate proton transfer in reaction centers from *Rhodobacter sphaeroides* mutated at AspL210 and AspM17, J. Biol. Chem. 281 (2006) 4413–4422.
[28] E. Takahashi, C.A. Wraight, A crucial role for Asp^{L213} in the proton transfer pathway to the secondary quinone of reaction centers from *Rhodobacter sphaeroides*, Biochim. Biophys. Acta 1020 (1990) 107–111.
[29] P. Maróti, C.A. Wraight, Flash-induced H^+ binding by bacterial photosynthetic reaction centers: comparison of spectrophotometric and conductimetric measurements, Biochim. Biophys. Acta 934 (1988) 314–328.
[30] R.R. Stein, A.L. Castellvi, J. Bogacz, C.A. Wraight, Herbicide-quinone competition in the acceptor complex of photosynthetic reaction centers from *Rhodopseudomonas sphaeroides*: a bacterial model for PS II-herbicide activity in plants, J. Cell. Biochem. 25 (1984) 243–259.
[31] F. Milano, L. Gerencsér, A. Agostiano, L. Nagy, M. Trotta, P. Maróti, Mechanism of quinol oxidation by ferricenium produced by light excitation in reaction centers of photosynthetic bacteria, J. Phys. Chem. B 111 (2007) 4261–4270.
[32] K. Mikkelsen, S.O. Nielsen, Acidity measurements with the glass electrode in H_2O–D_2O mixtures, J. Phys. Chem. 64 (1960) 632–637.
[33] P.K. Glasoe, F.A. Long, Use of glass electrodes to measure acidities in deuterium oxide, J. Phys. Chem. 64 (1960) 188–190.
[34] M.S. Graige, M.L. Paddock, G. Feher, M.Y. Okamura, Observation of the protonated semiquinone intermediate in isolated reaction centers from *Rb. sphaeroides*: implications for the mechanism of electron & proton transfer in proteins, Biochemistry 38 (1999) 11465–11473.
[35] C.A. Wraight, Proton and electron transfer in the acceptor quinone complex of bacterial photosynthetic reaction centers, Front. Biosci. 9 (2004) 309–327.
[36] J. Lavergne, C. Matthews, N. Ginet, Electron and proton transfer on the acceptor side of the reaction center in chromatophores of *Rhodobacter capsulatus*: evidence for direct protonation of the semiquinone state of Q_B, Biochemistry 38 (1999) 4542–4552.
[37] C.A. Wraight, P. Maróti, Temperature dependence of the 2nd electron transfer in bacterial reaction centers, Biophys. J. 86 (1) (2004) 148A (Part 2).
[38] H. Eyring, R. Lumry, J.W. Woodbury, Some applications of modern rate theory to physiological systems, Rec. Chem. Prog. 10 (1949) 100–114.
[39] E. Takahashi, C.A. Wraight, Potentiation of proton transfer function by electrostatic interactions in photosynthetic reaction centers from *Rhodobacter sphaeroides*: first results from site directed mutation of the H-subunit, Proc. Natl. Acad. Sci. U. S. A. 93 (1996) 2640–2645.
[40] M. Eigen, Proton transfer, acid-base catalysis, and enzymatic hydrolysis, Part I. Elementary processes, Angew. Chem. Int. Ed. Engl. 3 (1964) 1–72.
[41] G.J. Edens, M.R. Gunner, Q. Xu, D. Mauzerall, The enthalpy and entropy of reaction for formation of $P^+Q_A^-$ from excited reaction centers of *Rhodobacter sphaeroides*, J. Am. Chem. Soc. 122 (2000) 1479–1485.
[42] D. Mauzerall, J.M. Hou, V.A. Boichenko, Volume changes and electrostriction in the primary photoreactions of various photosynthetic systems: estimation of dielectric coefficient in bacterial reactions centers and of the observed volume changes with the Drude–Nernst equation, Photosynth. Res. 74 (2002) 173–180.
[43] K. Sharp, Entropy–enthalpy compensation: fact or artifact? Protein Sci. 10 (2001) 661–667.
[44] A. Cooper, C.M. Johnson, J.H. Lakey, M. Nöllmann, Heat does not come in different colours: entropy–enthalpy compensation, free energy windows, quantum confinement, pressure perturbation calorimetry, solvation and the multiple causes of heat capacity effects in biomolecular interactions, Biophys. Chem. 93 (2002) 215–230.
[45] J.E. Jackman, K.M. Merz, C.A. Fierke, Disruption of the active site solvent network in carbonic anhydrase II decreases the efficiency of proton transfer, Biochemistry 35 (1996) 16421–16428.
[46] W.B. Greenleaf, D.N. Silverman, Activation of the proton transfer pathway in catalysis by iron superoxide dismutase, J. Biol. Chem. 277 (2002) 49282–49286.

II.

Ágnes Maróti, Colin A. Wraight and Péter Maróti:

Protonated rhodosemiquinone at the Q_B binding site of M265IT mutant reaction center of photosynthetic bacterium *Rhodobacter sphaeroides.*

Biochemistry, American Chemical Society (2015) DOI: 10.1021/bi501553t

Impact factor: 3.194

BIOCHEMISTRY
including biophysical chemistry & molecular biology

Article

pubs.acs.org/biochemistry

Protonated Rhodosemiquinone at the Q_B Binding Site of the M265IT Mutant Reaction Center of Photosynthetic Bacterium *Rhodobacter sphaeroides*

Ágnes Maróti,[†] Colin A. Wraight,[†,§] and Péter Maróti*[,‡]

[†]Department of Pediatrics and [‡]Department of Medical Physics, University of Szeged, Szeged, Hungary H-6720

[§]Center for Biophysics and Computational Biology and Department of Plant Biology, University of Illinois, Urbana, Illinois 61801-3838, United States

ABSTRACT: The second electron transfer from primary ubiquinone Q_A to secondary ubiquinone Q_B in the reaction center (RC) from *Rhodobacter sphaeroides* involves a protonated Q_B^- intermediate state whose low pK_a makes direct observation impossible. Here, we replaced the native ubiquinone with low-potential rhodoquinone at the Q_B binding site of the M265IT mutant RC. Because the in situ midpoint redox potential of Q_A of this mutant was lowered approximately the same extent (≈100 mV) as that of Q_B upon exchange of ubiquinone with low-potential rhodoquinone, the inter-quinone ($Q_A \rightarrow Q_B$) electron transfer became energetically favorable. After subsequent saturating flash excitations, a period of two damped oscillations of the protonated rhodosemiquinone was observed. The $Q_BH^\bullet$ was identified by (1) the characteristic band at 420 nm of the absorption spectrum after the second flash and (2) weaker damping of the oscillation at 420 nm (due to the neutral form) than at 460 nm (attributed to the anionic form). The appearance of the neutral semiquinone was restricted to the acidic pH range, indicating a functional pK_a of <5.5, slightly higher than that of the native ubisemiquinone (pK_a < 4.5) at pH 7. The analysis of the pH and temperature dependencies of the rates of the second electron transfer supports the concept of the pH-dependent pK_a of the semiquinone at the Q_B binding site. The local electrostatic potential is severely modified by the strongly interacting neighboring acidic cluster, and the pK_a of the semiquinone is in the middle of the pH range of the complex titration. The kinetic and thermodynamic data are discussed according to the proton-activated electron transfer mechanism combined with the pH-dependent functional pK_a of the semiquinone at the Q_B site of the RC.

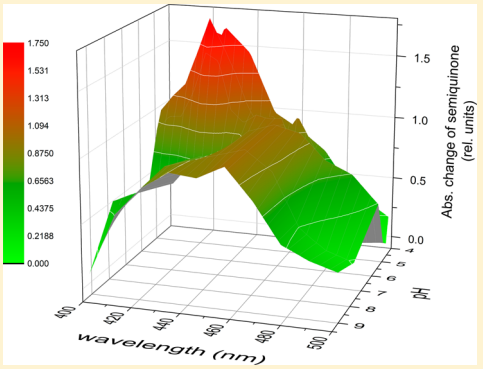

Coupled electron and proton transfers convert energy in many living organisms.[1,2] In the reaction center (RC) protein of photosynthetic bacterium *Rhodobacter sphaeroides*, the light-induced transfer of two electrons to the quinone at the Q_B binding site is accompanied by binding of two protons, resulting in fully reduced hydroquinone QH_2.[3−5] The H^+ ions are taken up from solution by long-range proton transfer (PT) over a distance of ∼15 Å, and a cluster of ionizable residues near the secondary quinone binding site is known to be involved in this delivery pathway. The bacterial RC provides a unique system for understanding the principles of long distance PT. The proton-coupled multielectron reactions, i.e., reactions with intermediate redox states like Q_B (but also others including the water-oxidizing complex of Photosystem II and hydrogenases), need to protect the cofactors from adventitious electron scavenging reactions. A minimum depth of ∼10 Å can be estimated from simple Marcus theory. If the electron transfer (ET) is intermolecular, then the Moser−Dutton rule[6] suggests that the distance should not be greater than 15 Å, which limits the depth at which the charge-accumulating site can be buried. However, if the ET is intramolecular (as for Q_B), the depth is limited by only biosynthetic cost and functional adequacy.[2,7] This necessitates long distance PT if H^+ ions are involved in the reactions. It was shown that the criteria of natural design of long distance PT pathways include the need to provide kinetic competence, high selectivity, and the overarching criterion of evolutionary stability or robustness.[8] A comparison of diverse proton-conducting materials, from gramicidin to cytochrome oxidase, led to the conclusion that rotationally mobile water is a major constituent of proton pathways, for energetic (especially entropic) reasons, and because it provides substantial immunity to mutational catastrophe.[2,8]

On the first ET after the first flash, the RC takes up a nonstoichiometric amount of H^+ ions, reflecting small changes in side chain pK_a values caused by the novel anionic charge of the semiquinone. Depending on the pK_1 of $Q_B^{-\bullet}/Q_BH^\bullet$ and the prevailing pH, the semiquinone itself can also be protonated (Figure 1). After the second flash, protons are delivered directly to the quinone headgroup and the second ET

Received: December 23, 2014
Revised: March 11, 2015

DOI: 10.1021/bi501553t
Biochemistry XXXX, XXX, XXX−XXX

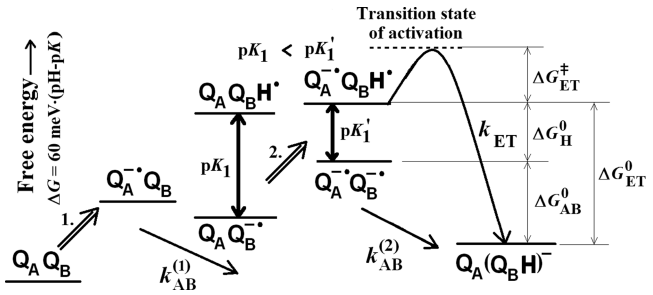

Figure 1. Uptake of the first H^+ ion by $Q_B^{-\bullet}$ in one- and two-electron states of the acceptor quinone complex of the RC after the first and second flashes, respectively. Red arrow 1 represents the light-induced transfer of an electron donor from the primary donor (not shown) to the primary quinone acceptor Q_A followed by the first $Q_A^{-\bullet}Q_B$ to $Q_AQ_B^{-\bullet}$ inter-quinone electron transfer [rate $k_{AB}^{(1)}$]. The generated state is mixed depending upon the proton uptake of $Q_B^{-\bullet}$ determined by the prevailing pH and pK_1 of $Q_B^{-\bullet}$. The second red arrow represents the second light-induced reduction of Q_A followed by the second inter-quinone ET (rate k_{ET}). The second electron transfer occurs from the protonated $Q_BH^\bullet$ semiquinone state whose equilibrium population is determined by pK_1' and the ambient pH. The observed rate of the second ET, $k_{AB}^{(2)}$, is given by eq 1. The free energy levels of the states involved in the proton-coupled ET are indicated for the wild-type RC.

is fully proton-coupled. The analysis of the free energy and pH dependencies of the rate has revealed that the reaction mechanism proceeds via rapid preprotonation of the semiquinone in the two-electron state of the acceptor quinone complex ($Q_A^{-\bullet}Q_B^{-\bullet} \leftrightarrow Q_A^{-\bullet}Q_BH^\bullet$) followed by rate-limiting electron transfer ($Q_A^{-\bullet}Q_BH^\bullet \rightarrow Q_AQ_BH^{-\bullet}$).[9] It is now understood to comprise a rate-limiting ET that is rate-modulated by pH because the protonated semiquinone, $Q_BH^\bullet$, is the actual electron acceptor species. The observed rate is

$$k_{AB}^{(2)} = k_{ET} f(Q_BH^\bullet) \quad (1)$$

where $f(Q_BH^\bullet)$ denotes the population of $Q_BH^\bullet$ and k_{ET} is the (maximal) rate of the forward electron transfer in the quinone complex. For a simple titration

$$k_{AB}^{(2)} = k_{ET}\frac{1}{1 + 10^{pH-pK_2}} \quad (2)$$

The PT equilibrium must be established at least 10 times faster than the rate-limiting ET, at all pH values. How fast the ET rate is, and therefore how fast the PT rate must be, depends on the functional pK_1 of the Q_B semiquinone. For the native ubiquinone$_{10}$ in RC of *Rba. sphaeroides*, the pK_1 should be very low as the Q_B^- semiquinone remains fully anionic at least down to pH 4.5, and therefore, the neutral (protonated) semiquinone as the transition intermediate of the second ET cannot be observed.[10,11]

A straightforward suggestion is to replace the ubiquinone at the Q_B site with a different type of quinone that can forward electrons and protons to quinol formation, and its semiquinone form exhibits a pK value higher than that of ubisemiquinone. Rhodoquinone (RQ) seems to fulfill these conditions. It is a required cofactor for anaerobic respiration in *Rhodospirillum rubrum*.[12] RQ is an aminoquinone that is structurally similar to ubiquinone (UQ), a ubiquitous lipid component involved in the aerobic respiratory chain. The only difference between the structures is that RQ has an amino group (NH_2) on the benzoquinone ring in place of a 3-methoxy substituent (OCH_3) in UQ. This difference of the structures causes considerable differences in (i) the redox midpoint potentials (E_m) measured polarographically {at pH 7, −63 mV for RQ and +43 mV for UQ (ubiquinone-10) in a mixture of ethanol and water [4:1 (v/v)] and −30 mV (RQ) and +50 mV (UQ) bound to chromatophores of *Rh. rubrum*}[13] and (ii) the pK of protonation of the semiquinones. The plots of the polarographic E_m versus pH curves can be used to estimate the numbers of electrons (e^-) and H^+ ions in the electrode reactions, but the plots fail to determine the increase in the pK of $RQ^{-\bullet}/RQH^\bullet$ relative to that of $UQ^{-\bullet}/UQH^\bullet$.[14] The shift is probably due to the higher level of electron donation of the amino substituent in RQ than the methoxy group in UQ to the quinone ring. The pK of rhodosemiquinone was estimated to be 7.3 at the Q_B site of the RC.[15] These results, however, must be regarded as very tentative because of the absence of more fundamental electrochemical information.[16]

The reduction of the low-potential rhodoquinone at the Q_B binding site requires the use of low-potential analogues of Q_A[15] or direct ET to Q_B along the inactive B branch.[17] Both methods have difficulties. Binding of different (non-native) quinones in the Q_A and Q_B sites calls for great challenge in the RC of *Rba. sphaeroides*. The incomplete binding of the quinones results in restricted inter-quinone ET with a mixture of Q_A^- and Q_B^- states after the first saturating flash. The observation of B branch ET to Q_B needs heavily modified RC with a total of five mutations, and even in that case, the quantum yield of Q_B reduction is very low (~5%). Because the many modified residues are not located in the region around Q_B, the integrity of the Q_B environment is supposed to be preserved.[18]

In this work, we used a different procedure for reducing rhodoquinone in the Q_B site. The Q_A binding site remained occupied by the native ubiquinone, but its redox midpoint potential was lowered by 100−120 mV upon mutation of M265 isoleucine to the smaller, polar residue of threonine in the Q_A binding pocket.[19] The H-bond structure and the extensive decrease in the redox midpoint potential of Q_A were studied earlier by delayed fluorescence of the bacteriochlorophyll dimer,[20,21] Fourier transform infrared,[22] and magnetic resonance[23] spectroscopy and quantum mechanical calculations of the ^{13}C couplings of the 2-methoxy dihedral angle.[24,25] The large decrease in the redox potential of Q_A is attributed to hydrogen bonding of the OH to the peptide C=O of ThrM261, which causes a displacement of the backbone strand that bears the hydrogen bond donor (AlaM260) to the C1 carbonyl of Q_A, lengthening the hydrogen bond to the semiquinone state, Q_A^-, and thereby destabilizing it. This greatly increases ΔE_m, the driving force for ET. If we combine the two low-potential quinones at Q_A (M265IT mutant) and Q_B (RQ substitution) sites, the driving force will remain sufficiently large to obtain efficient inter-quinone ET. We will have a chance to recognize the protonation of the semiquinone either from the typical light-induced optical absorption spectrum between 400 and 500 nm[26] or from comparison of the damping of the semiquinone oscillation[27] detected at wavelengths characteristic of the neutral and anionic forms of the semiquinone at the Q_B site of the RC.

MATERIALS AND METHODS

Chemicals and Reaction Centers. UQ_{10} (ubiquinone$_{10}$, 2,3-dimethoxy-5-methyl-6-decaisoprenyl-1,4-benzoquinone) was purchased from Sigma. RQ (rhodoquinone; 2-amino-3-methoxy-6-methyl-5-decaisoprenyl-1,4-benzoquinone) was ob-

DOI: 10.1021/bi501553t
Biochemistry XXXX, XXX, XXX−XXX

tained from *Rh. rubrum* grown photosynthetically under anaerobic conditions.[28] Separation of RQ from the quinone extractions was performed using preparative TLC plates.[29,30] The concentration of RQ in ethanol was determined from optical absorption coefficient of 1 mM^{-1} cm^{-1} at 500 nm.[31] Ferrocene (Eastman Kodak) and terbutryne (Chem. Service) used to reduce the oxidized dimer (P) and to block the inter-quinone electron transfer, respectively, were solubilized in ethanol. The buffer mix contained the following buffers (1−1 mM): 2-(*N*-morpholino)ethanesulfonic acid (MES, Sigma), succinate, or citric acid (Calbiochem) between pH 4.5 and 6.5; 1,3-bis[tris(hydroxymethyl)methylamino]propane (Bis-Tris propane, Sigma) between pH 6.3 and 9.5; Tris-HCl (Sigma) between pH 7.5 and 9.0; and 3-(cyclohexylamino)-propanesulfonic acid (CAPS, Calbiochem) above pH 9.5.

The details of the molecular biological techniques in generating the M265IT mutant from strain *Rba. sphaeroides*, the cultivation, and the preparation of RC protein have been described previously.[19] The UQ at the Q_B site was removed as described previously[32] and reconstituted by addition of RQ in large (>10) excess over RC. The occupancy of the Q_B site was >70% as determined from the ratio of the amplitudes of the slow and fast phases of the charge recombination measured at 865 nm.

Electron Transfer Measurements. The kinetics of flash-induced ET was measured by absorption changes using a single-beam spectrophotometer of local design.[33] The rates of charge recombination ($P^+Q_B^- \rightarrow PQ_B$) were obtained by monitoring the recovery of the dimer (P) absorbance at 430 nm (or 865 nm), following a saturating exciting flash. Electron transfer rate $k_{AB}^{(1)}$ ($Q_A^{-\bullet}Q_B \rightarrow Q_AQ_B^{-\bullet}$) was measured by tracking the absorption change at 398 nm following a saturating flash. The rate constants of the second ET to $Q_B^{-\bullet}$ were determined by monitoring the decay of semiquinone absorbances ($Q_A^{-\bullet}$ and $Q_B^{-\bullet}$) at a wavelength of 450 nm following a second saturating flash in a RC solution containing the exogenous reductant, ferrocene, which reduced the oxidized dimer P^+ within 1−5 ms.[11,34]

RESULTS

Rate and Temperature Dependence of $P^+Q_A^-$ Charge Recombination in the M265IT Mutant RC. The kinetics of P^+ dark decay following a flash was measured at 430 nm in the M265IT RC with native UQ at the Q_A binding site and empty Q_B binding site (Figure 2). The observed k_{AP} rates were 2−3 times faster than those for the wild-type RC[19] and showed temperature dependence. The Arrhenius plot of the temperature dependence of k_{AP} is presented in the inset of Figure 2: $\ln(k_{AP})$ follows a straight line revealing activation energy. The increased k_{AP} rates together with the temperature dependence suggest a thermally activated process of charge recombination and indicate that the free energy of the $P^+Q_A^-$ state in the M265IT mutant has been increased so that this state decays no longer directly to the PQ_A ground state by a tunneling effect. When the redox potential of Q_A is sufficiently low, a different pathway opens in which the electron is thermally excited to the relaxed state (M) of P^+I^- (I is bacteriopheophytin) with subsequent rapid decay from M to PQ_A.[35−37] The observed rate of $P^+Q_A^-$ recombination becomes

$$k_{AP} = k_d \times \exp\left(\frac{-\Delta G^{\circ}_{AM}}{RT}\right) \quad (3)$$

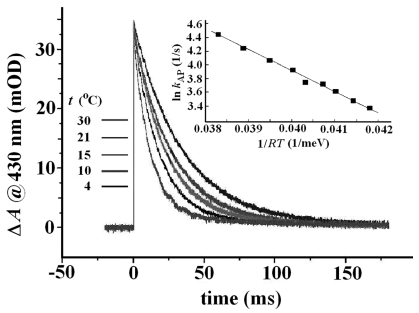

Figure 2. Temperature dependence of the kinetics of the $P^+Q_A^- \rightarrow PQ_A$ charge recombination measured by a flash-induced absorption change at 430 nm of the M265IT mutant RC of *Rba. sphaeroides*. The increasing rate constant k_{AP} of charge recombination with an increase in temperature is an indication of low-potential quinone at the Q_A binding site (inset). The shift in the free energy level of $P^+Q_A^-$ in the M265IT mutant relative to that of the wild type amounts to a ΔG°_{QA} of 107 meV (see the text). Conditions: 1.1 μM RC (Q_B-depleted), 0.03% LDAO, 1 mM MOPS buffer, and 2.5 mM KCl (pH 7).

where R is the universal gas constant, T is the temperature, and ΔG°_{AM} is the free energy gap between M and $P^+Q_A^-$ that is controlled by the equilibrium redox potential of Q_A/Q_A^-. The pre-exponential factor ($k_d = 2 \times 10^7$ s^{-1}) is the effective rate of recombination of P^+I^- to the ground state and is independent of the nature of the M265IT mutation.[35,36]

According to eq 3, the thermodynamic parameters of the recombination of the M265IT mutant can be derived from the slope ($-\Delta H$, change in enthalpy of the back reaction) and interception [$\ln(k_d) + \Delta S/T$, where ΔS is the change in entropy of the recombination] of the straight line in the Arrhenius plot. As we obtained a ΔH of 305 ± 10 meV and a $T\Delta S$ of −18 ± 1 meV for the enthalpic and entropic components of the free energy gap, respectively, $\Delta G^{\circ}_{AM} = \Delta H - T\Delta S = 323 \pm 11$ meV can be derived. The free energy gap (ΔG°_{AM}) between M and $P^+Q_A^-$ states in wild-type *Rba. sphaeroides* was found to be 430 meV.[35,37] Therefore, the free energy level of $P^+Q_A^-$ in the M265IT mutant is found to be increased by 430 meV − 323 meV = 107 meV (±11 meV); i.e., the shift of the midpoint redox potential of Q_A in M265IT relative to that of WT amounts to −110 mV at pH 7. This value is in excellent agreement with that obtained by delayed fluorescence measurements of the dimer.[20]

Q_B Site of M265IT Occupied by RQ. Upon addition of RQ to the Q_B-depleted RC, a slow phase with an $\sim(500\ ms)^{-1}$ rate constant appears in the charge recombination kinetics that disappears in the presence of the potent inhibitor terbutryne (data not shown). Subsequent saturating flashes evoke binary oscillation of the semiquinone in the presence of an external electron donor to the oxidized dimer, P^+ characteristic of the two-electron gate function of Q_B[10,38] (Figure 3). If UQ occupies the Q_B binding site of the M265IT mutant RC, then the oscillations in Q_B^- semiquinone formation are at least as strong as in wild-type RCs, consistent with a large value of electron equilibrium constant and effective transfer of the second electron.[19] If, however, RQ replaces UQ at the Q_B binding site, the magnitude of the semiquinone oscillation is significantly affected and the damping will be larger. The damping of the oscillation of the rhodosemiquinone upon subsequent saturating flashes is determined by (i) the occupancy of the Q_B site ($1 - \delta$) and (ii) the one-electron equilibrium partition coefficient [$\alpha = [Q_A^-Q_B]/([Q_A^-Q_B] +$

DOI: 10.1021/bi501553t
Biochemistry XXXX, XXX, XXX−XXX

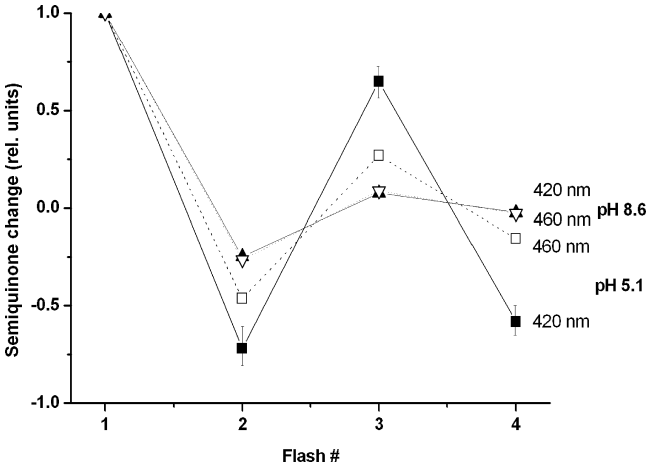

Figure 3. Changes of rhodosemiquinone at the Q_B site of the M265IT mutant RC upon subsequent saturating flashes measured at two wavelengths, 420 nm (characteristic of protonated RQ, $RQ_BH^{\bullet}$) and 460 nm (characteristic of the anionic form of RQ, $RQ_B^{-\bullet}$), and two pH values (5.1 and 8.6). The magnitudes are normalized to the change evoked by the first flash. The lines were fit by $\delta = 0.2$ and $\alpha = 0.09$ (pH 5.1 and 420 nm), 0.42 (pH 5.1 and 460 nm), 0.69 (pH 8.6 and 420 nm), and 0.67 (pH 8.6 and 460 nm) (see eq 4). Conditions: 1.1 μM RC, 100 μM RQ, 0.02% LDAO, 60 μM ferrocene, 5 mM buffer mix, and a flash repetition rate of 5 Hz.

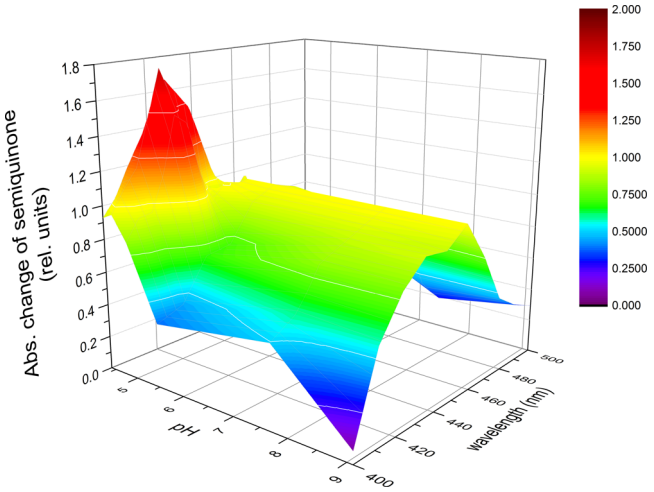

Figure 4. Quasi three-dimensional representation of the optical absorption spectra of rhodosemiquinone at the secondary quinone binding site (Q_B) of the M265IT mutant RC measured after a saturating flash in the presence of an electron donor to the oxidized dimer P^+ at several pH values. The 420 nm band of the spectra at low pH resembles the protonated spectrum of semiquinone in solution.[26] The spectra are normalized to the absorption at 450 nm.

$[Q_AQ_B^-])]$ in the acceptor quinone system.[27] The measured semiquinone absorption contains contributions from both Q_A^- and Q_B^- (protonated or deprotonated) and is given after the nth (>0) saturating flash by

$$\Delta A_n = (1-\delta)\frac{1-(-1)^n(1-\alpha)^n}{2-\alpha} + \delta \quad (4)$$

which is normalized to the absorption change after the first flash, ΔA_1. Figure 3 demonstrates the change in the semiquinone content after the nth flash: $\Delta Q^-_n = \Delta A_n - \Delta A_{n-1}$, i.e., the difference between two sequential flashes. By fitting the measured data to the model, we get $\delta = 0.2$ (the occupancy of the Q_B site by RQ is 80% in this experiment) and pH- and wavelength-dependent partition coefficients. At low pH, the damping is small, indicating effective electron transfer to Q_B. The oscillation at 420 nm (characteristic of protonated RQ, $RQ_BH^{\bullet}$) is larger than at 460 nm (typical of the anionic form of RQ, $RQ_B^{-\bullet}$) expressed by the smaller α at 420 nm than at 460 nm (0.09 and 0.42, respectively). At low pH (<pK_1), the protonated form of Q_B^- involves a free energy level lower than that of the anionic form (Figure 1). Therefore, because of the contribution of $RQ_BH^{\bullet}$, a smaller partition coefficient (higher one-electron equilibrium constant) was obtained. In crude terms, the protonation stabilizes the semiquinone state. At high pH (8.6), the oscillation is strongly damped and no distinctions can be made according to wavelengths: $\alpha = 0.69$ and 0.67 at 420 and 460 nm, respectively. The rhodosemiquinone is not protonated at all in this pH range.

This indirect statement can be confirmed by direct measurement of the second flash-induced absorption spectra of rhodosemiquinone in the 400−500 nm spectral range at different pH values (Figure 4). The generated spectral pofile is attributed mainly to the (anionic or ionic forms) of the Q_B semiquinone[26] as the spectral contribution of the oxidized external donor (ferrocinium) in this region and the accumulation of the $Q_A^{-\bullet}$ species are negligible. Similar spectra were obtained when the semiquinone appeared (after an odd number of flashes) or disappeared (after an even number of flashes), indicating that the contribution of RQ_B^- played the determining role. The spectra consisted of components from protonated RQ (characteristic band around 420 nm that appeared below pH 5) and deprotonated (anionic) RQ (characteristic band at 450 nm that dominates above pH 5). Although the appearance and disappearance of the band at 420 nm can be well recognized at low and neutral pH ranges, respectively, it is hard to predict a characteristic pK value for protonation of RQ_B^- as its band did not attain obviously its maximum at the lowest pH value (pH 4.3) used in these measurements. We predict a pK of ≲5 that is significantly smaller than 7.3 obtained after a simple (not extended) Henderson−Hasselbalch titration curve in ref 15.

Electron Transfer Rates. The exchange of UQ for RQ at the Q_B site of M265IT has a much larger effect on the energetics of the quinone acceptor system (manifested by variations of the $P^+Q_B^- \rightarrow PQ_B$ charge recombination or semiquinone oscillation) than on the kinetics of the first ($Q_A^-Q_B \rightarrow Q_AQ_B^-$) and second ($Q_A^-Q_B^- \rightarrow Q_AQ_BH$) electron transfers. The rates of the $k_{AB}^{(1)}$ reaction were the same with UQ as with RQ in the Q_B site (data not shown). Because the rate of the first electron transfer is under the control of conformational gating of the Q_B site,[39] the result indicates that substitution of RQ does not affect the dynamics of Q_B motion. The rates of the second ET with UQ or RQ at the Q_B site show similar and noninteger pH dependence below pH 8 (Figure 5). They demonstrate a highly moderate pH dependence at low pH (~0.1 decade/pH unit) but decrease at high pH by a factor of 10 per pH unit. For RQ, the rates are slightly smaller and the crossing point of the lines that approximate the low- and high-pH behavior has a pH value higher than those for UQ.

The rate of the second electron transfer is sensitive to the temperature: it increases upon elevation of the temperature in the physiological range. Figure 6 demonstrates this dependence for UQ and RQ at the Q_B site at different pH values in Arrhenius-type representation where the logarithm of the rate is

DOI: 10.1021/bi501553t
Biochemistry XXXX, XXX, XXX−XXX

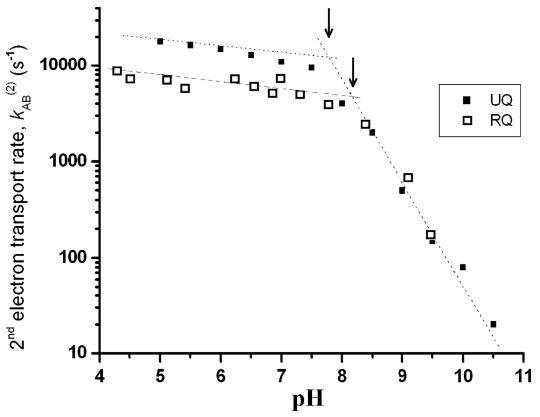

Figure 5. pH dependence of the rate of the second electron transfer in the M265IT mutant RC whose Q_B is occupied by either native UQ (■) or RQ (□). The rate was measured from the decay of semiquinone absorbance at 450 nm after the second flash. The lines represent the approximate weak pH dependence below pH 8 (~0.1 decade per pH unit) and the theoretical 1 decade/pH unit drop above pH 8. Note the shift of the crossing point of the straight lines upon UQ–RQ exchange at Q_B. Conditions: 2 μM RC in 2.5 mM KCl, 1 mM buffer mix, 0.02% LDAO, 40 μM UQ_{10} or 100 μM RQ_{10}, and 2–200 μM ferrocene (or its derivatives), depending on the rate (or pH).

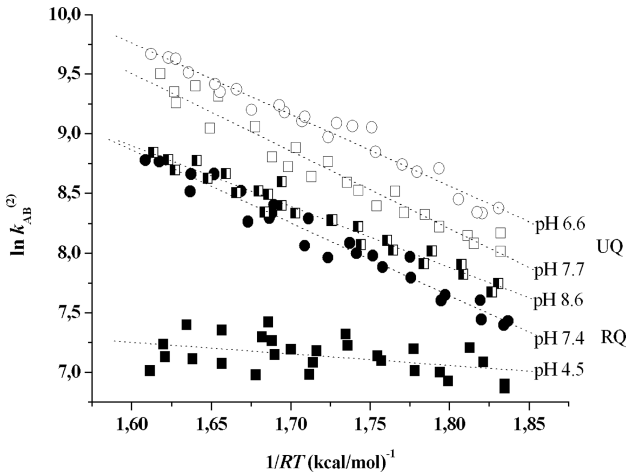

Figure 6. Temperature dependence of the rate of the second electron transfer at the physiological temperature range in the M265IT mutant RC with UQ (empty symbols) and RQ (filled symbols) at the Q_B binding site at several pH values. Conditions as in Figure 5. The fitted parameters of the straight lines (slope and intercept) are used to determine the thermodynamic parameter of activation of the second ET (see Table 1).

plotted as a function of the reciprocal of the temperature. As the measured data fit to straight lines, one can formally introduce observed activation parameters for the temperature dependence of the second ET:

$$k_{AB}^{(2)} = k_{max} \times \exp\left(-\frac{\Delta G_{obs}^{\ddagger}}{RT}\right) \quad (5)$$

where $k_{max} \approx 3.5 \times 10^9$ s^{-1} obtained from the exchange coupling between Q_A^- and Q_B^- in EPR studies,[40] R and T are the universal gas constant and the absolute temperature, respectively, and $\Delta G_{obs}^{\ddagger}$ is the observed free activation energy that can be decomposed into the enthalpy change of activation, $\Delta H_{obs}^{\ddagger}$ and entropic change of activation, $T\Delta S_{obs}^{\ddagger}$ ($\Delta G_{obs}^{\ddagger} = \Delta H_{obs}^{\ddagger} - T\Delta S_{obs}^{\ddagger}$). They can be derived from the slope (Slope) and interception (Int) of the straight line $\Delta H_{obs}^{\ddagger} = -$slope and $T\Delta S_{obs}^{\ddagger} = RT[\text{Int} - \ln(k_{max})]$. Their values are listed in Table 1. As one can see, neither the rates nor the activation parameters are very much different if UQ is replaced by RQ at the Q_B binding site of the M265IT mutant RC.

DISCUSSION

The results confirmed the incorporation of RQ into the Q_B site (~80%) and the reconstitution of the Q_B activity. It was demonstrated that the drop of the midpoint redox potential of Q_A in the M265IT mutant was large enough to compensate largely for a similar shift in the midpoint redox potential of Q_B when UQ was replaced by the low-potential RQ. Although the driving force and the electron equilibrium constants in the quinone complex became smaller, effective inter-quinone ET and turnover of the RC could be measured. The discussion will focus on the pH-dependent pK values of the Q_B^- semiquinones and the decomposition of the observed activation free energy of the second ET into contributions of both proton and electron transfer steps.

pK Values of Semiquinone at the Q_B Site. The pK of the ubisemiquinone has been estimated at $pK_1 \approx 3.8$ for the $(Q_A)Q_B^-/Q_BH$ one-electron equilibrium and $pK_1' \approx 4.5$ for the $(Q_A^-)Q_B^-/Q_BH$ two-electron equilibrium valid at pH 7.5.[4,41] These are mildly suppressed from the value in aqueous solution ($pK_a \approx 4.9$), but more importantly, the RC value appears to be pH-dependent because of the changing charge distribution, and possibly sensitive to the nature of the environment, i.e., detergent versus native membrane. Several acidic groups with Q_B^- constitute a cluster of strongly interacting components resulting in a remarkable and unexpected pH dependence of flash-induced proton uptake.[42] The protonation of the semiquinone does not follow a simple titration curve, and to preserve the formalism, pH-dependent pK values should be introduced.[41] The weak pH dependence of the rate of the second ET up to pH 8 suggests that the pK of the semiquinone is not constant but is continuously modulated by interactions with a changing electrostatic environment. Recently, a molecular probe (stigmatellin) was introduced to measure the electrostatic potential at the Q_B site.[43] The apparent pK of the semiquinone at a definite pH depends on minor changes in the intrinsic pK_a values of Q_B^- and the amino acids involved, and on their strengths of interaction. By measuring the decrease of the rate constant of the second ET in several mutants, we observed a considerable decrease in the operational pK of Q_B^-/Q_BH with a change of a single amino acid at key positions: the estimated pK of 4.5 (native) dropped to 3.9 (L210DN), 3.7 (M17DN), and 3.1 (H173EQ) at pH 7.[11] The results may simply suggest that the point at which pK approaches and exceeds the ambient pH (thereby allowing significant levels of $Q_BH^•$) will depend on interaction with components of the acidic cluster.

While the values of the pK of ubisemiquinone fall in the lower part, the pK for rhodosemiquinone lies at the upper limit of the range of those of carboxylates (4–5), where the protein electrostatics are most complex. A similar type of interaction as discussed above for UQ may be responsible for the increase in the operational pK of rhodosemiquinone that was large enough to be able to measure the protonated rhodosemiquinone below pH 5.5. The estimated pK, however, was much smaller in our study than that reported previously.[15] The lower pK value was supported by recent low-temperature electron paramagnetic

DOI: 10.1021/bi501553t
Biochemistry XXXX, XXX, XXX–XXX

Table 1. Standard (°) and Activation (‡) Free Energy (ΔG), Enthalpy (ΔH), and Entropic Energy ($T\Delta S$) Changes of the Second Electron Transfer in the M265IT RC with either UQ or RQ at the Q_B Binding Site[a]

RC	Q_B site	pH	$\Delta H^{\ddagger}_{obs}$ (kcal/mol)	$T\Delta S^{\ddagger}_{obs}$ (kcal/mol)	$\Delta G^{\ddagger}_{obs}$ (kcal/mol)	ΔG°_{H} (kcal/mol)	pK_2	ΔG°_{ET} (kcal/mol)	$\Delta G^{\ddagger}_{ET}$ (kcal/mol)	k_{ET} (μs^{-1})
M265IT	UQ	6.6	6.0	−1.5	7.5	3.3	3.8	−7.0	3.9	4.4
	UQ	7.7	6.1	−2.0	8.1	4.2	4.3	−7.9	3.6	7.6
	RQ	4.5	6.5	−1.2	7.7	2.3	2.6	−3.6	5.2	0.4
	RQ	7.4	5.1	−2.9	8.0	2.7	5.2	−4.1	5.0	0.6
	RQ	8.6	1.0	−7.6	8.6	3.9	5.6	−5.2	4.6	1.4
WT	UQ	7.8	4.2	−4.8	9.0	4.8	4.3	−6.2	4.2	2.6

[a]The observed activation parameters were obtained from the temperature dependence of $k^{(2)}_{AB}$ and the free energies ΔG°_{H}, ΔG°_{ET}, and $\Delta G^{\ddagger}_{ET}$ were calculated from eqs 10, 9, and 8, respectively. The values of pK_2 and k_{ET} were derived from the equations $\Delta G^{\circ}_{H} = 2.3RT(pH - pK_2)$ and $k_{ET} = k_{max} \times \exp(-\Delta G^{\ddagger}_{ET}/RT)$, respectively. For the maximal electron transfer rate, $k_{max} = 3.5 \times 10^9\ s^{-1}$;[40] for the reorganization energy, $\lambda = 1.2$ eV,[15] and for the free energy gap between the quinones in two-electron states, $\Delta G^{\circ}_{AB} = -60$ meV (UQ in WT and RQ in M265IT) and $\Delta G^{\circ}_{AB} = -160$ meV (UQ in M265IT).[19,20]

resonance (EPR) and electron nuclear double-resonance (ENDOR) investigations in which no changes of the spectra were found with a decrease in pH from the alkaline to the acidic range as low as pH 4.5.[17]

The protonated ubisemiquinone in isolated RC (UQ^-_B) has a very low pK value (~4.0), similar (4.1) to the pK_a of the protonated 1,4-semiquinone radical.[44,45] Substituents on the quinone ring can influence the electron density on the ring and thus modify both the redox midpoint potential and pK values.[46] The hydroxy groups increase slightly the pK. Because of the properties of electron donation of methyl groups into the ring, the methyl groups increase the pK by ~0.25 pH unit/group. The effect of methoxy groups is very similar to that of the methyl groups. The substitution of amino groups in 9,10-anthraquinone (AQ) gives a hint of the magnitude of the pK shift in RQ relative to UQ. The pK_1 of AQ was found to be 5.3[46,47] that increased by $\Delta pK = 0.5$ to $pK_1 = 5.8$ in 1-amino-AQ.[48]

It is well-established that spatial orientations and restrictions of the substituents can seriously modify the electron donating capacity.[24,25] While the 2-methoxy group of UQ is free for conformational change and takes an out-of-plane conformation in the Q_B binding pocket, the 3-methoxy group is unable to conduct a similar conformational change, probably because of steric restriction *in situ*. In RQ, this position is substituted with an amino group; therefore, no significant contribution can be expected from conformation-related pK changes. The observed and predicted changes in pK published in the literature for different substituents support our results of a moderate (1−1.5) increase in the pK of rhodosemiquinone with respect to ubisemiquinone.

In chromatophores, the protonation of the stable Q_B ubisemiquinone ($Q_AQ_BH^{\bullet}$) was readily observable, with a functional pK of 6.[49] This also suggests slight changes in the interactions of the RC embedded in chromatophores relative to isolated RC. In addition to the functional pK for Q_B^-, other differences may exist between isolated RCs and chromatophores. The midpoint redox potential of the primary quinone, $E_m(Q_A^-/Q_A)$, is strongly pH-dependent in chromatophores[50] but not in isolated RCs.[51,52] However, determinations of the free energy gap between P* and $P^+Q_A^-$ in chromatophores reveal a pH dependence identical to that seen in isolated RCs and cast serious doubt on the potentiometric determinations of $E_m(Q_A^-/Q_A)$ probably because of poor mediation of the Q_A binding site of the protein.[53] It was suggested that Q_A may actually be titrated through the Q_B site, reflecting titration of the quinone pool or perhaps a redox mediator in the Q_B site. Nevertheless, this remained an open question whose answer is critical to our understanding of the acceptor quinones.

The semiquinone has two different pK values in one-electron (pK_1) and two-electron (pK_1') states of the quinone acceptor complex (Figure 1). We were able to determine the pK_1 from the oscillation of the flash-induced absorption changes of the stable semiquinone, when Q_A was oxidized. The determination of pK_1' of the transient semiquinone important in the second ET is not straightforward, but a realistic estimate can be offered. The difference between pK_1 and pK_1' is due to the extra (electrostatic) interaction of Q_A^- with Q_B^- that can be deduced from equilibrium and kinetic electron transfer and proton uptake measurements and electrostatic calculations. The long-range interactions between the two quinone sites prepare the Q_B site for the subsequent electron transfer from Q_A.[54] The electrostatic influence of Q_A^- on the apparent pK_a of the acidic cluster that controls the pH dependence of the electron equilibrium in the quinone complex causes a difference of 0.5−1 unit between pK values in states Q_AQ_B and $Q_A^-Q_B$.[41] This result is consistent with the conclusions drawn from the pH dependence of the H^+/Q_A^- and H^+/Q_B^- stoichiometries.[33,55] Light activation causes proton uptake as the acid cluster reprotonates in accordance with the pK shifts induced by the semiquinone anions. The pH dependence of the H^+ uptake stoichiometries, H^+/Q_A^- and H^+/Q_B^-, can be deconvoluted into discrete contributions. Q_A^- causes pK shifts of 0.7−0.8 pH unit estimated for the pK_1' of the Q_B semiquinone in the two-electron state, $Q_A^-Q_B^-$, and for the first pK of the quinol, QH^-, in the three-electron state, $Q_A^-Q_BH^-$.[15,56] The 0.7−0.8 unit upshift in the pK of the ubiquinone in the $Q_A^-Q_B^-$ state was similar to that inferred for the rhodoquinone occupant.[15] In this work, the protonation of the rhodosemiquinone was observed in the one-electron state ($Q_AQ_B^- \leftrightarrow Q_AQ_BH$) with a pK_1 of 7.3. On the second electron transfer, $k^{(2)}_{AB}$ displayed a well-behaved pH dependence (see eq 2 with a pH-independent pK): it was constant below pH 7 and decelerated 10-fold per pH unit above a pK of 8.0 in the $Q_A^-Q_B^-$ state. In contrast, our kinetic and thermodynamic data were consistent with the significantly smaller and pH-dependent functional pK_1 of the rhodosemiquinone.

Activation Analysis of the Second ET. The fast proton pre-equilibrium is followed by a rate-limiting ET. The states involved in the $k^{(2)}_{AB}$ reaction are shown in Figure 1. The observed activation parameters are characteristic to both the proton equilibrium and the subsequent electron transfer step. On one hand, the rate of the second ET increases with a decrease in the activation barrier, $\Delta G^{\ddagger}_{ET}$, and on the other hand

DOI: 10.1021/bi501553t
Biochemistry XXXX, XXX, XXX−XXX

decreases due to the increase in the free energy to protonate the semiquinone [$\Delta G^{\circ}_{H} = 2.3RT(pH - pK_2)$] that results in a smaller population of the $Q_B^{-\bullet}$ state. The connected proton and electron transfer steps give the complex behavior of the apparent activation. Whatever rate model is used for the ET, the proton pre-equilibrium (acid association) parameters (ΔG°_{H}, etc.) combine with those of the true activation step ($\Delta G^{\ddagger}_{ET}$, etc.) to give the observed activation energies ($\Delta G^{\ddagger}_{obs}$, etc.) that will not be, however, simply the sum of the components.

The rate-limiting step is a nonadiabatic ET, and the Marcus formalism should be used.[57]

$$k_{AB}^{(2)} = \frac{k_{max} \times \exp\left(-\frac{\Delta G^{\ddagger}_{ET}}{RT}\right)}{1 + \exp\left(\frac{\Delta G^{\circ}_{H}}{RT}\right)} \quad (6)$$

If eqs 5 and 6 are compared, then

$$\Delta G^{\ddagger}_{obs} = \Delta G^{\ddagger}_{ET} + RT \times \ln\left[1 + \exp\left(\frac{\Delta G^{\circ}_{H}}{RT}\right)\right] \quad (7)$$

Here, the activation free energy of ET, $\Delta G^{\ddagger}_{ET}$, can be expressed from the free energy of the ET (defined as the free energy of the final minus the initial state), ΔG°_{ET}, and the reorganization energy, λ:

$$\Delta G^{\ddagger}_{ET} = \frac{(\Delta G^{\circ}_{ET} + \lambda)^2}{4\lambda} \quad (8)$$

The standard free energy levels follow a simple summation rule. The free energy for electron transfer, ΔG°_{ET}, is the difference in the free energy between initial and final states, ΔG°_{AB}, and the free energy to protonate $Q_B^{-\bullet}$, ΔG°_{H}:

$$\Delta G^{\circ}_{ET} = \Delta G^{\circ}_{AB} - \Delta G^{\circ}_{H} \quad (9)$$

.

Inserting eq 9 into eq 8 and inserting eq 8 into eq 7, we obtain

$$\Delta G^{\ddagger}_{obs} = \frac{(\Delta G^{\circ}_{AB} - \Delta G^{\circ}_{H} + \lambda)^2}{4\lambda} + RT \times \ln\left[1 + \exp\left(\frac{\Delta G^{\circ}_{H}}{RT}\right)\right] \quad (10)$$

ΔG°_{H} and pK_2 at a definite pH can be obtained by solution of eq 10 with λ = 1.2 eV (=27.7 kcal/mol)[15] and ΔG°_{AB} = −160 meV for UQ[19,20] and ΔG°_{AB} = −60 meV for RQ at the Q_B site. Although the latter values refer to the differences in free energy between the semiquinones in one-electron states, similar values can be taken for the two-electron states. In the WT RC, a very small (β < 0.05) partition coefficient was found for the two-electron equilibrium in the acceptor quinone system at pH <8.[58] The measured and calculated values are listed in Table 1. The functional (pH-dependent) pK_1' values are somewhat higher for RQ than for UQ. Although the increase is not as large as reported previously,[15] a fraction of protonated RQ could be detected in our experiments in the low-pH range (see Figure 4). This observation is in good agreement with conclusions of recent EPR and ENDOR studies.[17]

The $T\Delta S^{\ddagger}_{obs}$ entropy change is small and negative. The negative value makes sense as an activation parameter. By our estimates, the entropic component from the electron transfer, $T\Delta S^{\ddagger}_{ET}$, is quite small and pH-independent. Most of the observed activation entropy is due to the protonation equilibrium, i.e., entropy of mixing. Accordingly, it should have an increasingly negative entropy contribution with pH. Indeed, the entropy of activation decreases (becomes more negative) because H^+ ions are being brought from an increasingly dilute solution as the pH is increased.

CONCLUSIONS

With a decrease in the potential of the UQ at the Q_A site in the M265IT mutant, the activity of the Q_B site occupied by the low-potential RQ can be reconstituted. The second electron transfer reaction followed the mechanism of proton-activated electron transfer. The flash-induced rhodosemiquinone showed partly neutral (protonated) character below pH 5 and was completely anionic above pH 5.5. Kinetic and thermodynamic assays of the second ET supported the low value of the functional pK of RQ at the Q_B site that was slightly higher than that of the native ubiquinone. The pK is pH-dependent because of the pH-dependent local potential whose main contributor is the cluster of acidic residues around Q_B. The complex deprotonation of the cluster makes the positive local potential at low pH gradually more and more negative at high pH. The pH dependence of the pK is responsible for the fact that the second ET rate has a noninteger pH dependence below pH 8.

AUTHOR INFORMATION

Corresponding Author

*Department of Medical Physics, University of Szeged, Rerrich Béla tér 1., Szeged, Hungary H-6720. Phone: 36-62-544-120. Fax: 36-62-544-121. E-mail: pmaroti@sol.cc.u-szeged.hu.

Funding

This work was supported by TÁMOP 4.2.2.A-11/1KONV-2012-0060, TÁMOP 4.2.2.B, COST CM1306, and OTKA K116834.

Notes

The authors declare no competing financial interest.

ACKNOWLEDGMENTS

Thanks to Dr. E. Takahashi (University of Illinois) for the M265IT mutant and to G. Sipka (University of Szeged) for the three-dimensional representation of Figure 4.

DEDICATION

[†]Deceased July 10, 2014. This work is dedicated to his memory.

ABBREVIATIONS

ET, electron transfer; P, bacteriochlorophyll dimer; QA and QB, primary and secondary quinone acceptors, respectively; UQ10, ubiquinone; RC, (bacterial) reaction center; RQ, rhodoquinone.

REFERENCES

(1) Cramer, W. A., and Knaff, D. B. (1990) *Energy Transduction in Biological Membranes: A Textbook of Bioenergetics*, Springer-Verlag, New York.

(2) Wraight, C. A. (2006) Chance and design: Proton transfer in water, channels and bioenergetic proteins. *Biochim. Biophys. Acta 1757*, 886–912.

DOI: 10.1021/bi501553t
Biochemistry XXXX, XXX, XXX–XXX

(3) Okamura, M. Y., Paddock, M. L., Graige, M. S., and Feher, G. (2000) Proton and electron transfer in bacterial reaction centers. *Biochim. Biophys. Acta 1458*, 148−163.
(4) Zhu, Z., and Gunner, M. R. (2005) Energetics of quinone-dependent electron and proton transfers in *Rhodobacter sphaeroides* photosynthetic reaction centers. *Biochemistry 44*, 82−96.
(5) Wraight, C. A., and Gunner, M. R. (2009) The Acceptor Quinones of Purple Photosynthetic Bacteria- Structure and Spectroscopy. In *Advances in Photosynthesis and Respiration: The Purple Phototrophic Bacteria* (Hunter, C. N., Daldal, F., Thurnauer, M., and Beatty, J. T., Eds.) pp 379−405, Springer, Dordrecht, The Netherlands.
(6) Moser, C. C., Page, C. C., Cogdell, R. J., Barber, J., Wraight, C. A., and Dutton, P. L. (2003) Length, Time and Energy Scales of Photosystems. *Adv. Protein Chem. 63*, 71−109.
(7) Takahashi, E., and Wraight, C. A. (2006) Small weak acids reactivate proton transfer in reaction centers from *Rhodobacter sphaeroides* mutated at AspL210 and AspM17. *J. Biol. Chem. 281*, 4413−4422.
(8) Wraight, C. A. (2005) Intraprotein proton transfer: Concepts and realities from the bacterial photosynthetic reaction center. In *Biophysical and Structural Aspects of Bioenergetics* (Wikström, M., Ed.) Chapter 12, pp 273−313, The Royal Society of Chemistry, Cambridge, U.K.
(9) Graige, M. S., Paddock, M. L., Bruce, J. M., Feher, G., and Okamura, M. Y. (1996) Mechanism of proton-coupled electron transfer for quinone (Q_B) reduction in reaction centers of *Rb. sphaeroides*. *J. Am. Chem. Soc. 118*, 9005−9016.
(10) Wraight, C. A. (1979) Electron acceptors of bacterial photosynthetic reaction centers II. H^+ binding coupled to secondary electron transfer in the quinone acceptor complex. *Biochim. Biophys. Acta 548*, 309−327.
(11) Maróti, Á., Wraight, C. A., and Maróti, P. (2015) The rate of second electron transfer to Q_B^- in bacterial reaction center of impaired proton delivery shows hydrogen-isotope effect. *Biochim. Biophys. Acta 1847*, 223−230.
(12) Lonjers, Z. T., Dickson, E. L., Chu, T. P. T., Kreutz, J. E., Neacsu, F. A., Anders, K. R., and Shepherd, J. N. (2012) Identification of a New Gene Required for the Biosynthesis of Rhodoquinone in *Rhodospirillum rubrum*. *J. Bacteriol. 194* (5), 965−971.
(13) Erabi, T., Higuti, T., Kakuno, T., Yamashita, J., Tanaka, M., and Horio, T. (1975) Polarographic studies on ubiquinone-10 and rhodoquinone bound with chromatophores from *Rhodospirillum rubrum*. *J. Biochem. 78* (4), 795−801.
(14) Song, Y., and Buettner, G. R. (2010) Thermodynamic and kinetic considerations for the reaction of semiquinone radicals to form superoxide and hydrogen peroxide. *Free Radical Biol. Med. 49* (6), 919−962.
(15) Graige, M. S., Paddock, M. L., Feher, G., and Okamura, M. Y. (1999) Observation of the protonated semiquinone intermediate in isolated reaction centers from *Rhodobacter sphaeroides*: Implications for the mechanism of electron and proton transfer in proteins. *Biochemistry 38*, 11465−11473.
(16) Wraight, C. A. (1982) The involvement of stable semiquinones in the two-electron gates of plant and bacterial photosystems. In *Function of Quinones in Energy Conserving Systems* (Trumpower, B., Ed.) Chapter 3, pp 59−72, Academic Press, San Diego.
(17) Paddock, M. L., Flores, M., Isaacson, R., Shepherd, J. N., and Okamura, M. Y. (2010) EPR and ENDOR investigation of rhodosemiquinone in bacterial reaction centers formed by B-branch electron transfer. *Appl. Magn. Reson. 37* (1−4), 39−48.
(18) Paddock, M. L., Chang, C., Xu, Q., Abresch, E. C., Axelrod, H. L., Feher, G., and Okamura, M. Y. (2005) Quinone (Q_B) reduction by B-branch electron transfer in mutant bacterial reaction centers from *Rhodobacter sphaeroides*: Quantum efficiency and X-ray structure. *Biochemistry 44*, 6920−6928.
(19) Takahashi, E., Wells, T. A., and Wraight, C. A. (2001) Protein control of the redox potential of the primary acceptor quinone in reaction centers from *Rhodobacter sphaeroides*. *Biochemistry 40*, 1020−1028.
(20) Rinyu, L., Martin, E. W., Takahashi, E., Maróti, P., and Wraight, C. A. (2004) Modulation of the free energy of the primary quinone acceptor (Q_A) in reaction centers from *Rhodobacter sphaeroides*: Contributions from the protein and protein−lipid(cardiolipin) interactions. *Biochim. Biophys. Acta 1655*, 93−101.
(21) Onidas, D., Sipka, G., Asztalos, E., and Maróti, P. (2013) Mutational Control of Bioenergetics of Bacterial Reaction Center Probed by Delayed Fluorescence. *Biochim. Biophys. Acta 1827*, 1191−1199.
(22) Wells, T. A., Takahashi, E., and Wraight, C. A. (2003) Primary Quinone (Q_A) Binding Site of Bacterial Photosynthetic Centers: Mutations at Residue M265 Probed by FTIR Spectroscopy. *Biochemistry 42*, 4064−4074.
(23) Martin, E., Samoilova, R. I., Narasimhulu, K. V., Lin, T. J., O'Malley, P. J., Wraight, C. A., and Dikanov, S. A. (2011) Hydrogen bonding and spin density distribution in the Q_B semiquinone of bacterial reaction centers and comparison with the Q_A site. *J. Am. Chem. Soc. 133* (14), 5525−5537.
(24) Taguchi, A. T., O'Malley, P. J., Wraight, C. A., and Dikanov, S. A. (2013) Conformational differences between the methoxy groups of Q_A and Q_B site ubiquinones in bacterial reaction centers: A key role for methoxy group orientation in modulating ubiquinone redox potential. *Biochemistry 52*, 4648−4655.
(25) Taguchi, A. T., Mattis, A. J., O'Malley, P. J., Dikanov, S. A., and Wraight, C. A. (2013) Tuning Cofactor Redox Potentials: The 2-Methoxy Dihedral Angle Generates a Redox Potential Difference of >160 mV between the Primary (Q_A) and Secondary (Q_B) Quinones of the Bacterial Photosynthetic Reaction Center. *Biochemistry 52*, 7164−7166.
(26) Land, E. J., Simic, M., and Swallow, A. J. (1971) Optical absorption spectrum of half-reduced ubiquinone. *Biochim. Biophys. Acta 226*, 239−240.
(27) Kleinfeld, D., Abresch, E. C., Okamura, M. Y., and Feher, G. (1984) Damping of oscillations in the semiquinone absorption in reaction centers after successive flashes. Determination of the equilibrium between $Q_A^-Q_B$ and $Q_AQ_B^-$. *Biochim. Biophys. Acta 765*, 406−409.
(28) Asztalos, E., Sipka, G., and Maróti, P. (2015) Fluorescence relaxation in intact cells of photosynthetic bacteria: Donor and acceptor side limitations of reopening of the reaction center. *Photosynth. Res.*, DOI: 10.1007/s11120-014-0070-0.
(29) Moore, H. W., and Folkers, K. (1966) Structure of rhodoquinone. *J. Am. Chem. Soc. 88*, 567−570.
(30) Daves, G. D., Wilczynski, J. J., Friis, P., and Folkers, K. (1968) Synthesis of rhodoquinone and other multiprenyl-1,4-benzoquinones biosynthetically related to ubiquinone. *J. Am. Chem. Soc. 90*, 5587−5593.
(31) Giménez-Gallego, G., Ramírez-Ponce, M. P., Lauzurica, P., and Ramírez, J. M. (1982) Photooxidase system of *Rhodospirillum rubrum*. III. The role of rhodoquinone and ubiquinone in the activity preparations of chromatophores and reaction centers. *Eur. J. Biochem. 121*, 343−347.
(32) Okamura, M. Y., Isaacson, R. A., and Feher, G. (1975) Primary acceptor in bacterial photosynthesis: Obligatory role of ubiquinone in photoactive reaction centers of *Rhodopseudomonas sphaeroides*. *Proc. Natl. Acad. Sci. U.S.A. 72*, 3491−3495.
(33) Maróti, P., and Wraight, C. A. (1988) Flash-induced H^+ binding by bacterial photosynthetic reaction centers: Comparison of spectrophotometric and conductimetric methods. *Biochim. Biophys. Acta 934*, 314−328.
(34) Milano, F., Gerencsér, L., Agostiano, A., Nagy, L., Trotta, M., and Maróti, P. (2007) Mechanism of quinol oxidation by ferricenium produced by light excitation in reaction centers of photosynthetic bacteria. *J. Phys. Chem. B 111*, 4261−4270.
(35) Woodbury, N. W., Parson, W. W., Gunner, M. R., Prince, R. C., and Dutton, P. L. (1986) Radical-pair energetics and decay mechanisms in reaction centers containing anthraquinones, naph-

DOI: 10.1021/bi501553t
Biochemistry XXXX, XXX, XXX−XXX

thoquinones or benzoquinones in place of ubiquinone. *Biochim. Biophys. Acta 851*, 6−22.
(36) Shopes, R. J., and Wraight, C. A. (1987) Charge recombination from the $P^+Q_A^-$ state in reaction centers from *Rhodopseudomonas viridis*. *Biochim. Biophys. Acta 893*, 409−425.
(37) Sebban, P. (1988) Activation free energy of $P^+Q_A^-$ absorption decay in reaction centers from *Rb. sphaeroides* reconstituted with different anthraquinones. *FEBS Lett. 233*, 331−334.
(38) Vermeglio, A. (1977) Secondary electron transfer in reaction centers of *Rhodopseudomonas sphaeroides*: Out-of phase periodicity of two for the formation of ubisemiquinone and fully reduced ubiquinone. *Biochim. Biophys. Acta 459*, 516−524.
(39) Stowell, M. H. B., McPhillips, T. M., Rees, D. C., Soltis, S. M., Abresch, E., and Feher, G. (1997) Light-Induced Structural Changes in Photosynthetic Reaction Center: Implications for Mechanism of Electron-Proton Transfer. *Science 276*, 812−816.
(40) Calvo, R., Isaacson, R., Paddock, M. L., Abresch, E. C., Okamura, M. Y., Maniero, A.-L., Brunel, L.-C., and Feher, G. (2001) EPR Study of the Semiquinone Biradical $Q_A^{-\bullet}Q_B^{-\bullet}$ in Photosynthetic Reaction Centers from *Rb. sphaeroides* at 326 GHz: Determination of the Exchange Interaction J_0. *J. Phys. Chem. B 105*, 4053−4057.
(41) Wraight, C. A. (2004) Proton and electron transfer in the acceptor quinone complex of photosynthetic reaction centers from *Rhodobacter sphaeroides*. *Front. Biosci. 9*, 309−337.
(42) Cheap, H., Tandori, J., Derrien, V., Benoit, M., de Oliveira, P., Köpke, J., Lavergne, J., Maróti, P., and Sebban, P. (2007) Evidence for delocalized anticooperative flash induced proton bindings as revealed by mutants at M266His iron ligand in bacterial reaction centers. *Biochemistry 46*, 4510−4521.
(43) Gerencsér, L., Boros, B., Derrien, V., Hanson, D. K., Wraight, C. A., Sebban, P., and Maróti, P. (2015) Stigmatellin probes the electrostatic potential in the Q_B site of photosynthetic reaction center. *Biophys. J. 108*, 379−394.
(44) Rao, P. S., and Hayon, E. (1973) Ionization constants and spectral characteristics of some semiquinone radicals in aqueous solution. *J. Phys. Chem. 77*, 2274−2276.
(45) Willson, R. L. (1971) Semiquinone free radicals: Determination of acid dissociation constants by pulse radiolysis. *J. Chem. Soc. D*, 1249−1250.
(46) Swallow, A. J. (1982) Physical Chemistry of Semiquinones. In *Function of Quinones in Energy Conserving Systems* (Trumpower, B., Ed.) Chapter 3, pp 59−72, Academic Press, San Diego.
(47) Mukherjee, T. (2000) Photo and Radiation Chemistry of Quinones. *PINSA-A: Proc. Indian Natl. Sci. Acad., Part A 66A* (No. 2), 239−265.
(48) Pal, H., Mukherjee, T., and Mittal, J. P. (1994) One-electron reduction of 9,10-anthraquinone, 1-amino-9,10-anthraquinone and 1-hydroxy-9,10-anthraquinone in aqueous isopropanol-acetone mixed solvent: A pulse radiolysis study. *Radiat. Phys. Chem. 44*, 603−609.
(49) Lavergne, J., Matthews, C., and Ginet, N. (1999) Electron and proton transfer on the acceptor side of the reaction center in chromatophores of *Rhodobacter capsulatus*: Evidence for direct protonation of the semiquinone state of Q_B. *Biochemistry 38*, 4542−4552.
(50) Prince, R. C., and Dutton, P. L. (1978) Protonation and the reducing potential of the primary electron acceptor. In *The Photosynthetic Bacteria* (Clayton, R. K., and Sistrom, W. R., Eds.) pp 439−453, Plenum Press, New York.
(51) McPherson, P. H., Nagarajan, V., Parson, W. W., Okamura, M. Y., and Feher, G. (1990) pH-dependence of the free energy gap between DQ_A and $D^+Q_A^-$ determined from delayed fluorescence in reaction centers from *Rhodobacter sphaeroides* R-26. *Biochim. Biophys. Acta 1019*, 91−94.
(52) Turzó, K., Laczkó, G., Filus, Z., and Maróti, P. (2000) Quinone-dependent delayed fluorescence from reaction centers of photosynthetic bacteria. *Biophys. J. 79*, 14−25.
(53) Maróti, P., and Wraight, C. A. (2008) The redox midpoint potential of the primary quinone of reaction centers in chromatophores of *Rhodobacter sphaeroides* is pH independent. *Eur. Biophys. J. 37*, 1207−1217.
(54) Alexov, E., and Gunner, M. R. (1999) Calculated protein and proton motions coupled to electron transfer: Electron transfer from Q_A^- to Q_B in bacterial photosynthetic reaction centers. *Biochemistry 38*, 8254−8270.
(55) McPherson, P. H., Okamura, M. Y., and Feher, G. (1988) Light induced proton uptake by photosynthetic reaction centers from *Rhodobacter sphaeroides* R-26. I. Protonation of the one-electron states $D^+Q_A^-$, DQ_A^-, $D^+Q_AQ_B^-$, and $DQ_AQ_B^-$. *Biochim. Biophys. Acta 934*, 348−368.
(56) McPherson, P. H., Schönfeld, M., Paddock, M. L., Okamura, M. Y., and Feher, G. (1994) Protonation and Free Energy Changes Associated with Formation of Q_BH_2 in Native and Glu-L212 → Gln Mutant Reaction Centers from *Rhodobacter sphaeroides*. *Biochemistry 33*, 1181−1193.
(57) Marcus, R. A., and Sutin, N. (1985) Electron transfers in chemistry and biology. *Biochim. Biophys. Acta 811*, 265−322.
(58) Kleinfeld, D., Okamura, M. Y., and Feher, G. (1985) Electron transfer in reaction centers of *Rhodopseudomonas sphaeroides*. II. Free energy and kinetic relations between the acceptor states $Q_A^-Q_B^-$ and $Q_AQ_B^{2-}$. *Biochim. Biophys. Acta 809*, 291−310.

DOI: 10.1021/bi501553t
Biochemistry XXXX, XXX, XXX−XXX

III.

Ágnes Maróti, Colin A. Wraight and Péter Maróti:

Equilibrium- and kinetic isotope effects of electron transfer in bacterial reaction center of photosynthetic bacteria.

COST CM1306 conference, Visegrád (2014) talk.

No impact factor.

COST 1306 Conference on
Understanding Movement and Mechanism in Molecular Machines
15th-17th September 2014 Visegrád, Hungary
Oral presentation

Equilibrium- and kinetic isotope effects of electron transfer in bacterial reaction center of photosynthetic bacteria

Ágnes Maróti[1], Colin A. Wraight[2] and Péter Maróti[3]

Departments of [1]Paediatrics and [3]Medical Physics, University of Szeged, Hungary
[2]Center for Biophysics and Computational Biology, and Department of Plant Biology, University of Illinois, Urbana, IL 61801-3838 USA

The 2nd electron transfer in reaction center of photosynthetic bacterium *Rba. sphaeroides* is a two step process in which protonation of Q_B^- precedes interquinone electron transfer. The thermal activation and pH dependence of the overall rate constants of different RC variants were measured and compared in solvents of water (H_2O) and heavy water (D_2O). The electron transfer variants where the electron transfer is rate limiting (wild type and M17DN, L210DN and H173EQ mutants) do not show solvent isotope effect and the significant decrease of the rate constant of the second electron transfer in these mutants is due to lowering the operational pK_a of Q_B^-/Q_BH: 4.5 (native), 3.9 (L210DN), 3.7 (M17DN) and 3.1 (H173EQ) at pH 7. On the other hand, the proton transfer variants where the proton transfer is rate limiting demonstrate solvent isotope effect of pH-independent moderate magnitude (2.11±0.26 (WT+Ni^{2+}), 2.16±0.35 (WT+Cd^{2+}) and 2.34±0.44 (L210DN/M17DN)) or pH-dependent large magnitude (5.7 at pH 4 (L213DN)). Upon deuteration, the free energy and the enthalpy of activation increases in all proton transfer variants by about 1 kcal/mol and the entropy of activation becomes negligible in L210DN/M17DN mutant. The results are interpreted as manifestation of equilibrium and kinetic solvent isotope effects and the structural, energetic and kinetic possibility of alternate proton delivery pathways are discussed.

IV.

Ágnes Maróti, Colin A. Wraight and Péter Maróti:

Spectroscopic evidence for protonated semiquinone in reaction center protein of photosynthetic bacteria.

Molecular Machines Conference, Ringberg, Germany (2014) poster.

No impact factor.

Integrating spectroscopic and theoretical methods to analyse molecular machines

10.-13. December 2014,
Schloss Ringberg, Kreuth, Germany

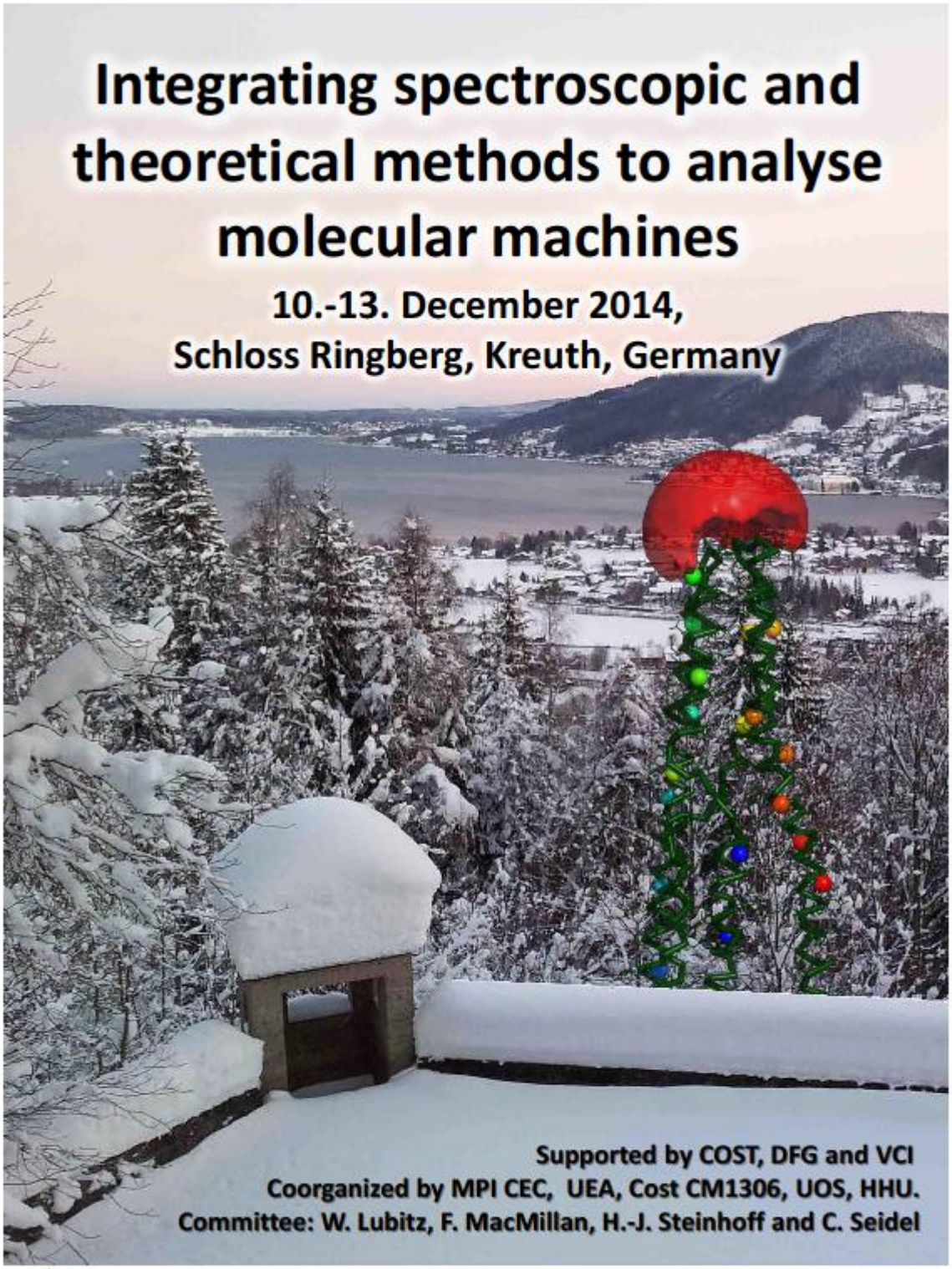

Supported by COST, DFG and VCI
Coorganized by MPI CEC, UEA, Cost CM1306, UOS, HHU.
Committee: W. Lubitz, F. MacMillan, H.-J. Steinhoff and C. Seidel

mpi cec

UEA
University of East Anglia

UNIVERSITÄT OSNABRÜCK

HEINRICH HEINE
UNIVERSITÄT DÜSSELDORF

P - 14

Spectroscopic evidence for protonated semiquinone in reaction center protein of photosynthetic bacteria

Ágnes Maróti[1], Colin A. Wraight[2†] and Péter Maróti[3]

Departments of [1]Pediatrics and [3]Medical Physics, University of Szeged, Rerrich Béla tér 1. 6720 Hungary
[2]Center for Biophysics and Computational Biology, and Department of Plant Biology, University of Illinois, Urbana, S. Goodwin Avenue, IL 61801-3838 USA
† This work is dedicated to the memory of Colin Wraight (1945-2014).

Coupled electron and proton transfers carry out energy conversion in many living organisms. In reaction center protein of photosynthetic bacteria the transfer of the second electron to the quinone at the Q_B binding site is accompanied by uptake of a proton from the aqueous bulk phase [1]. Although the protonation of $Q_B^{\bullet-}$ precedes rate-limiting electron transfer from $Q_A^{\bullet-}$, unambiguous evidences for observation of protonated semiquinone intermediate, $Q_BH^{\bullet}$ in isolated RC had so far not been reported. The reason for that could be the low pK (<4.5) of the ubisemiquinone [2]. In this work, we replaced the native ubiquinone in the Q_B site with rhodoquinone (RQ), which has a higher pK [1,3]. Unfortunately, the midpoint potential of RQ is lower by ~ 80 mV that makes the interquinone electron transfer thermodynamically unfavorable. To overcome this problem, we used the M265IT mutant where the midpoint potential of Q_A was reduced by ~100 mV. The pH dependence of the flash-induced semiquinone optical absorption spectrum between 400 nm and 500 nm does not follow a simple Henderson-Hasselbalch titration curve but is extended due to the strong interaction of the semiquinone with the cluster of acidic residues around the Q_B site [4]. The poster deals with the kinetics and energetics of the 2nd electron transfer reaction in Q_B site of RC where the native UQ is replaced by RQ.

Thanks to TÁMOP 4.2.2.A-11/1KONV-2012-0060, TÁMOP 4.2.2.B and COST (CM1306) programs.

References

[1] Graige, M. S., Paddock, M. L., Feher, G., Okamura, M. Y. *Biochemistry* **1999**, 38, 11465.
[2] Maróti, Á., Wraight C. A., Maróti, P. *Biochim Biophys Acta* (in press).
[3] Paddock, M. L., Flores, M., Isaacson, R., Shepherd, J. N., Okamura, M. Y. *Appl. Magn. Reson*. **2010**, 37, 39.
[4] Gerencsér, L., Boros B., Derrien, V., Hanson, D. K., Wraight, C. A., Sebban, P., Maróti, P. *Biophysical Journal* (in press).

Spectroscopic evidence for protonated semiquinone in reaction center protein of photosynthetic bacteria

Ágnes Maróti[1], Colin A. Wraight[2†] and Péter Maróti[3]

Department of [1]Pediatrics, and Department of [3]Medical Physics, University of Szeged, Rerrich Béla tér 1. 6720 Hungary

[2]Center for Biophysics and Computational Biology and Department of Plant Biology, University of Illinois, Urbana, S. Goodwin Avenue, IL 61801-3838 USA

† This work is dedicated to the memory of Colin A. Wraight (1945-2014).

Introduction

Coupled electron and proton transfers carry out energy conversion in many living organisms. In reaction center protein of photosynthetic bacterium *Rhodobacter sphaeroides* the light-induced transfer of two electrons to the quinone at the Q_B binding site is accompanied by binding of two protons resulting in fully reduced hydroquinone QH_2. The electron transfer steps and uptake of protons are sequential: e^-, H^+, e^- and H^+.

The transfer of the second (interquinone) electron from $Q_A^{\bullet-}$ is preceded by a very fast protonation of $Q_B^{\bullet-}$ and followed by binding of the second proton to $Q_AQ_BH^-$.

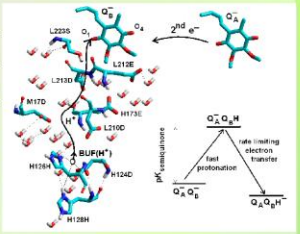

Aims and methods

Although the protonated semiquinone, $Q_BH^{\bullet}$ is an essential intermediate of the second interquinone electron transfer, no unambiguous evidences of observation had so far been reported. The reason for that could be the low pK (<4.5) of the semiquinone [Maróti et al. 2015]. In this work, we replaced the native ubiquinone in the Q_B site with rhodoquinone (RQ), which is supposed to have a higher pK and about 80 mV lower midpoint redox potential than the native ubiquinone. The low potential RQ at Q_B makes the interquinone electron transfer thermodynamically unfavorable. To overcome this problem, we used the M265IT mutant where the midpoint potential of Q_A was reduced by ~100 mV.

Quinones

Rhodoquinone (RQ) is a required cofactor for anaerobic respiration in *Rhodospirillum rubrum* [Lonjers et al. 2012]. It is an aminoquinone that is structurally similar to ubiquinone (Q), a ubiquitous lipid component involved in the aerobic respiratory chain. The only difference between the structures is that RQ has an amino group (NH_2) on the benzoquinone ring in place of a methoxy substituent (OCH_3) in Q. This difference of the structures causes considerable difference of their redox midpoint potentials (E_m): from +50 mV (UQ) to −30 mV (RQ) in *Rhodospirillum rubrum* [Erabi et al. 1975] and of pK of protonation of semiquinone (probably due to the higher electronegativity of nitrogen than carbon atom): from <4.5 (UQ) to 7.3 [Graige et al. 1999].

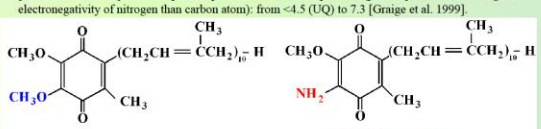

The reduction of the low potential rhodoquinone at the Q_B binding site requires the use of low potential analogues of Q_A [Graige et al. 1999] or direct electron transfer to Q_B along the inactive B branch [Paddock et al. 2010]. Both methods have difficulties. Binding different (non-native) quinones in the Q_A and Q_B sites calls for great challange in RC of *Rba. sphaeroides*. The incomplete binding of the quinones results in restricted interquinone electron transfer with a mixture of Q_A^- and Q_B^- states after the first saturating flash. The observation of B branch electron transfer to Q_B needs heavily modified RC with a total of five mutations and even in that case, the quantum yield of Q_B reduction is very low (about 5%). As the many modified residues are not located in the region around Q_B, the integrity of the Q_B environment is supposed to be preserved [Paddock et al. 2005].

Mutant RC: M265IT

Here, we used a different procedure for reducing rhodoquinone in the Q_B site. The Q_A binding site remained occupied by the native ubiquinone but its redox midpoint potential was lowered by 100-120 mV upon mutation of M265 isoleucine to threonine in the Q_A binding pocket [Takahashi et al. 2001]. The H-bond structure and the extensive decrease of the redox midpoint potential of Q_A were studied by delayed fluorescence of the bacteriochlorophyll dimer [Rinyu et al. 2004; Onidas et al. 2013], FTIR [Wells et al. 2003] and magnetic resonance [Martin et al. 2011] spectroscopies and quantum mechanical calculations of the 13C couplings of the 2-methoxy dihedral angle [Taguchi et al. 2013a,b]. The large drop in the redox potential of Q_A is attributed to hydrogen bonding of the OH to the peptide C=O of ThrM261, which causes a displacement of the backbone strand that bears the hydrogen bond donor (AlaM260) to the C1 carbonyl of Q_A, lengthening the hydrogen bond to the semiquinone state, Q_A^-, and thereby destabilizing it. This greatly increases ΔE_m, the driving force for electron transfer from Q_A^- to Q_B. If the native ubiquinone at Q_B is occupied by a low potential quinone (RQ), the driving force will remain large enough to get efficient interquinone electron transfer.

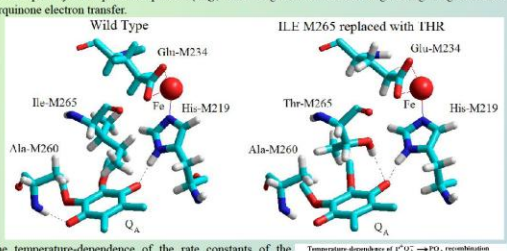

The temperature-dependence of the rate constants of the charge recombination measured by flash-induced absorption change at 430 nm is a good indication of the low potential of the quinone at the Q_A binding site. In wild type RC, the charge recombination occurs exclusively directly (probably by tunneling) to the ground state Q_A and the rate constant is highly independent on the temperature. If Q_A has low potential (e.g. in M265IT mutant), the recombination may occur also through the reduced bacteriophephytine (I, indirect pathway). As I is thermally populated, the observed recombination rate will show temperature-dependence.

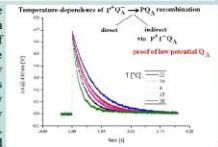

Results and discussion

Rhodosemiquinone oscillation

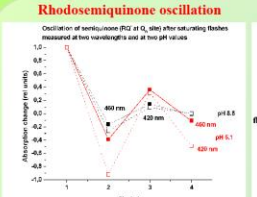

Control of damping of the oscillation

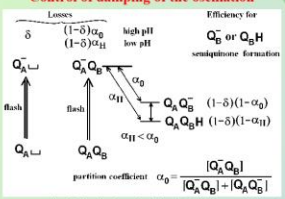

The damping of oscillation of rhodosemiquinone upon subsequent saturating flashes is determined by 1) the occupancy of the Q_B site (1-δ), and 2) the one-electron equilibrium partition coefficient (α) in the acceptor quinone system. At low pH, the damping is small indicating large Q_B site occupancy and effective electron transfer to Q_B (small δ and α). Additionally, the oscillation at 420 nm (characteristic of protonated RQ, $RQ_BH^{\bullet}$) is larger than at 460 nm (anionic form of RQ, $RQ_B^{\bullet-}$). It is due to higher stabilization (smaller partition coefficient) of the protonated form than that of the anionic form.

Light-induced absorption spectra of rhodosemiquinone

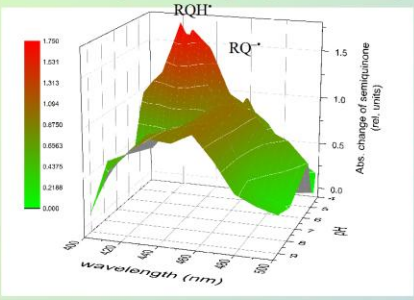

Quasi 3D representation of the optical absorption spectra of rhodosemiquinone at the secondary quinone binding site (Q_B) measured after a series of saturating flashes in the presence of electron donor to the oxidized dimer P$^+$ at several pH values. Similar spectra were obtained when the semiquinone appeared (after odd number of flashes) or disappeared (after even number of flashes). The spectra consist of components from protonated RQ (characteristic band around 420 nm that appears below pH 5) and deprotonated (anionic) RQ (characteristic band at 450 nm that dominates above pH 5). The predicted pK is much smaller than 7.3 given by Graige et al. 1999.

pH dependence of the rate of the 2nd electron transfer

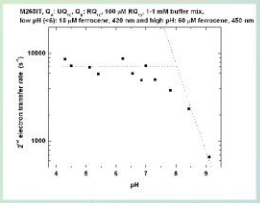

The rate constant of the 2nd ET is at a maximum or plateau below pH 5 ($k_{AB}^{(2)} \approx 7\text{-}8 \cdot 10^3\ s^{-1}$), decreases slowly between pH 5 and 7, and more steeply only at pH > 8 (one decade/pH unit).

Activation analysis of the rate of the 2nd electron transfer

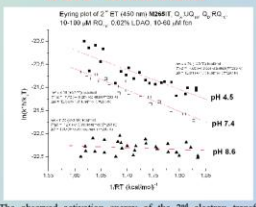

The observed activation energy of the 2nd electron transfer includes components from protonation and electron transfer. The decrease of the activation enthalpy can be observed at high pH due to the increase of the energy level of the protonated semiquinone. The pH-dependences of the activation parameters are similar in RCs of UQ or RQ at the Q_B site.

Protonation of rhodosemiquinone

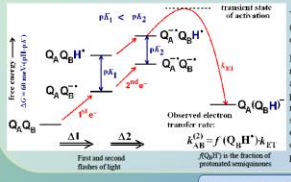

The k_{ET} electron transfer is rate limiting, but the observed (net) rate of 2nd ET is modulated by the pH-dependent equilibrium population of the protonated semiquinone $Q_BH^{\bullet}$.

In contrast to ubisemiquinone, the proton uptake of rhodosemiquinone can be observed to $Q_BH^{\bullet}$ at low pH with an apparent pK_2 < 5. The spectrum of stable rhodosemiquinone produced after odd number of flashes (and removed after even number of flashes) was obtained by measurement of the semiquinone oscillation. Although the pK_2 of the protonation of the rhodosemiquinone in the transient two-electron state could not be measured directly, it can be somewhat larger than pK_1 due to the extra negative charge on Q_A.

Conclusions

The flash-induced optical absorption spectrum of rhodosemiquinone between 400 nm and 500 nm showed partly neutral (protonated) character below pH 5 and was completely anionic above pH 5.5. The apparent pK of RQ at the Q_B site is low, similar to that of native ubiquinone and pH-dependent due to the strong interaction with the cluster of acidic residues in the Q_B site. The pH-dependence of the rates and activation energy of the 2nd electron transfer reaction in the Q_B site of the RC where the native UQ is replaced by RQ can be explained by the mechanism of proton activated electron transfer.

References

Erabi T, Higuti T, Kakuno T, Yamashita J, Tanaka M, Horio T (1975) Polarographic studies on ubiquinone-10 and rhodoquinone bound with chromatophores from *Rhodospirillum rubrum*. J. Biochem (Tokyo) 78(4) 795-801.

Graige MS, Paddock ML, Feher G, Okamura MY (1999) Observation of the protonated semiquinone intermediate in isolated reaction centers from *Rhodobacter sphaeroides*: Implications for the mechanism of electron and proton transfer in proteins. Biochemistry 38 11465-11473.

Lonjers ZT, Dickson EL, Cho TPT, Krentz JE, Neacsu FA, Anders KR, Shepherd JN (2012) Identification of a New Gene Required for the Biosynthesis of Rhodoquinone in *Rhodospirillum rubrum*. J Bacteriol 194(5) 965-973.

Maróti Á, Wraight CA, Maróti P (2015) The rate of second electron transfer to Q_B^- in bacterial reaction center of impaired proton delivery shows hydrogen-isotope effect. Biochim Biophys Acta 1847 223–230.

Martin E, Samoilova RI, Narasimhulu KV, Lin TJ, O'Malley PJ, Wraight CA, Dikanov SA (2011) Hydrogen bonding and spin density distribution in the Q_A semiquinone of bacterial reaction centers and comparison with the Q_A site. J Am Chem Soc 133(14) 5525-5537.

Onidas D, Sipka G, Asztalos E, Maróti P (2013) Mutational Control of Bioenergetics of Bacterial Reaction Center Probed by Delayed Fluorescence. Biochim Biophys Acta Bioenergetics 1827 1191-1199.

Paddock ML, Flores M, Isaacson R, Shepherd JN, Okamura MY (2010) EPR and ENDOR investigation of rhodosemiquinone in bacterial reaction centers formed by B-branch electron transfer. Appl Magn Reson 37(1-4) 39-48.

Paddock ML, Chang C, Xia Q, Abresch EC, Axelrod HL, Feher G, Okamura MY (2005) Quinone (Q_B) reduction by B-branch electron transfer in mutant bacterial reaction centers from *Rhodobacter sphaeroides*: quantum efficiency and X-ray structure. Biochemistry 44 6920-6928.

Rinyu L, Martin EW, Takahashi E, Maróti P, Wraight CA (2004) Modulation of the free energy of the primary quinone acceptor (Q_A) in reaction centers from *Rhodobacter sphaeroides*: contributions from the protein and protein–lipid(cardiolipin) interactions. Biochim Biophys Acta 1655 93–101.

Taguchi, A. T., O'Malley, P. J., Wraight, C. A., and Dikanov, S. A. (2013a) Conformational differences between the methoxy groups of Q_A and Q_B site ubiquinones in bacterial reaction centers: A key role for methoxy group orientation in modulating ubiquinone redox potential. Biochemistry 52, 4648–4655.

Taguchi AT, Mattis AJ, O'Malley PJ, Dikanov SA, Wraight CA (2013b) Tuning Cofactor Redox Potentials: The 2-Methoxy Dihedral Angle Generates a Redox Potential Difference of −160 mV between the Primary (Q_A) and Secondary (Q_B) Quinones of the Bacterial Photosynthetic Reaction Center. Biochemistry 52, 7164–7166.

Takahashi E, Wells TA, Wraight CA (2001) Protein control of the redox potential of the primary acceptor quinone in reaction centers from *Rhodobacter sphaeroides*. Biochemistry 40 1026-1038.

Wells TA, Takahashi E, Wraight CA (2003) Primary Quinone (Q_A) Binding Site of Bacterial Photosynthetic Centers: Mutations at Residue M265 Probed by FTIR Spectroscopy. Biochemistry 42 4064-4074.

Acknowledgements: Thanks to **Gábor Sipka** for construction of the 3D picture and to **TÁMOP 4.2.2.A-11/1KONV-2012-0060, TÁMOP 4.2.2.B** and **COST (CM1306)** for the financial support.

V.

Zita Gyurkovits, **Ágnes Maróti**, Lóránd Rénes, Gábor Németh, Attila Pál, and Hajnalka Orvos:

Adrenal haemorrhage in term neonates: a retrospective study from the period 2001–2013

The Journal of Maternal-Fetal Neonatal Medicine, Early Online: 1–4, 2014. DOI: 10.3109/14767058.2014.976550

Impact factor: 1.21

THE JOURNAL OF MATERNAL-FETAL & NEONATAL MEDICINE

http://informahealthcare.com/jmf
ISSN: 1476-7058 (print), 1476-4954 (electronic)

J Matern Fetal Neonatal Med, Early Online: 1–4
 DOI: 10.3109/14767058.2014.976550

informa healthcare

ORIGINAL ARTICLE

Adrenal haemorrhage in term neonates: a retrospective study from the period 2001–2013

Zita Gyurkovits[1], Ágnes Maróti[2], Lóránd Rénes[1], Gábor Németh[1], Attila Pál[1], and Hajnalka Orvos[1]

[1]*Department of Obstetrics and Gynaecology and* [2]*Department of Paediatrics, University of Szeged, Szeged, Hungary*

Abstract

Objective: To assess the incidence, risk factors and clinical presentations of neonatal adrenal haemorrhage (NAH) in uncomplicated, singleton and term deliveries.
Methods: A retrospective analysis of 26 416 term neonates delivered between 2001 and 2013, and screened with abdominal ultrasonography.
Results: Of the 26 416 neonates, 74 (0.28%) displayed NAH; the male/female ratio was 1.55:1. Vaginal delivery was significantly more frequent than caesarean section among them (71 versus 3; 95.9% versus 4.1%). Unilateral bleeding occurred on the right side in 36 (48.7%), and on the left in 34 (45.9%), without a significant difference; bilateral haematomas were found in four cases (5.4%). The most common risk factors were macrosomia (16, 21.6%) and fetal acidaemia (23, 31%), while four (5.4%) neonates exhibited pathological acidaemia. Clinical presentations included jaundice in 37 (50%), anaemia in six (8.1%) and an adrenal insufficiency in only one (1.3%) case. In three cases, neuroblastoma was diagnosed.
Conclusions: Vaginal delivery, macrosomia and fetal acidaemia are the most important risk factors for NAH. The adrenal glands on both sides were similarly involved. In the healthy neonates with NAH, the clinical presentations were mild, with spontaneous regression. Differentiation of NAH from tumours is of considerable importance.

Keywords

Adrenal haemorrhage, neonate, ultrasonographic screening

History

Received 20 July 2014
Revised 14 September 2014
Accepted 10 October 2014
Published online 7 November 2014

Introduction

Adrenal bleeding in the perinatal period may remain asymptomatic and, as routine neonatal abdominal screening is not common practice worldwide, its exact incidence cannot be determined. Earlier estimates indicated 1.7–2.1 per 1000 births, depending on the mode of diagnosis, which in most cases is ultrasonographic (USG) screening [1]. The pathogenesis is still unclear; the extensive vascularity and the relatively large size enhance the vulnerability of the adrenal glands to venous pressure changes, and mechanical compression also has a role during delivery [2]. Predisposing factors include prematurity, prolonged labour, a difficult delivery, macrosomia, perinatal hypoxia, coagulation disorders and septicaemia, though in most cases the aetiology cannot be established [3]. Neonatal adrenal haemorrhage (NAH) can occur *in utero*, but it usually appears perinatally; 5–10% of the cases involve bilateral haemorrhage; interestingly, in the unilateral cases, right adrenal gland involvement has been reported more frequently [4]. The clinical features are variable: anaemia, persistent indirect hyperbilirubinaemia, abdominal distension with an abdominal mass, and a bluish discolouration of the scrotum [5]. Whereas minor bleeding into the adrenal cortex may remain asymptomatic, a severe blood loss can be life-threatening, with hypovolaemic shock or an adrenal insufficiency. The differential diagnosis of suprarenal masses should include neuroblastoma, the predominant neonatal malignancy, teratomas, subdiaphragmatic extralobar pulmonary sequestration, vascular thrombosis and congenital adrenal cystic lesions [6].

In this study, we set out to review the incidence, risk factors and clinical presentations of NAH in term infants in our neonatal department over a 13-year period.

Methods

This was a retrospective study on singleton pregnancies of women who delivered at the Department of Obstetrics and Gynaecology, University of Szeged, Hungary, between 01.01.2001 and 31.12.2013. The inclusion criteria included a gestational age at delivery of at least 37 completed weeks; 26 416 full-term mature neonates of either sex, born between gestational weeks 37 and 41, were enrolled. Neonates who needed neonatal intensive care immediately after birth were not included in the study. The maternal data, gestational age, parity, mode of delivery and the presence of gestational diabetes mellitus were reviewed.

Every baby had ultrasound examination on day 2 of their life; this practice was adapted to screen renal abnormalities.

Address for correspondence: Zita Gyurkovits, Department of Obstetrics and Gynaecology, University of Szeged, Semmelweis Street 1, 6725 Szeged, Hungary. Tel: +36 70 4083878. Fax: +36 62 545711. E-mail: gyurkovits2000@yahoo.com

Considering that our university is a tertier center with a numerous transfers from other regions without proper antenatal care, our department decided to introduce renal screening. The significance of renal screening is well-known in the literature, where sonographic screening of the kidneys and the urinary tract was described as a very effective and non-invasive screening method after birth. It allows planning for appropriate diagnostic tests and therapeutic procedures in a timely fashion [7–9].

Suprarenal masses were diagnosed via postnatal USG of the abdomen on the second day of postnatal life, and the site of adrenal haemorrhage was recorded.

From the data in the files on the neonates, we analysed the presence of risk factors and comorbidities, such as a high birthweight, fracture of the clavicle, cephalhaematoma, anaemia, hyperbilirubinaemia, hypoglycaemia and respiratory disorders. The neonatal outcome was investigated from the aspects of the umbilical cord blood pH, the base excess (BE) and the 5–10 min Apgar scores. The neonatal outcomes were compared between two groups: the neonates with NAH and the control group, 5167 consecutive healthy term neonates born in a 2-year period (2012 and 2013). We found that this approach is statistically proper and allows a sufficiently correct and relevant basis of reference as a control group for comparison with the NAH group.

Immediately after delivery, a segment of the umbilical cord was double-clamped, and blood was drawn from the artery into preheparinized plastic syringes. Coagulation was inhibited with EDTA. The whole-blood samples were analysed within 5 min of collection for pH and BE. Acidaemia was defined as an umbilical blood pH <7.2 or/and an umbilical BE <-12 mmol/l (a BE of -12 mmol/l is approximately 2SDs below the mean), and pathological fetal acidaemia was diagnosed when the umbilical blood pH was <7.0. Maternal acidaemia as a cause of the cord blood acidaemia was excluded.

Macrosomia was defined as a birthweight >4000 g, and anaemia as a haemoglobin level more than 2SDs below the mean value for the corresponding age [10]. The definition of hypoglycaemia was a blood glucose level <2.6 mmol/l. Hyperbilirubinaemia was defined according to the Clinical Practice Guideline of the American Academy of Paediatrics published in 2004 [11].

Statistical analysis was performed by using the chi-square test; a level $p<0.05$ was considered to be statistically significant.

Results

Abdominal USG was applied in the total of 26 416 singleton neonates included in the study from the 13-year period; 74 of the neonates demonstrated NAH, an incidence of 0.28%. The vast majority, 71 (95.9%) of these 74 neonates, were delivered by vaginal delivery, and only 3 (4.1%) by caesarean section; the frequency of caesarean section in the NAH group was significantly lower than that in the control group (40.6%).

The haemorrhagic lesions were evaluated by USG as inhomogeneous lesions with decreased echogenicity that were mixed solid-liquid or echogenic masses.

NAH was more frequent in boys (60.8%) than in girls (39.2%); the difference was significant. Thirty six neonates (48.7%) had a unilateral haematoma on the right side, while 34 (45.9%) had one on the left, with no significant difference between the sides. Bilateral haematomas were found in four cases (5.4%).

The mean birthweight and gestational age were 3640 ± 424 g and 39.1 ± 1.0 weeks, respectively; 29 (39%) of the 74 were primipara and 45(61%) were multipara.

Sixteen (21.6%) of the 74 neonates were macrosomic, i.e. a significantly higher proportion as compared with the macrosomic neonate rate (7.1%) for the entire population at our department. Four mothers (5.4%) were diagnosed with gestational diabetes mellitus, a similar level of incidence as in our previous data.

As concerns the general condition at birth of the neonates with NAH, in 23 (31%) the umbilical cord blood pH was <7.2, or/and had BE <-12 mmol/l; fetal acidaemia was therefore significantly more frequent in the NAH group. Four (5.4%) of the 23 displayed pathological acidaemia with an umbilical cord blood pH <7.0. Five neonates (6.7%) had a 5- or 10-min Apgar score <7 ($p<0.05$).

The most common significant clinical features in the neonates with NAH were indirect hyperbilirubinaemia, in 37 (50.0%) cases, and anaemia in six (8.1%) cases ($p<0.001$). Other clinical presentations included birth trauma, e.g. cephalhaematoma (5; 6.7%); as compared with the controls, this was very close to the limit of significance. In cases of clavicle fracture (1; 1.3%) and hypoglycaemia (2; 2.7%), significance calculations could not be carried out, because of the low incidence, but both clinical presentations were observed with similar incidence in the NAH and control groups.

We have not found any abnormal palpable masses among these 74 babies although all the newborns were examined at least two times by specialised neonatologists. There was no significant difference in the rates of respiratory disorders between the NAH and control group (8.1% versus 6.3%).

Table 1 summarises the statistical data and an analysis of the NAH and control groups. No perinatal mortality occurred in either study group.

One neonate (1.3%) with bilateral NAH developed an adrenal insufficiency and was treated with glucocorticoid. Coagulation disorder and sepsis were not observed. The mean time for complete resolution of the haemorrhage was 18 ± 8 weeks. Three of the suprarenal masses proved to be congenital neuroblastomas (as confirmed by colour Doppler USG and pathological analysis) developing from the adrenal glands; these neonates were transferred and treated in another unit.

Discussion

This is the largest retrospective study that we are aware of which reports on the prevalence of NAH among term neonates. During a 13-year period, 74 neonates were diagnosed with NAH by abdominal USG, reflecting an incidence of 0.28% among the healthy term infants. Previous studies have indicated a wide range of incidence, from 0.003% up to 0.55%, depending on whether the selected population was symptom-free or treated in an intensive care unit [12,13]

Table 1. Outcome measures of neonates with NAH and the control group.

Comorbidities	NAH ($n = 74$)	Control ($n = 5167$)	p
Males	45 (60.8%)	2602 (50.3%)	<0.05*
Caesarean section	3 (4.1%)	2100 (40.6%)	<0.001*
Vaginal delivery	71 (95.9%)	2955 (57.2%)	<0.001*
Umbilical cord pH <7.2	23 (31%)	775 (15%)	<0.001*
Apgar score <7 at 5 min	5 (6.7%)	93 (1.8%)	<0.05*
Macrosomia	16 (21.6%)	366 (7.1%)	<0.001*
Anaemia	6 (8.1%)	87 (1.7%)	<0.001*
Indirect hyperbilirubinaemia	37 (50%)	1522 (29.4%)	<0.001*
Cephalhaematoma	5 (6.7%)	150 (2.9%)	0.052
Clavicle fracture	1 (1.3%)	50 (1.0%)	–
Hypoglycaemia	2 (2.7%)	163 (3.1%)	–
Respiratory disorder	6 (8.1%)	326 (6.3%)	0.52

Significance at $p < 0.05$ is indicated by*.

and also on whether the mode of diagnosis was USG, CT or autopsy.

Most of the neonates with NAH in our study were delivered by vaginal delivery, which is consistent with earlier findings and reflects the possible role of mechanical compression and also a hypoxic-ischaemic event with subsequent reperfusion injury during vaginal delivery [14]. Although the precise mechanisms leading to adrenal haemorrhage are still unclear, the available evidences have implicated the role of adrenocorticotropic hormone (ACTH), adrenal vein spasm and thrombosis, the limited venous drainage in the pathogenesis of this condition. The adrenal gland has a rich arterial supply, in contrast to its limited venous drainage, which is critically dependent on a single vein. Furthermore, in stressful situations, ACTH secretion increases, which stimulates adrenal arterial blood flow and cause adrenal vein spasm so the limited venous drainage capacity may cause venous stasis and may lead to haemorrhage [10].

The occurrence of NAH was particularly high in the macrosomic group and in those with fetal acidaemia or birth asphyxia, which is again consistent with other reports in the literature [15]. Furthermore, the common clinical presentations were similar to those in previous reviews, i.e. anaemia and persistent indirect bilirubinaemia [16].

On the other hand, our study revealed that the right and left sides were equally likely to be involved, in contrast with former reports suggesting that the probability of right adrenal gland haemorrhage involvement was higher. The mechanism for a right-sided predilection is presumed to be the compression of the adrenal gland between the liver and the spine and the pressure fluctuation in the inferior vena cava, which is directly connected to the right adrenal gland. However, at our department each infant undergoes abdominal USG screening. This therefore furnished reliable data on a high number of neonates, clearly demonstrating the equal likelihood of left and right NAH.

It is noteworthy that the incidence of NAH exhibited a slightly increasing tendency during this 13-year period, despite the continuously falling rate of vaginal delivery in our department.

This phenomenon may be explained in part by the rising frequency of macrosomic neonates. During the last 2–3 decades an overall increase in the proportion of macrosomic newborns has been found. The causes of the increasing prevalence of large newborns are complex and insufficiently explained, however this is a common phenomenon in many developed countries. The incidence of macrosomia varies between 5% and 20%, the highest ratio is found in the Nordic countries [17]. In Hungary, the incidences of macrosomia (birthweight >4000 g) in the recent decades are shown in Figure 1.

A number of risk factors for fetal macrosomia have been recognised, the strongest is the gestational maternal diabetes. Other modifiable risk factors are maternal pre-gestational anthropometric characteristics, like BMI, excessive weight gain during pregnancy, nutritional intake, level of physical activity, smoking and metabolic parameters. Non-modifiable factors include genes, fetal sex, parity, maternal age and height [18,19].

In the event of a suprarenal mass, it is of the highest importance to differentiate bleeding from a malignancy, such as a neuroblastoma, which originates from the neural tube cells. The tumour can be differentiated by the presence of vascular flow with colour Doppler USG or CT and via the catecholamine metabolite levels in the urine in the case of a neuroblastoma. While conservative therapy is appropriate for NAH, adrenal tumours may need surgical excision. An adrenal mass can be followed up for one month with serial USG without any adverse effects on the therapy and prognosis of the tumour [20], persistence or enlargement suggesting an adrenal neoplasm. We diagnosed three cases of neuroblastoma; at the time of detection, all of them were symptom-free, the early diagnosis therefore was promoting a good prognosis.

NAH, and particularly the bilateral form, needs a careful follow-up to prevent the later consequences, including prolonged jaundice, anaemia or an adrenal insufficiency. In our study, jaundice was observed in 50% and anaemia in 8.1% of the NAH cases; they required only conservative treatment. An adrenal insufficiency was diagnosed in only one patient, who needed adequate hormone supplementation.

The limitation of our study is its retrospective nature, which is why the exact descriptions of haemorrhages were not recorded. Although an adrenal insufficiency is more frequent among preterms than among mature neonates [21], preterms were not included in the study as they were transferred to

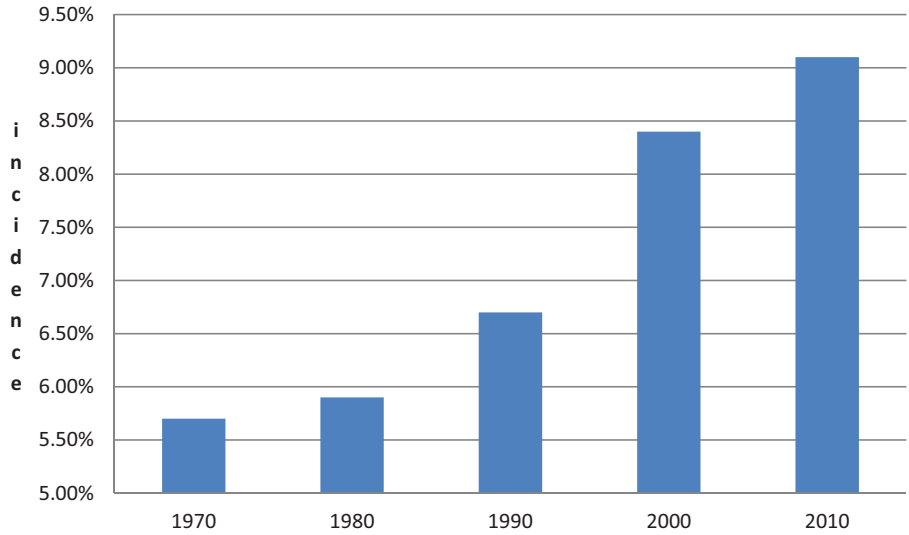

Figure 1. Incidence of macrosomia (birthweight >4000 g) in Hungary from 1970 until 2010.

another department. Due to the same reason, the medical follow-up of the neonates with an adrenal insufficiency or neuroblastoma was not feasible.

Primary coagulation disorders and sepsis are also well-known risk factors for bleeding, but they did not play a role in the aetiology in our work.

In conclusion, this is the largest series of scanning for NAH in healthy neonates that has been reported so far. The findings highlight the diverse and non-specific clinical presentation of NAH, though most of the cases had merely mild consequences and needed only conservative treatment.

We still continue our screening protocol regarding abdominal ultrasound screening for every term neonate, as benefits overweigh the harms, according to our opinion. Particularly, the follow-up of the newborns with any congenital abnormalities became much more effective and precise with this protocol. However, as further data and investigations are still needed to clarify the presence and importance of the later consequences, for other neonatal units we only recommend abdominal ultrasound screening in the risk groups, like macrosomic neonates with vaginal delivery or fetal acidaemia. A long term follow-up for the consequences of adrenal haemorrhage is still needed. The importance of abdominal USG screening is to be stressed, especially for vaginally delivered macrosomic neonates, for those with fetal acidaemia and for newborns suffering from birth trauma, unexplained anaemia and prolonged icterus.

Declaration of interest

The authors report no conflicts of interest.

References

1. Demirel N, Baş AY, Zenciroğlu A, et al. Adrenal bleeding in neonates: report of 37 cases. Turk J Pediatr 2011;53:43–7.
2. Felc Z. Ultrasound in screening for neonatal adrenal hemorrhage. Am J Perinatol 1995;12:363–6.
3. Katar S, Oztürkmen-Akay H, Devecioğlu C, et al. A rare cause of hyperbilirubinemia in a newborn: bilateral adrenal hematoma. Turk J Pediatr 2008;50:485–7.
4. Lai LJ, Chen LM, Chu PY, et al. Neonatal adrenal hemorrhage associated with scrotal hematoma: an unusual case report and literature review. Pediatr Neonatol 2012;53:210–12.
5. Velaphi SC, Perlman M. Neonatal adrenal hemorrhage: clinical and abdominal sonographic findings. Clin Pediatr 2001;40:545–8.
6. Postek G, Streich H, Narębski K. Assessment of diagnostic methods in adrenal gland hemorrhage in neonates on the basis of own material from the years 2007–2011. Pol J Radiol 2011;76:62–4.
7. Bereczki CS, Orvos H, Sumegi V, et al. Postnatal renal pelvis dilatation – results of 9650 screened neonates (Abstr). Pediatr Nephrol 2004;19:C217.
8. Gruessner SE, Klein K, Peter C, et al. Ultrasound screening of the kidneys and urinary tract in 11.887 newborn infants: a 10-year experience. Open J Obstet Gynecol 2012;2:389–93.
9. Drnasin K, Saraga-Babić M, Saraga M. Clinical importance of pyelocalyceal dilation diagnosed by postnatal of the ultrasonographic screening urinary tract. Med Sci Monit. 2013;19:125–31.
10. Tulassay T, Seri I, Evans J. Renal vascular disease in the newborn. In: Taeugah HW, Ballard RA, Avery ME, eds. Schaffers and avery's diseases of newborn. 7th ed. Philadelphia: WB Saunders Company; 1998:1177–87.
11. American Academy of Pediatrics. Clinical practice guideline. Management of hyperbilirubinemia in the newborn infant 35 or more weeks of gestation. Pediatrics 2004;114:297–308.
12. White PC. Adrenocortical insufficiency. In: Behrman RE, Kliegman RM, Jenson HB, eds. Nelson text book of pediatrics. 18th ed. Philadelphia, PA: Saunders; 2007:2357–8.
13. Lee MC, Lin LH. Ultrasound screening of neonatal adrenal hemorrhage. Acta Paediatr Taiwan 2000;41:327–30.
14. DeSa DJ, Nicholls S. Haemorrhagic necrosis of the adrenal gland in perinatal infants: a clinico-pathological study. J Pathol 1972;106:133–49.
15. Örün E, Yıldırım M, Yılmaz AE, et al. Is routine abdominal ultrasonography necessary in macrosomic newborns with difficult delivery? Matern Fetal Neonatal Med 2012;25:1195–6.
16. Qureshi UA, Ahmad N, Rasool A, Choh S. Neonatal adrenal hemorrhage presenting as late onset neonatal jaundice. J Indian Assoc Pediatr Surg 2009;14:221–3.
17. Henriksen T. The macrosomic fetus: a challenge in current obstetrics. Acta Obstet Gynecol Scand 2008;87:134–45.
18. Kramer MS, Morin I, Yang H, et al. Why are babies getting bigger? Temporal trends in fetal growth and its determinants. J Pediatr 2002;141:538–42.
19. Rooth G. Increase in birthweight: a unique biological event and an obstetrical problem. Eur J Obstet Gynecol Reprod Biol 2003;106:86–7.
20. Yao W, Li K, Xiao X, et al. Neonatal suprarenal mass: differential diagnosis and treatment. J Cancer Res Clin Oncol 2013;139:281–6.
21. Mutlu M, Karagüzel G, Aslan Y, et al. Adrenal hemorrhage in newborns: a retrospective study. World J Pediatr 2011;7:355–7.